Tectono-stratigraphic evolution of the El Qaa fault block, Sinai, Egypt - an ArcGIS and MOVE study

Barbara Biskopstø Hansen

Master of Science thesis

in Petroleum Geology

Department of Earth Science

University of Bergen

June 2015

ABSTRACT

The Gulf of Suez is a classic example of a failed rift system and due to the extensive erosion it has become perfect for studying structural style and stratigraphy in a 3D environment, where the sedimentary architecture can be studied in more details. There have been many studies in specific areas within the Gulf of Suez focusing on these subjects, but less focus has been on construction and restoration of cross-sections and 3D modelling in the area, which is the focus of this study, in addition to a geological map generated in this thesis.

The work in this study includes the mapping of prerift and synrift units, faults, folds and dip data and an analysis of the tectono-stratigraphic evolution of the El Qaa fault block. The geological map is generated in ArcGIS by mapping lithological boundaries, tracing faults and folds and adding dip data. Based on the geological map, six cross-sections were constructed and restored using the 2D/3D MOVE software and the interpreted cross-sections are used to construct a 3D model of the present day structural style in the El Qaa fault block.

The tectono-stratigraphic evolution can be divided into 4 main synrift stages. Synrift stage 1 (Burdigalian-Langhian) is the first rotation of the prerift units that caused an angular unconformity between the prerift and synrift units. Synrift stage 2 (Langhian) is a further rotation of the units as the Rudeis Formation and the Delta Lope complex 1 was deposited. Synrift stage 3 (Seravallian) contains the deposition of the Delta Lobe Complex 2 and 3. Synrift stage 4 (Seravallian-Present day) is the latest rotation of the units caused by the increased displacement on the Coastal Fault Belt as the fault activity in the rift migrates towards the rift axis.

The lower Delta Lobe Complex 1 is a short, steep and coarse-grained delta with a local catchment-area that is feeding the delta with sediments derived from the uplifting rift shoulder on the East Boundary Fault Belt. The Delta Lobe Complex 1 is deposited in similar structural settings as the much smaller western delta in the Alkyonides half graben in the Gulf of Corinth which has a high subsidence rate and high accommodation development. The upper prograding Delta Lobe Complex 2 and 3 are deposited in a more tectonically quiet period, with a low subsidence rate and low accommodation development, it extends ca. 13,5 across the El Qaa half graben. The upper deltas show similarities with the deltas on the Horda platform containing the Krossfjord, Sognefjord and Fensfjord Formations, in being larger and possible having a well-developed catchment-area feeding the deltas.

The study illustrates the importance of understanding how the sedimentary architecture in a rift basin is formed and the main factors controlling the sediment dispersal.

ACKNOWLEDGEMENTS

This present study was conducted at the Department of Earth Science, University of Bergen, in the time period from 2013-2015, as a part of my master degree in petroleum geology.
I would like to acknowledge several people that have been important for me and my research project.

First I would like to thank my supervisor, Professor Rob Gawthorpe and my co-supervisor Martin Muravchik for the helpful discussions, guidance and constructive comments and feedback on my thesis. In addition I would like to thank Martin for all the help regarding ArcGIS and data.

Rosa Polanco Ferrer I would like to thank for all the help and advice on the structural modelling software 2D/3D MOVE. Mike Young I would like to thank for all the helpful comments on the thesis and for taking the time to look through it.

In addition I would like to thank my son John Tóri and Leivur for their patience, support and encouragement during my years of study. And my mom and Fríðbjørg for the good advice regarding writing this master thesis.

And last but not least I would like to thank my fellow students at the University of Bergen for five great years.

.....

Barbara Biskopstø Hansen Bergen, 1 June 2015

CONTENT

1 INTRODUCTION

1.1 Rationale

Extensional rift basins have been widely studied for the last two decades and the Gulf of Suez is a classic example of a failed rift system. The extensive erosion made by the Wadi Sidri and Wadi Feiran system created outcrops in this area that are perfect for studying the tectono-stratigraphic evolution in a 3D environment, where one is able to follow structures both across and along strike. To get a better understanding of the fault evolution, structural and stratigraphic analysis are needed, and constructing 3D models are one way of improving the understanding and to get an insight on how rift systems are build and thereby being able to locate if and where hydrocarbons could be found.

There have been several studies focusing on the structural evolution and the sedimentary response in the Gulf of Suez e.g. (Moustafa, 1993; Gupta et al., 1999; Sharp et al., 2000b; Bosworth and Mcclay, 2001). Furthermore, there have been many studies on specific areas within the Gulf of Suez, e.g. Gawthorpe et al. (1990) focuses on the Miocene Abu Alaqa Group, Lewis et al. (in press) on the Hadahid fault block and McClay and Khalil (1998) on the Araba-Abu Durba area. Other have generated models describing sedimentary response to fault evolution regarding extensional rift basins (Leeder and Gawthorpe, 1987; Ravnås and Steel, 1998; Sharp et al., 2000a). There has been less focus on the entire El Qaa fault block on a bigger scale, including both restoration of cross-sections and 3D modelling, which is the focus of this thesis.

1.2 Aims and objectives

The overall aim of this study is the mapping of the stratigraphy and the structures of the El Qaa fault block (east margin of the Suez rift) and analysis of the tectono-stratigraphic evolution using Google Earth, ArcGIS and 2D/3D MOVE. The overall aim can be subdivided into the following objectives:

- Mapping of the Prerift and synrift stratigraphic units in the El Qaa fault block.
- Mapping of the faults and folds in the study area
- Construction of six cross-sections across the fault block
- Restoration of cross-section using 2D/3D MOVE
- Construction of a 3D model of the present day El Qaa fault block
- Interpretation of the tectono-stratigraphic evolution of the El Qaa fault block.

1.3 Methods

The project has been done using satellite images and field work done by a number of professors and researchers at the Bergen University, together with publications that provide ground truthing of the remote sensing based mapping undertaken in this thesis.

1.4 Study area

The Study area the Suez Rift is located at the northern end of the Red Sea in Egypt. It is a failed rift that originated due to extension caused by the separation between the African plate and the Arabian plate. The Suez Rift is considered to be an abandoned rift (Patton et al., 1994) that extended northward from the Red Sea, it is about 300 km long, 50 km wide in the northern end, 80-90 km wide in the southern end and consists mainly of rotational fault blocks bounded by large normal faults. The boundaries of the Suez Rift have a characteristic zig-zig pattern (Bosworth and Mcclay, 2001). Around the Late middle Miocene the rifting in the Gulf of Suez stopped or diminished remarkably at the onset of the Gulf of Aqaba (Dead Sea transfer fault system), which is the NE rift arm extending from the Red Sea (Figure 1-1).

Figure 1-1: Location of the Study area, the El Qaa Fault block in the Gulf of Suez, Sinai, Egypt (Map retrieved from Google Earth 28.05.2015)

1.5 Thesis layout

Following the introduction chapter, this thesis is divided into six chapters; **chapter 2** contains the background information on general rift system concepts and background on the Gulf of Suez; **chapter 3** describes where the data is from and what kind of software (ArcGIS and 2D/3D MOVE) was used in this thesis, furthermore it describes the work-flow and methods used in this study; **chapter 4** represents the results from the mapping, construction of cross-sections, restoration (backstripping) and the 3D model; **chapter 5** is the synthesis and discussion on the tectonic evolution of the study area and goes into more detail on the fault growth and activity, delta types present and a short description of the limitations and possible future work; **chapter 6** summarizes the main conclusions made from this study.

2 GEOLOGICAL BACKGROUND

To be able to understand the tectono-stratigraphic evolution in a rift basin, it is important to understand the basics behind extensional rift system, such as why and how the rifting starts and furthermore, how the rift evolution is controlled mainly by fault growth, drainage evolution, changes in sediment supply and sea-level. This rift evolution is recorded in the sedimentary architecture and can be extracted by making a tectono-stratigraphic analysis of the rift basin, which is the main goal of this thesis. The aim of this chapter is to give an overview of these previous mentioned basic concepts regarding extensional rift systems starting from the lithospheric scale towards more detailed fault growth evolution and the sedimentary response. The chapter is divided into two parts, **part 2.1** focuses on the structural styles and sedimentology for general rift basins and **part 2.2** focuses on the Gulf of Suez.

2.1 Structural Styles and synrift sedimentology in Rift Basins

2.1.1 Structural styles for general rift basins:

How rift basins evolve depend on the thermal state of the crust, how thick the crust is at the rift initiation stage, amount of extension and how large the affected area is, if extension is orthogonal or oblique, the composition and erodibility of the prerift and synrift deposits involved throughout the rifting. Another important control on the orientation of the faults is old fabric in the basement rocks, these can be reactivated and thereby forcing the new faults to follow old structures (Ravnås and Steel, 1998).

Rifts at a lithospheric scale

Huismans et al. (2011) describes the two end-members of rift systems in a lithospheric scale, and proposes that these are the direct consequence of their differences in lithospheric rheological properties (Huismans and Beaumont, 2011). Type 1 (Figure 2-1, A and B) is a magma-poor rift system characterized by a narrow (< 100 km wide) rift-zone with large basin-bounding faults, reaching deep into the crust, the flanks are usually uplifted and the rift is asymmetric. Type 1 has a two-layer rheology with a brittle top-layer (upper lithosphere) that breaks first and ductile bottom-layer (lower lithosphere). At the transition

between oceanic and continental plate a serpentinized continental mantle lithosphere can be exposed. The Iberia-NewFoundland and Labradore-Southern Greenlands margins are examples of Type 1 margins (Huismans and Beaumont, 2011). Type 2 (Figure 2-1, C and D) is characterized by an ultra-wide (> 350 km wide) rift-zone and a very thin continental crust. Synrift basins are faulted and created early in the rifting process, the late synrift sediments are undeformed and capped by evaporates and other sediments deposited in shallow water conditions. There is little synrift subsidence or uplifts of flanks due to the underlying continental mantle lithosphere being replaced by hot asthenosphere. Type 2 has a 3 layer rheology where the middle layer (lower crust) acts as a decoupling layer that separates the upper and lower lithosphere, in contrast to type 1, the lower lithospheric layer breaks first, since the extension is spread over a large area, the crust is only relative thin and takes much longer time before it breaks. The central South Atlantic and the Exmouth plateau are examples of type 2 margins (Huismans and Beaumont, 2011). Huismans et al. (2014) propose a third type of margin (Figure 2-1, E and F), that differs from Type 2 in having a middle layer (mid-crust) that is strongly bonded to the lower lithosphere, and breaks along with the lower lithosphere leaving the upper crust in direct contact with the asthenosphere. Underplating of hot depleted lower cratonic lithospheric that floats laterally towards the rift axis can occur on all three types of margins (Figure 2-1, B, D and F). Where underplating occurs, the formation of oceanic lithosphere is delayed. For type 2 and 3 the underplate material will only be exposed at the rift margins if it flows beneath the rift axis, when it ruptures (Huismans and Beaumont, 2014).

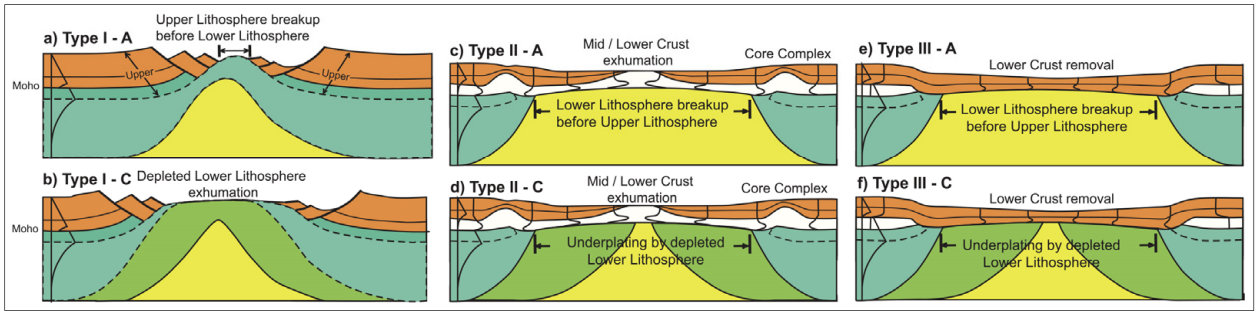

Figure 2-1: Diagram depicts the difference between type 1, 2 and 3 endmembers of rift margins. (Type A) is where the asthenosphere underplates and (Type C) is where the depleted cratonic lower lithosphere underplates. Modified from Huismans and Beaumont (2014).

Fault blocks/half grabens

A rift can consist of one or many faulted tilt blocks or half grabens bounded by basin-bounding faults, which are the fundamental morphological element in rifts (Leeder and

Gawthorpe, 1987; Ravnås and Steel, 1998). As the faults propagate the hangingwall collapses/subsides and the footwall uplifts, which causes the blocks to rotate, creating a domino fault block system (Figure 2-2).

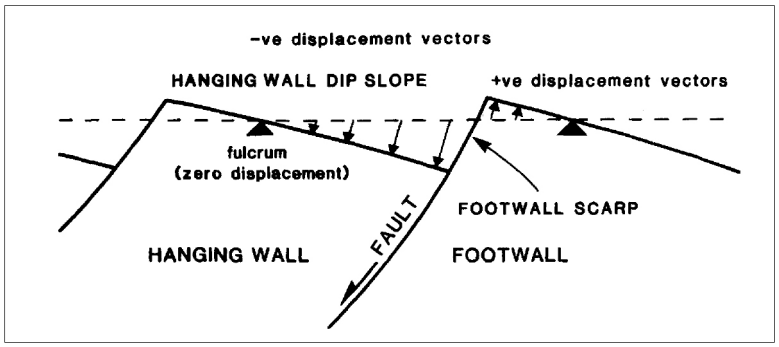

Figure 2-2: Diagram showing a simple rotated domino fault block and the position of the fulcrum point. Modified from Leeder and Gawthorpe (1987).

The variation in displacement along-strike and perpendicular to a fault and the rotation of the blocks, are unique element of rift-basins and control the complex asymmetric infill architecture (Leeder and Gawthorpe, 1987; Ravnås and Steel, 1998). The fulcrum point is the line/point separating the uplifting part from the subsidence part of a fault block, at this point the hangingwall displacement is zero (Leeder and Gawthorpe, 1987). The location of the fulcrum depends on the geometry of the fault, the balance between uplift/subsidence and the presence of secondary structures (antithetic and synthetic faults) in the tilted block (Leeder and Gawthorpe, 1987).

Transfer/accommodation zones

Transfer zones and accommodation zones or relay ramps occur between overlapping fault tips where the strain is being shifted (transferred) from one fault to another due to the stress between them (Patton et al., 1994). Patton et al. (1994) describes 2 major types of transfer zones (Figure 2-3), conjugate and synthetic. Conjugate is when two fault with opposite dip direction link, this can be further divided into divergent system, when the faults face dip towards each other and convergent systems, when the fault face dip away from each other. If the faults dip in the same direction it is a synthetic transfer zone (Patton et al., 1994).

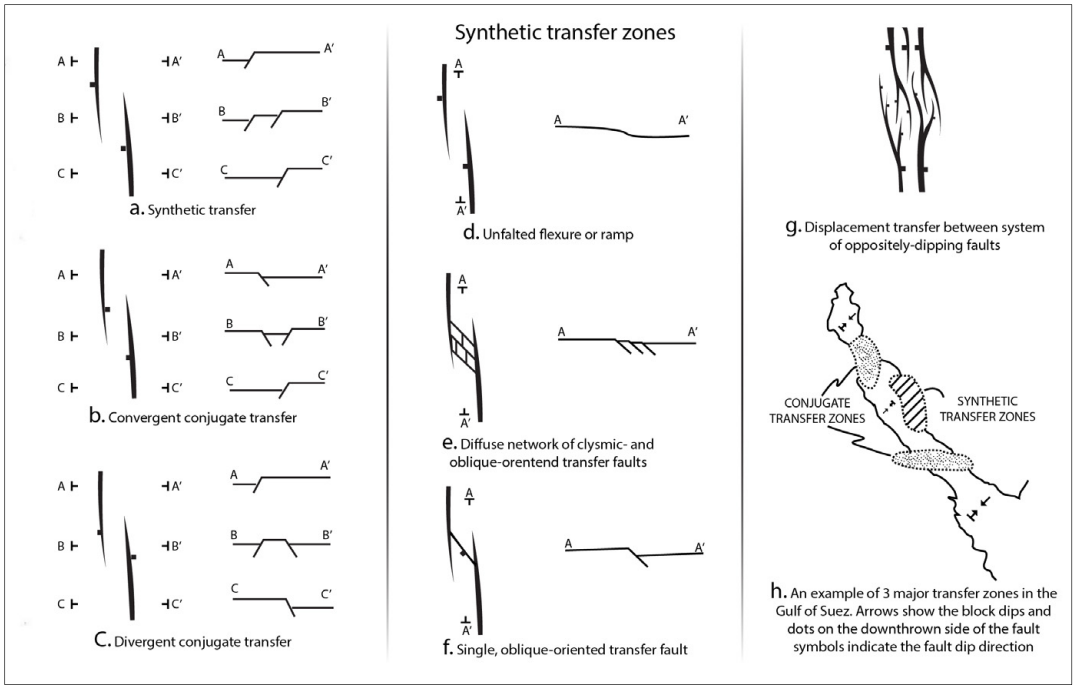

Figure 2-3: Diagram that shows idealized examples of displacement transfer between en echelon, overlapping normal faults (after Morley et al., 1990). Modified from Patton et al. (1994).

Rift areas are often submitted to periodically rifting, that is multiple active rifting periods each followed by a quiescence period. This has been observed in areas such as the North Sea-Norwegian sea, where the successive rifting episodes where active for 4-6 Ma at the time, and the entire rifting went on for some tens of Ma (Ravnås and Steel, 1998).

Fault growth and linkage

The initial rifting begins with the nucleation of several isolated fault segments, a normal fault array (Cowie et al., 2000; Gawthorpe and Leeder, 2000). Figure 2.4A-C shows a schematic overview of the development from the initial stage of rifting with several small, largely isolated faults distributed over a large area. The depocentres created at rift initiation (Figure 2-4) are small and shallow and the subsidence rate is slow (Cowie et al., 2000). As the extension continues and the stress increases (Figure 2-4B) the fault tips propagate to form longer faults that interact and link with one another (Cowie et al., 2000; Gawthorpe and Leeder, 2000). When a fault ruptures the elastic strain in the surrounding rock is disturbed causing shadow zones (stress-level decreases) and enhancement zones (stress-level increases) to develop around the fault. Faults with overlapping enhancement zones will grow more rapidly and faults with overlapping shadow zones will eventually die out (Cowie

et al., 2000). Generally the maximum fault displacement (d_{max}) scales with the length of the fault (L) and is largest near the centre of the fault segments and decreases towards the fault tips (Cowie et al., 2000; Sharp et al., 2000b). A fault array including many short fault segments can act as one long fault, causing the maximum displacement (d_{max}) to shift away from the centre along-strike in a fault, depending on the location of the fault in the overall array. Figure 2-4C depicts the linkage of shorter faults into longer through-going fault zones, at this point the amount of active fault decreases, since many faults ending up in the shadow-zones, of newly segmented longer faults, become inactive. These long faults usually have displacement variation along a fault scarp, due to differences in length before linkage, but as the fault grows longer the displacement is more evened out and (Cowie et al., 2000).

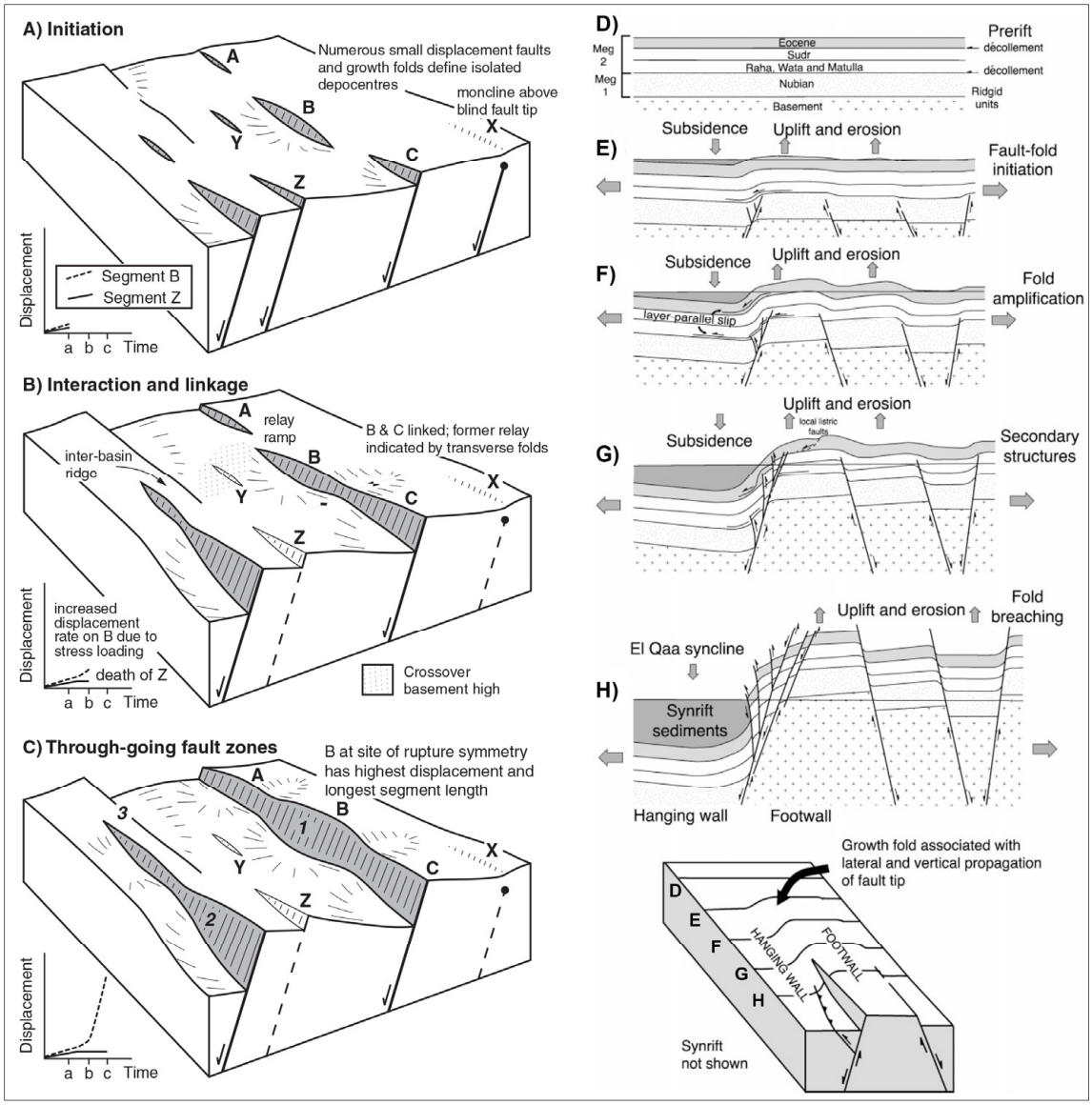

Figure 2-4: (A to D) shows a schematic 3D evolution of the linkage of fault segments. (D to H) depicts the evolution of a monocline developing over a blind fault and until it ruptures. Modified from (Gawthorpe and Leeder, 2000; Sharp et al., 2000b)

As a blind fault propagates upward, the surface expression is folding (Figure 2-4 A-C, fault x). Figure 2-4 D-H is a schematic diagram showing the development from a blind fault causing folding of the surface above the fault tip and as the fault tip migrates towards the surface second- and third-generation synthetic and antithetic faults develop in the hangingwall syncline, until the fault eventually breaks through the surface (Leeder and Gawthorpe, 1987; Gawthorpe et al., 1997).

Fault activity

Cowie et al. (2005) focus on the temporal inward increased activity of the faults towards the rift axis. The conclusion of their study of the rifting in the northern North Sea, in the Late Jurassic, on the Viking Graben and the platform surrounding is summarized in Figure 2-5. Stage 1 (A) is the rift initiation, at this stage the faults are small and dipping both towards and away from the rift axis, the fault activity is distributed across the entire rifting-area and the thermal gradient (D) is laterally weak at this stage. Stage 2 (B) at this stage the faults dipping inwards are more active and increase in displacement and the out-ward dipping faults die out, (E) now shows an increase towards the middle in the thermal gradient, viscosity and strain rate which causes the increase activity in the inward dipping faults. The last stage (C) illustrates clearly the fault closest to the rift axis now obtain the largest displacement and faults towards the rift margins are less active or inactive, the zone active rifting thereby decreases with time, in this case from the northern North Sea the active rifting zone was ~200 km wide at rift initiation and decreased to ~50 km wide during the 40 Ma of active rifting, (F) clearly illustrates the largest Thermal gradient, viscosity structure and Strain Rate is concentrated in the centre of the rift axis, where the lithosphere is thinnest.

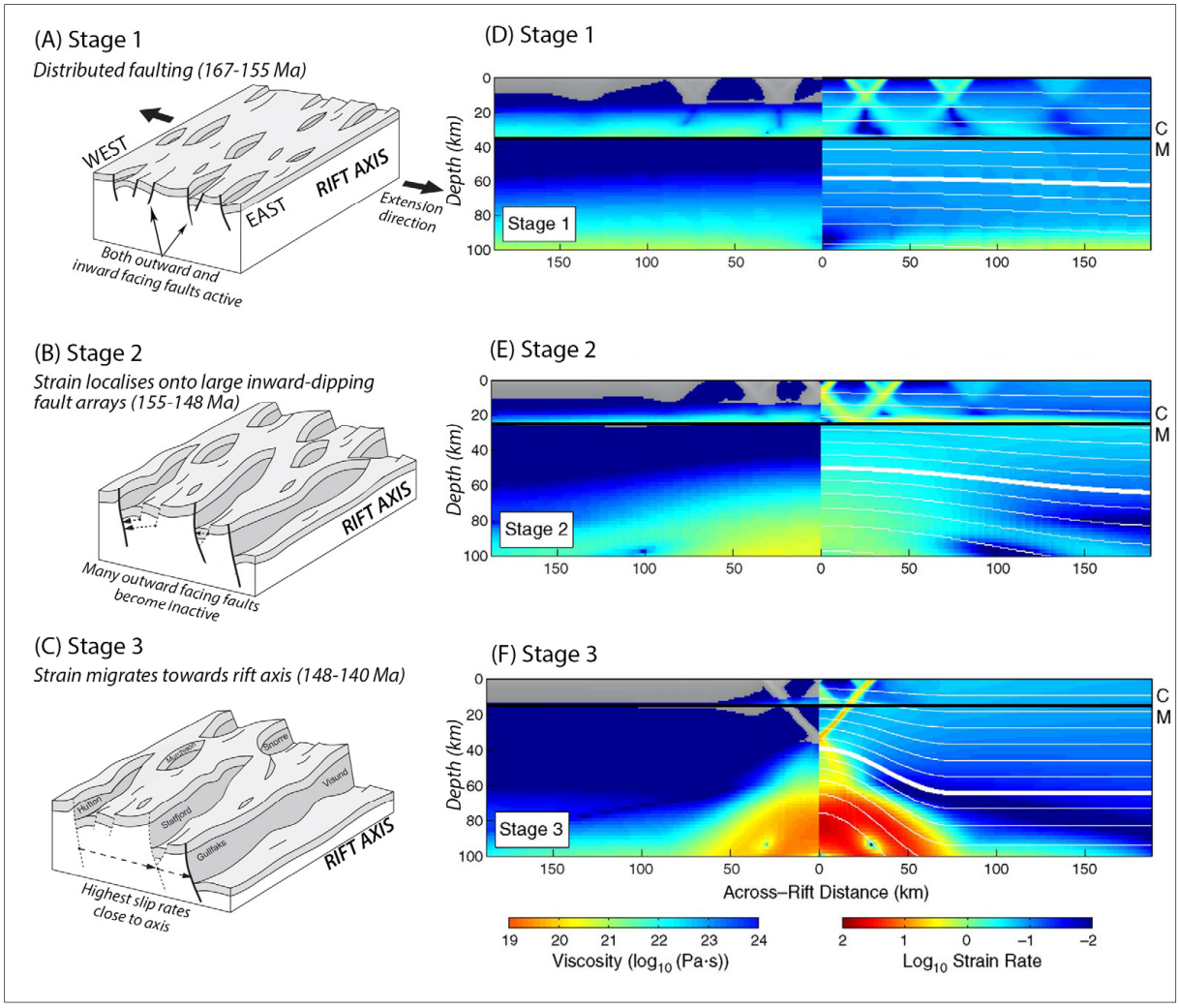

Figure 2-5: Diagram on the left (A, B and C) illustrates temporal the migration of fault activity towards the rift axis, (A) being at rift initiation, (B) middle part of the rifting and (C) illustrates the later part of rifting when the fault activity moves further towards the rift axis and the displacement increases in the faults closest to the rift axis. D, E and F illustrates the simulation Cowie et al. (2005) made (based on the model from (Behn et al., 2004), which illustrates the increase towards the rift axis, in the temperature gradient, viscosity and Strain Rate from stage 1 to 3. Figure modified from Cowie et al. (2005).

2.1.2 Synrift sedimentology and stratigraphy for rift basins

The sedimentary deposition and distribution in rifts is very complex due to the asymmetry of half grabens and the constant change in topography and morphology as the extension widens (Ravnås and Steel, 1998; Gawthorpe and Leeder, 2000). The two most unique aspects of marine rift systems are, the very steep slope of the basin floor that is steepening due to ongoing rotation of the fault blocks (Figure 2-6), and the variations in sediment supply and distribution, that changes throughout the rifting phases (Ravnås and Steel, 1998). The major controls for this complex sedimentary architecture are, fault growth and linkage,

drainage and drainage catchments and climate (sea/lake level changes) (Gawthorpe and Leeder, 2000).

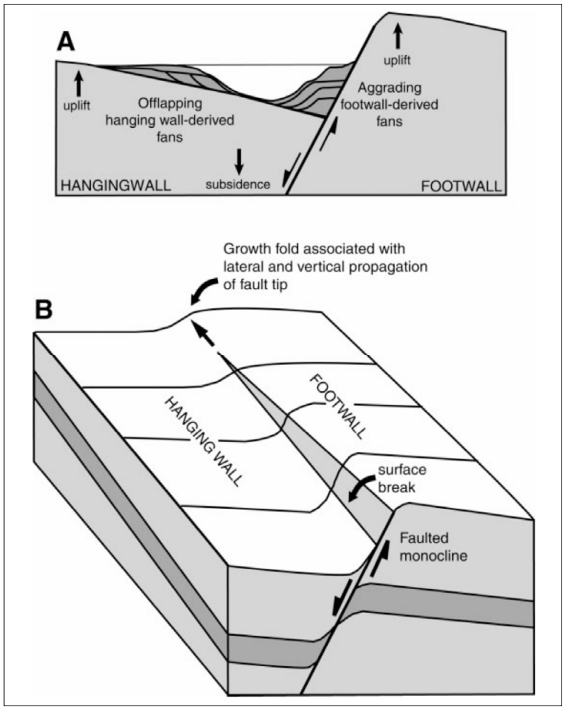

Figure 2-6: Diagram showing the asymmetry in a half graben and the sedimentary deposition in response to the hangingwall and footwall slopes. Modified from Sharp et al. (2000b).

Fault growth impact on drainage and sedimentary response

Fault growth and linkage determines the geometry of the basin and is a major control on the evolution of drainage systems, size of catchment areas and the creation of accommodation space in the rift, and is thereby controlling the sediment distribution and deposition in the hangingwall depocentres (Cowie et al., 2006). Figure 2-7A shows the surface response to the initial fault growth when subsidence rate is low and low gradient rivers run in between fault segments, depositing relative mature, coarse sediment in the shallow depocentres, developed adjacent to small displacement faults (Cowie et al., 2006). Figure 2-7B depicts the surface response to the linkage of faults and the increase of subsidence rate at this point. The sediment yield is highest at the largest displacement in the fault, here the transport is short and the slope is very steep, this results in more angular, less sorted and maybe coarser sediments, derived from the fault scarp. Sediment yield decreases along-strike the fault towards the fault tip, due to lower gradient and longer transport, even if the catchment area increases, resulting in more mature sediment that are very similar to fluvial sediments from early rift initiation (Cowie et al., 2006).

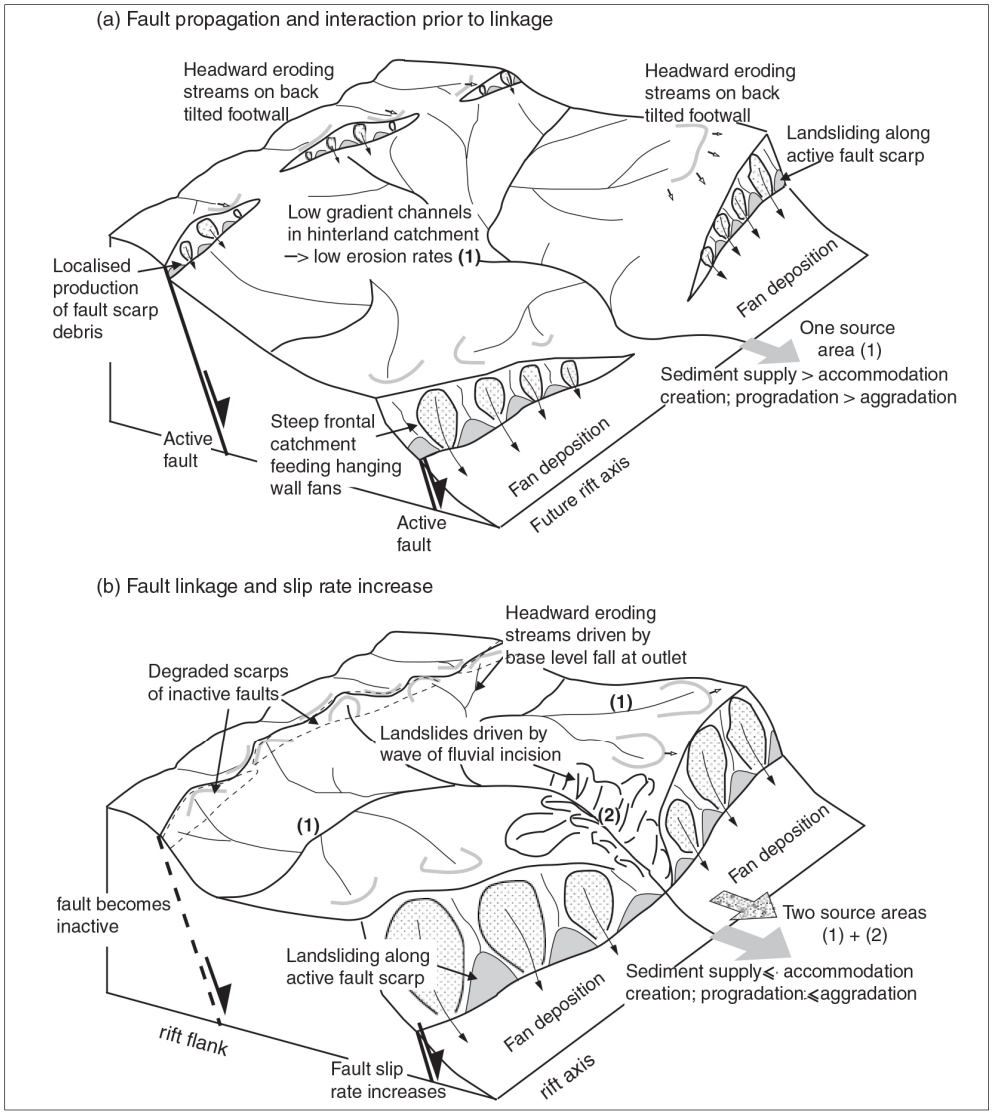

Figure 2-7: Schematic diagram showing the surface response from the initial fault growth and the linkage of faults. Modified from (Cowie et al., 2006).

There are two distinct tectono-stratigraphic styles in a basin, the first is the sedimentary response to the growth of a blind fault causing folding of the sediments above, where strata becomes thinner towards the monocline and rotates and thickens away from the monocline (fault zone). The second is after the fault has breached the surface, where the stratigraphy changes and the strata now thickens and diverges towards the fault scarp (Figure 2-8) (Gawthorpe and Leeder, 2000). In a rift containing multiple fault blocks the basins are filled in a fill-spill manor, if the first basin is filled up sediments spill over into the second basin and so on, this is why the basins further away from the hinterland (sediment source) often only depend on sediments from the fault block itself.

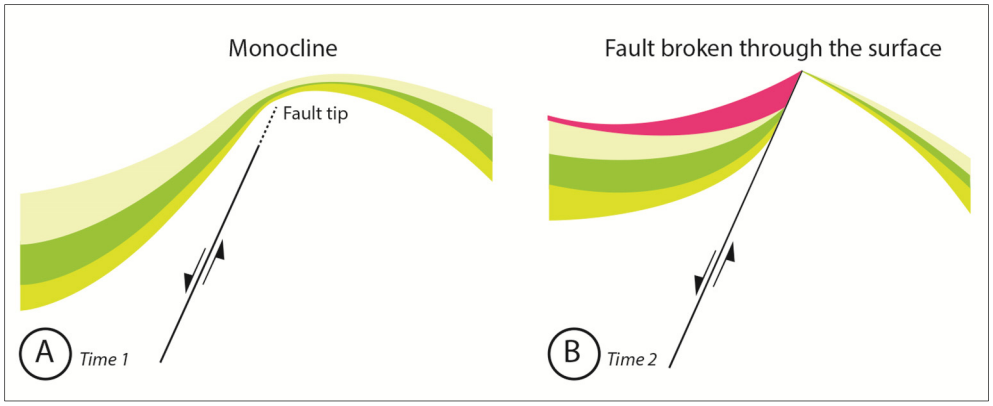

Figure 2-8: (A) Monocline forming above a blind fault. (B) Depicts the sediments forming a wedge towards the fault scarp after the fault has broken through the surface.

Drainage and drainage catchments

The size of the drainage catchments area is controlled by Hack´s power law ($L=1.4A^{-0,6}$) that represents the empirical relationship between the length (L) of the longest stream within the catchment area and the catchment area itself (A) (Rigon et al., 1996; Ravnås and Steel, 1998; Gawthorpe and Leeder, 2000). Drainage systems and the overall subsidence control the amount of water discharge and sediment supply and thereby also the size of the alluvial fans, fan deltas and the submarine fans (Gawthorpe and Leeder, 2000). The drainage systems are transverse or parallel to the rift axis (axial), antecedent or consequent. Usually the hangingwall has the larger sediment yield potential, since they tend to have a larger catchment area then the footwall (Ravnås and Steel, 1998) they also produce larger fans because of the gentle slope. In the rift axis where the steep footwall slope meets the shallower hangingwall slope, the sediment deposition consists of talus cones, alluvial fans, fan deltas and submarine fans (Figure 2-10) (Gawthorpe and Leeder, 2000). A steep slope gives a fast response time for drainage systems to create. The sediment successions in the footwall fault scarp reflect the subsidence meanwhile the hangingwall successions reflect both the changes in hangingwall and the adjacent footwall conditions. Secondary structures, transfer zones and segmentation of the footwall could all tribute to the movement of the drainage divide (Ravnås and Steel, 1998).

Climate / sea level change

Climate has a major impact on the sediment supply and drainage development, due to seasonal variations in temperature, wind and rainfall (Ravnås and Steel, 1998) affecting the

vegetation biomass and water balance (Gawthorpe and Leeder, 2000). This controls the balance between the axial and transverse rivers and the water discharge, if they are balanced, the axial rivers will aggrade and can cause avulsion around growing transverse fans, but if the water discharge increases and sediment supply decreases the axial rivers will degrade, causing incision, forming of soil and the growth of terraces (Gawthorpe and Leeder, 2000). The erodibility of the prerift lithology is also a factor regarding the amount of sediment supply (Ravnås and Steel, 1998).

Basins types and main depositional lithologies:

Rift basins can be characterized into 4 types based on the sediment supply and the pre-rotational sea-level compare to the fulcrum. Sediment-overfilled, these are typically closest to the hinterland and the sediment supply outruns the accommodation space created and the fulcrum lies below the pre-rotational sea-level and these contain coarser material, and after they are filled the excess sediments are transferred to the next basin. The sediment-balanced basins, also close to the hinterland, manage to keep the sediment supply rate and the accommodation rate just about equal. In these above mentions basin types a three-fold lithology (Sandstone-claystone-sandstone), representing the initial, early, climax and late rifting phases, forms (Figure 2-9B). Sediment-underfilled and sediment starved basins don't fill up because the accommodation rate outruns the sediment supply rate, these are either partly emerged or completely submerged basins and a two-fold lithology (Figure 2-9A) forms (conglomerate-sandstone-claystone), the lack of a coarse cap is due to the low sediment supply at late rifting stages (Ravnås and Steel, 1998).

The early synrift, rift climax and late synrift signatures are represented in both three-fold and the two fold stratigraphy (Figure 2-9) seen in rifts. The lowermost coarse materiel represents the initial and early rift stage, the mud represents the rift climax stage and the coarse sandy material on top in the three-fold lithology represent the late synrift stage, when the sediment supply increases and the block rotation decrease, causing new drainage system to develop. This top coarse sandy layer is absent in the two-fold lithology either because of severe extension or a limitation in sediment supply, these are either sediment-underfilled or sediment-starved basins.

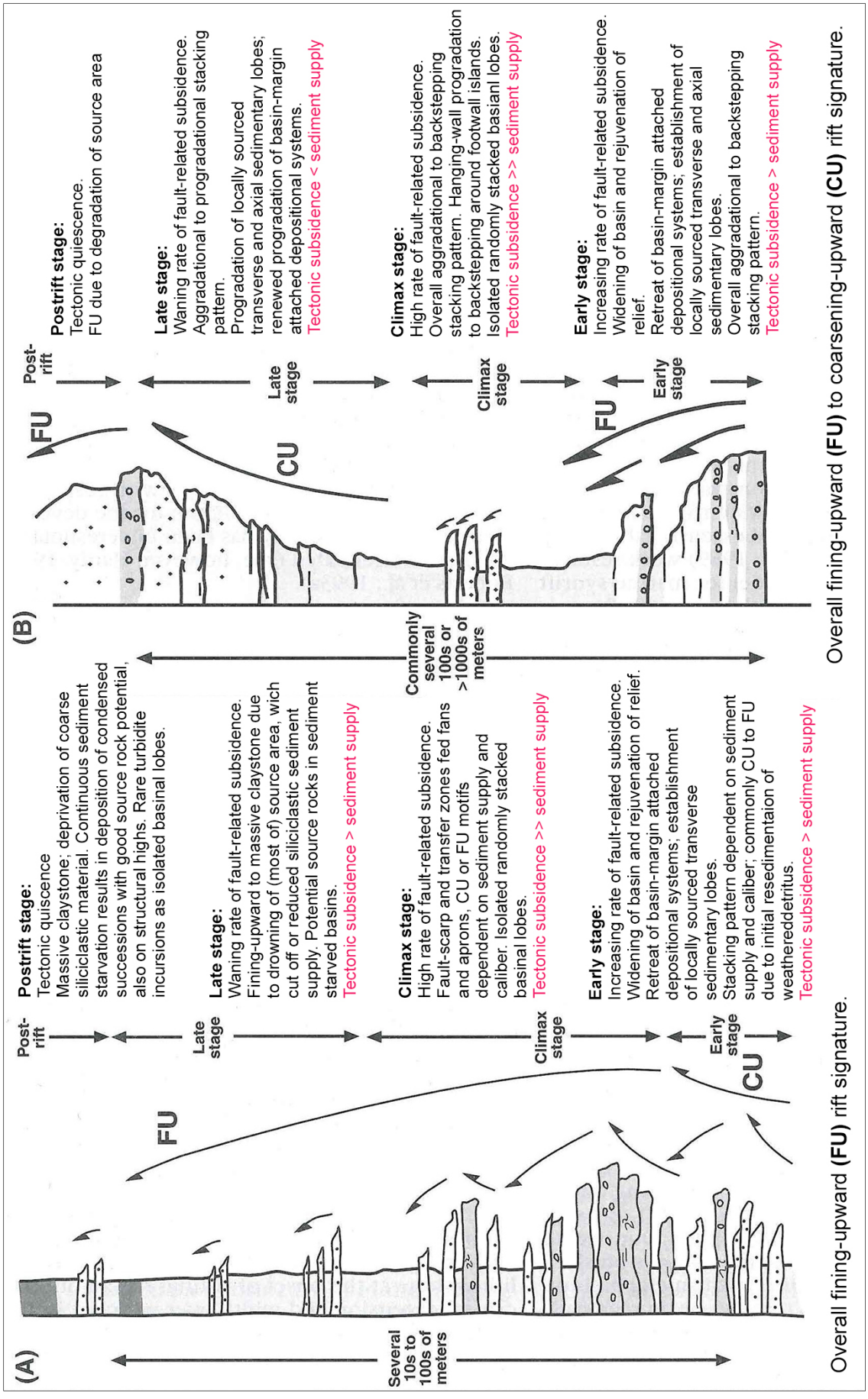

Figure 2-9: (A) Twofold and (B) tree-fold stratigraphy in rift systems. Modified from Ravnås and Steel (1998).

The geometry, evolution of drainage catchments and the resulting sediment deposition are summarized in Figure 2-10, which depicts the changing environment throughout the rifting. Figure 2-10A is the initial rifting phase, at this point many small isolated faults form with adjacent shallow depocentres that have different sediment infill architecture depending on their location compared to sea-level. The increasing on-going displacement causes an overall deepening trend in the stratigraphy and as the faults grow the stratigraphy onlaps laterally. If the fault has broken through the surface a wedge is formed towards the fault scarp, but if the fault is blind the stratigraphy thins towards above the blind fault. Since the topography at this point is relative low the drainage is diverted around the fault tips, causing large alluvial fans to develop at relay zones areas and syncline form where the axial sediment input is large. Figure 2-10B illustrates fault interaction and linkage of fault forming larger faults with deeper depocentres. Transverse drainage developed on both hangingwall and footwall, supplying sediment to the deltas. Large deltas develop at the fault segment linkage as a result from the antecedent drainage on the rift shoulder closer to the hinterland. In the basin furthest away (left side in Figure 2-10) footwall islands develop with adjacent sediment-starved basins, due limited intrabasinal sediment supply. Turbidites develop along-strike in the fault, due to the tilting of basin floor and are interfingering transverse building fans and deltas. Figure 2-10C depicts a sea-level fall, at shallow places where the subsidence rate is low, the facies shift basinward and offlap and incision occurs. In the footwall fan deltas where the subsidence rate typically is higher than sea-level fall, the deposits aggrade or prograde. At this point terraces, incised valley and forced regression are formed. Figure 2-10D depicts the deep water basin, at this point the major master faults have formed causing high displacement rates and sediments bypass the footwall and are deposited into the deeper basins, causing slope failure and slumps, chutes scars and debris flows to develop in the fault scarp. The footwalls uplift causes reverse drainage, meaning it changes direction down the hangingwall instead. As the fault scarp degrades major slides occur and basinal megabreccias are deposited. The turbidites generated adjacent to the footwall are vertically stacked due to tilting of basin floor (Leeder and Gawthorpe, 1987).

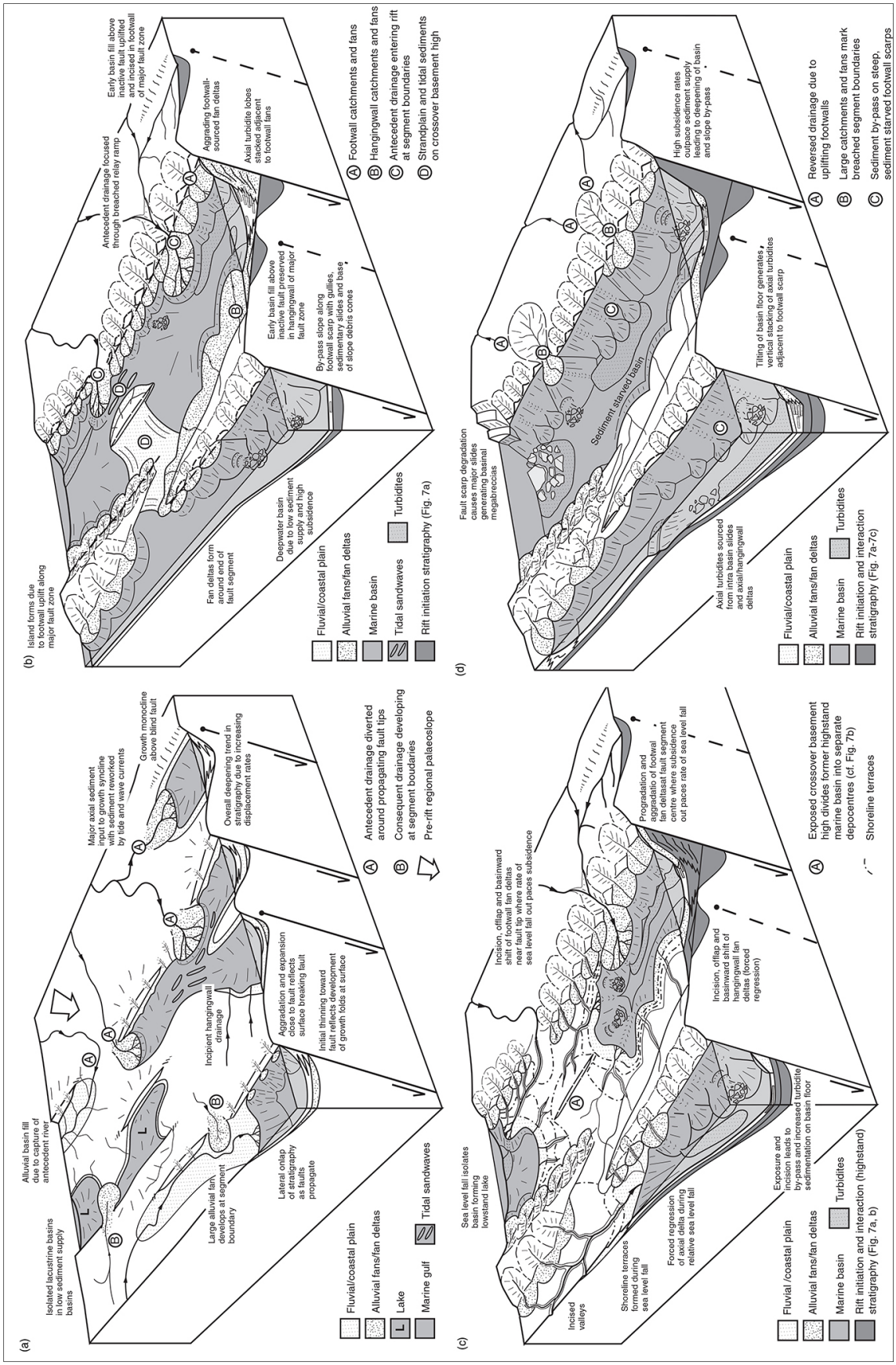

Figure 2-10: A schematic overview of basin evolution, drainage catchments, sedimentary deposition throughout the rift stages. Figure modified from Gawthorpe and Leeder (2000).

2.2 Structural styles and synrift sedimentology for Gulf of Suez Rift

The Study area is located on the eastern side of the Gulf of Suez in Egypt and consists of the NE-dipping El Qaa fault block (Figure 2-11).

2.2.1 Structural styles for the Gulf of Suez

The Gulf of Suez rift is an abandoned rift-arm that extends NW from the Red Sea (Figure 2-11) and developed in the Oligocene-Miocene time, caused by the separation of the Arabian plate moving away from the African plate. The rifting rotates around a pole in the north, as the Arabian plate rotated counter clockwise away from the African plate, causing a scissor-like extension that decreases northward.

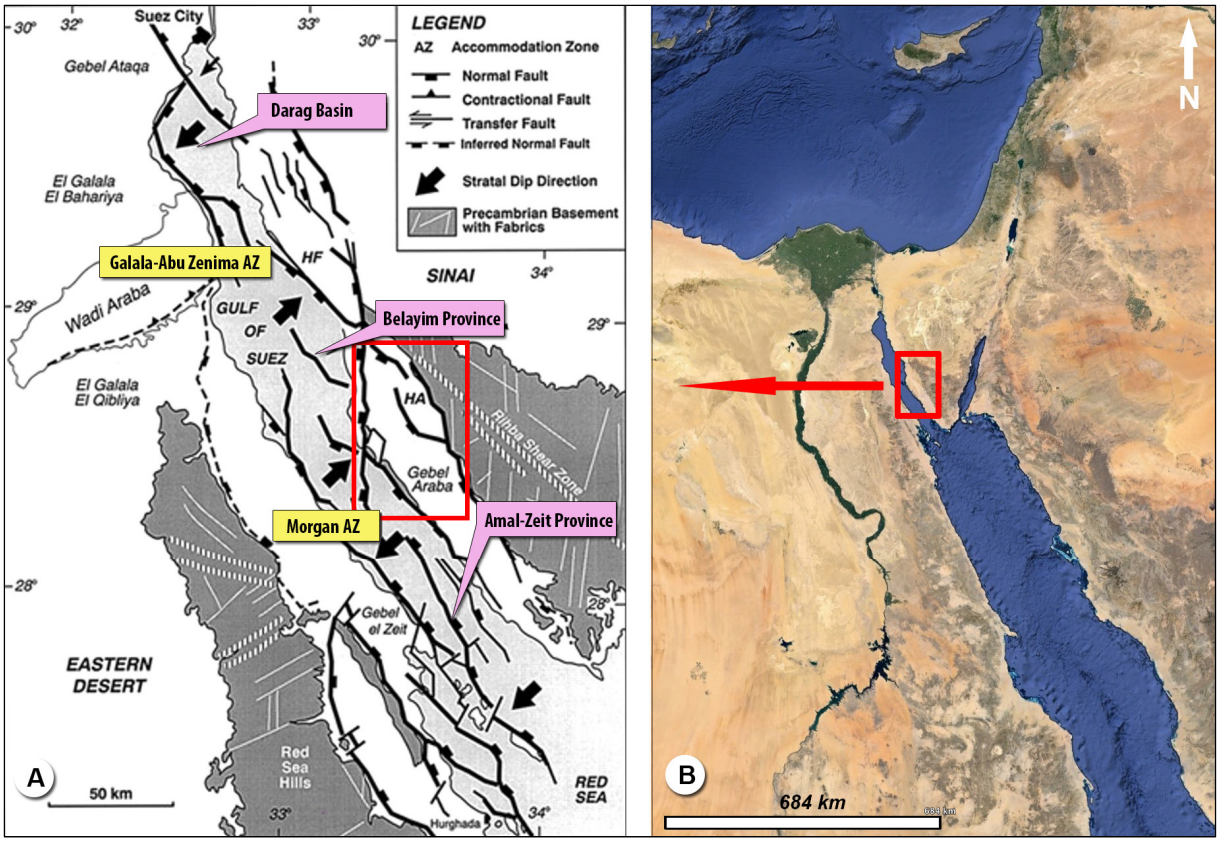

Figure 2-11: (A) Map of the Suez Rift area. Modified from Younes et al. (2002). (B) Location of the map (Map retrieved from Google Earth 28.05.2015).

The Gulf of Suez rift is up to 300 km long and up to 80 km wide (80 km in the south-end and 50 km in the north-end). The dominated margin-bounding normal faults in the Gulf of Suez strike (NW-NNW) and are linked by smaller oblique faults trending (NNW, E-W and N-S), this has resulted in the characteristic zig-zag pattern along the borders of the Suez Rift and in the centre (Patton et al., 1994; Sharp et al., 2000a). The Gulf of Suez rift can be divided into 3

large asymmetric dip-provinces (main half grabens), the Darag Basin in the north, the Belayim Province in the centre, and the Amal-Zeit Province in the south (Figure 2-11). These half grabens are bounded by large normal faults that strike parallel to the Gulf and have 4-6 km large throws, and are dipping towards the east in the north and south province and towards the west in the centre Belayim Province. Within these grabens are second order half grabens/sub-basins consisting of smaller faults (Sharp et al., 2000a; Bosworth and Mcclay, 2001). Two large, up to 20 km wide, complex accommodation zones (AZ) are separating the basins, the northern Galala-Abu Zenima AZ and the southern Morgan AZ (Figure 2-11). The fault systems in the accommodation zones are trending oblique to the rift fault direction (Bosworth and Mcclay, 2001).

The study area comprises the El Qaa fault block (half graben) which is 25 km wide and 40 km long and is dipping (10-20°) towards the NE, bounded by large displacement (2-5 km) normal faults, that strike NW to NNW and dip down to the west (Figure 2-12). The western margin boundary, the Coastal Fault Belt (**CFB**) consists of the Nezzazat fault that has up to 5 km displacement, dip down to the west at an angle of ~65° (Sharp et al., 2000b; Whipp, 2011), and contains the fault segments from north to south, the Nezzazat fault (NNF), Ekma fault (EF), Durba fault (DF) and the Araba fault (AF). The individual sub-fault blocks on the western side, from south to north, are Gebel Araba, Gebel Abu Durba, Gebel Ekma and the Gebel Nezzazat (McClay and Khalil, 1998). On the eastern side, the block is bounded by the sinuous Eastern Boundary Fault Belt (**EBFB**), which contains the Baba-Sidri Fault, the Hadahid Fault, Gebah fault and the Sinai Massif fault. The overlap zone between the Hadahid fault/monocline, Gebah fault and the Baba-Sidri fault is the Feiran Transfer zone, this zone overlaps by about 12 km and is 3-5 km wide (Sharp et al., 2000b; Whipp, 2011). The northern Baba-Sidri fault contains 2 fault segments, which are from the north, the Baba-fault, the Sidri fault and the Alaqa fault. The large displacement (ca. 4 km) Sinai Massif fault is the southernmost fault in the study area it transfers throw by splaying off into two new faults, the Hadahid (2,5 km throw) fault and the Gebah fault (1,5 km throw) (Moustafa and El-Raey, 1993; Whipp, 2011). The Gebah fault consists of 4 fault-segments, which are from south to north, the Gebel El Turr (GTF), Mukattab-Feiran (MFF), East Sidri (ESF) and North Sidri faults (NSF) (Gupta et al., 1999) (Figure 2-12). The Hadahid fault is made up of 8

segments dipping towards the west, the displacement in these segments varies but there is an overall decrease in displacement from south to north (Whipp, 2011).

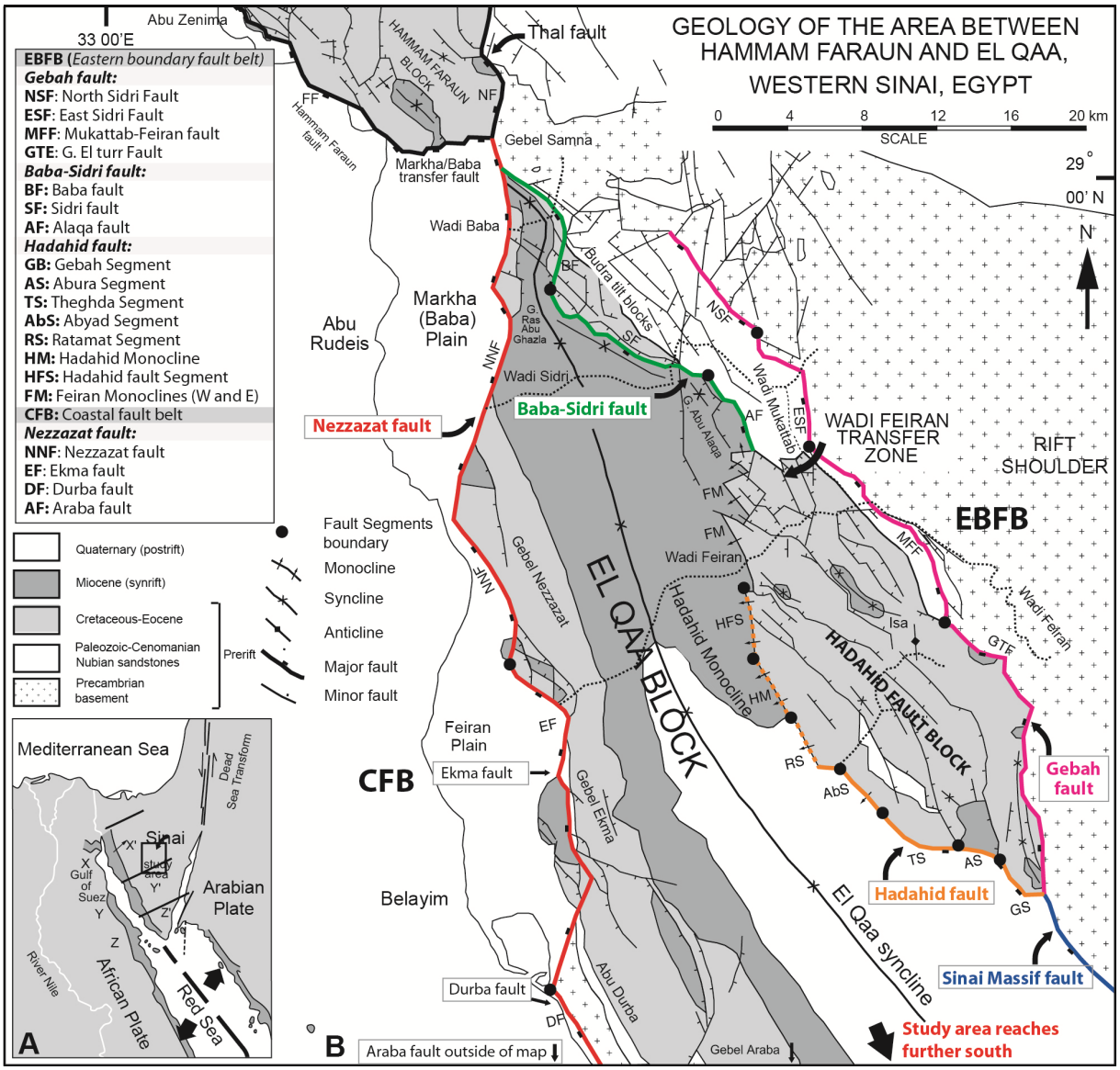

Figure 2-12: (A) Location of the study Area, El Qaa fault block. (B) Map modified from Sharp et al. (2000b). Including faults segments names and their boundaries.

One of the most important controls on the fault orientations in the Gulf of Suez, is the reactivation of the older fabric, such as faults, joints, dikes and shear zones, that are present in the Basement rocks and have a dominant NW-trending (Bosworth and Mcclay, 2001). Patton et al. (1994) divided the Gulf of Suez into 4 major fault-orientation trends, The Clysmis trend, N-Oblique trend, NW-oblique trend and the Cross-trend. The Clysmic trend NW-NNW (310-340° azimuth) is the most abundant fault-trend and these faults can be

found throughout all of the Gulf of Suez and seem to have been active since the rifting started. The N-oblique trend (350-10° azimuth), oblique to the Clysmic trend, is the second most abundant fault-trend in the Gulf of Suez and the faults are found mostly at the "termination of major rift blocks" (Patton et al., 1994). The third is the NW-oblique trend (280-310° azimuth), these fault can be found between Dara ridge and the Gebel Esh El Mellaha, and in the Wadi Baba area and are only weakly following old basement fabrics. The least frequent fault-trend is the Cross-trend NEE (50-75° azimuth), mostly found at the south-western end, in the Dara ridge, Gebel Zeit, and the Gebel Esh El Mellaha area and run parallel to the most obvious of the pre-existing basement fabrics. The cross-trend faults have less throw relative to the above mentioned trends (Patton et al., 1994). Figure 2-13 is a diagram describing the abundance of faults in the 4 trends.

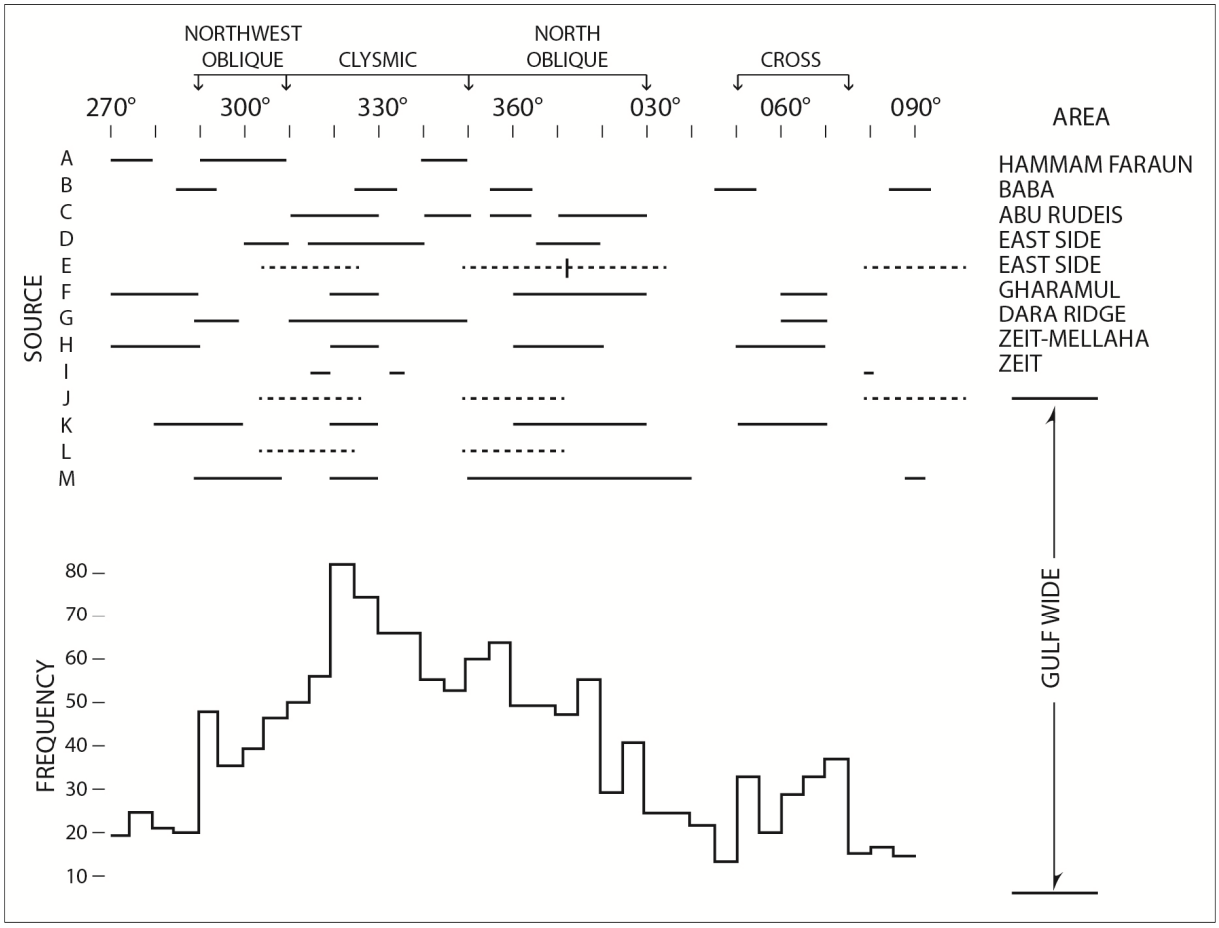

Figure 2-13: Diagram summarizing the abundance of the four major fault trends suggested by Patton et al., 1994. Diagram modified from Patton et al. (1994).

2.2.2 Synrift sedimentology and stratigraphy for the Gulf of Suez

The stratigraphy used in this chapter is based on the Hamman Faraun – El Qaa region in the Suez Rift (Figure 2-14) and has been divided into: Basement, Megasequence 1, Megasequence 2 and Megasequence 3 (Sharp et al., 2000b).

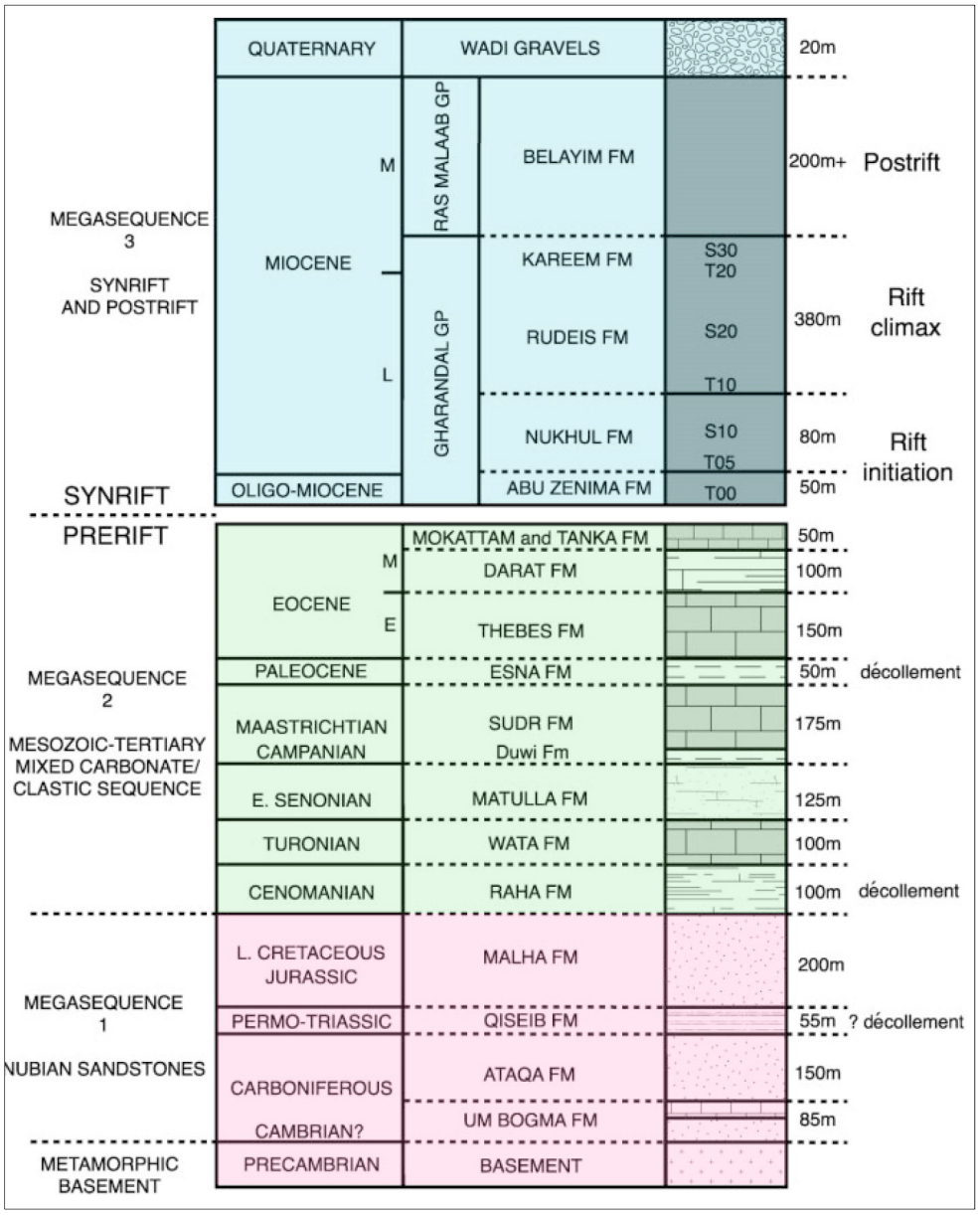

Figure 2-14: Stratigraphic section of the Hamman Faraun-El Qaa region. Modified from Sharp et al., (2000a).

Basement:

The basement is composed of Precambrian gneisses, volcanic rocks and meta-sediments, that where deformed and metamorphosed during the Pan-African orogeny (1000-550 Ma).

The basement was peneplained creating a planar unconformity that separates the basement bedrock from the overlaying sedimentary rocks (Sharp et al., 2000b).

Megasequence 1: Nubian sandstones

This sequence is composed of non-marine sediments that were deposited between the Cambrian to Early Cretaceous and consists mostly of sandstone. The formations are, starting from the oldest, the Um Bogma Formation, the base is a sandstone unit and the top is a limestone-dolomite unit, then the Ataqa Formation (sandstone), the Permo-Triassic Qiseib Formation, a variable colour siltstone and the Malha Formation (white kaolinitic sandstone) (Moustafa, 1993).

Megasequence 2: Mesozoic-tertiary mixed carbonate/clastic sequence

This sequence is composed of marine sediments with different facies that were deposited between the Late Cretaceous to Eocene, and consists of sandstone, siltstone, claystone, shale, marl limestone and dolomite. The lower part is represented by the mixed facies of the late Cretaceous Raha, Wata, and Matulla Formations (Moustafa, 1993). The upper part is composed by the late Cretaceous to the Eocene carbonate units Sudr Formation (chalk), Esna Formation (shale), Thebes Formation (limestone), Darat Formation (marl-limestone), Mokattam Formation (nummulitic limestone) and Tanka Formation (chalky limestone) (Moustafa, 1993).

Megasequence 3: Synrift and postrift

Is divided into 2 groups: Gharandal group (clastic sediments) and Ras Malaab Group (evaporite sediments) (Sharp et al., 2000b).

The Gharandal group comprises the rift initiation and the rift climax stages:

Rift initiation: The formations are Abu Zenima Formation, non-marine sediments red beds that are made of red and white sandstone and the Nukhul Formation, tidal to marginal marine sediments.

Rift climax: Rudeis Formation, open marine sediments. Lower Rudeis consists mainly of fine-grained marl and minor sandstone. The upper Rudeis, consists of glauconitic and

fossiliferous coarse sandstone successions (Bosworth and Mcclay, 2001). Kareem Formation, shelly calcarenites, patch-reef limestones and polymictic conglomerates.

The Ras Malaab group contains evaporite sediments:

Postrift: The postrift sediments are represented by the Belayim Formation, mainly composed of halite. Most of the postrift sediments are Quaternary such as unconsolidated coarse clastics and several gravel terraces (Moustafa, 1993).

The development of the Suez Rift with time

The evolution of the Suez Rift can be divided into three different phases (Figure 2-15), 1. Rift initiation, 2. Rift climax and 3. Postrift stage.

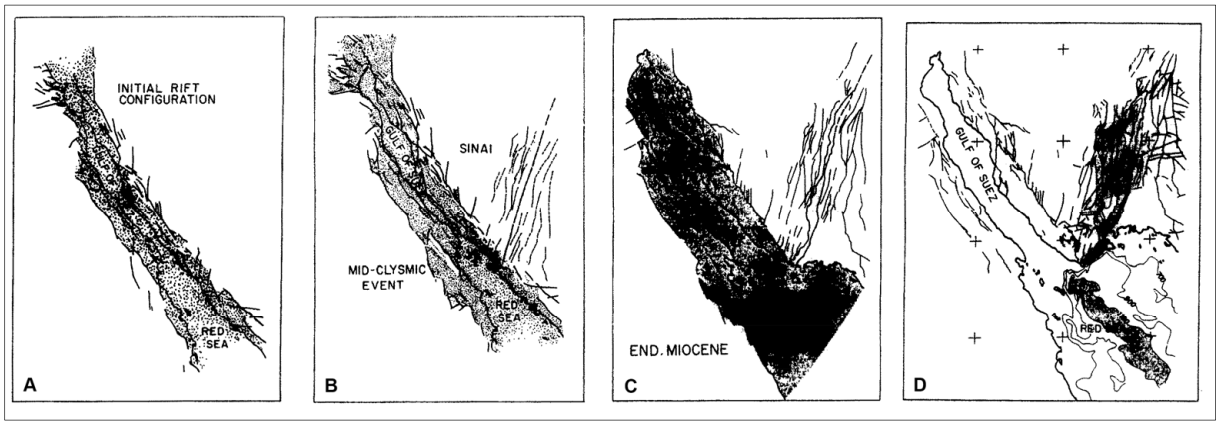

Figure 2-15: Different stages throughout the Suez Rift evolution. Modified from Steckler et al. (1988).

1. Rift Initiation stage:

The initial rifting stage took place at the late Oligocene associated with locally preserved Abu Zenima Formation (24-21,5 Ma) fluvial red beds that passes transitionally into the shallow marine Nukhul Formation (21,5-19,7 Ma). The subsidence rate was very slow at this stage (Bosworth et al., 2001). In this phase there is also evidence for igneous activity, since the Abu Zenima Formation, is capped by a basaltic flow (Patton et al., 1994). There was little uplift associated with the initial rifting, from tens to hundreds of meters (Patton et al., 1994). In this early stage of the rifting, the fault developed the characteristic “domino-style tilted (rotational) fault blocks” (Bosworth et al., 2001). In the hangingwall of these faults the

Nukhul Formation was deposited and at the end of this period the Nukhul Formation carbonates sealed of many of the faults that had been active before (Bosworth et al., 2001).

2. Rift-climax stage

The Suez Rift was most active during the Burdigalian (19-16 Ma). The deposition of the deeper water Rudeis Formation over the shallower Nukhul Formation is interpreted to reflect an increase in the subsidence and extensional rates. At this stage there are many key-erosional boundaries that represent major changes in stratigraphic facies, indicating sudden changes in the depositional environment, accommodation space and the source of sediments. A major event of structural reorganization called “Clysmic-event” happened in Mid-Rudeis times causing a reorganization of the fault blocks in the rift and new faults to develop (Moustafa and El-Raey, 1993). The Globigerina marls are below this unconformity and above are the limestone-conglomerate. Many faults died out after the “Clysmic-event”(Patton et al., 1994). The geometry changed to larger structures, that dominated the rest of the rifting, until the faults eventually died out or the displacement decreased significantly (Patton et al., 1994).

3. Postrift phase:

Approximately in the Middle Miocene the Dead Sea transform fault was activated and the extension in the Suez Rift almost came to an end. The Suez Rift was also at this time blocked totally or partly from the Mediterranean Sea, which led to extensive evaporate deposition (Patton et al., 1994; Bosworth and Mcclay, 2001). At this time the subsidence rate was much less and the rifting came to an end. The Suez Rift is still active but mostly due to thermal subsidence, the mantle is slowly cooling and as a result it gets thicker, heavier and subsides (Steckler et al., 1988).

3 DATA AND METHODS

This chapter describes the workflow behind the analysis made in this study. **Part 3.1** shortly explains what kind of data is used and where it was obtained from. **Part 3.2** is divided into two sections, section one explains how the data (lithology, faults and dip data) were mapped in the ArcGIS 10.1 Software and section two explains further work on the data using 2D/3D MOVE (Midland valley software), to produce cross-sections that where restored before a 3D model was constructed of the present day structural settings in the El Qaa fault block. The final **part 3.3** shortly explains the theory behind the different tools used in MOVE for this thesis, "Unfolding", "Move on fault" and "Decompaction". Se Figure 3-1 for a flowchart over the entire workprocess.

3.1 Data and software

The data used in this master thesis are mapped lithological units (polygons), traced faults (polylines) and dip data (points). The geological maps were generated using high resolution satellite images in Google Earth and ArcGIS 10.1 ("Add Base Map", will show the Google Maps in ArcGIS), a geospatial processing program, the Coordinate system was WGS_1984_UTM_Zone_36N. Geological maps made by Moustafa (2004), M. Muravchik and Whipp (2011) where used as a guide to map the lithological units, trace the faults and to insert dip data that was not digitally available. The Digital elevation models (DEM) used are ca. 30 m, 1 arc-second raster images, these where downloaded from NASA, EOSDIS webpage (NASA, 2014). The DEM dataset contains information on elevation (x, y and z values) in this case each square in the raster image represents a ca. 30x30m area, meaning that smaller topographic anomalies in areas smaller than 30 meters may not show up in topographic surfaces that are generated from these DEM's.

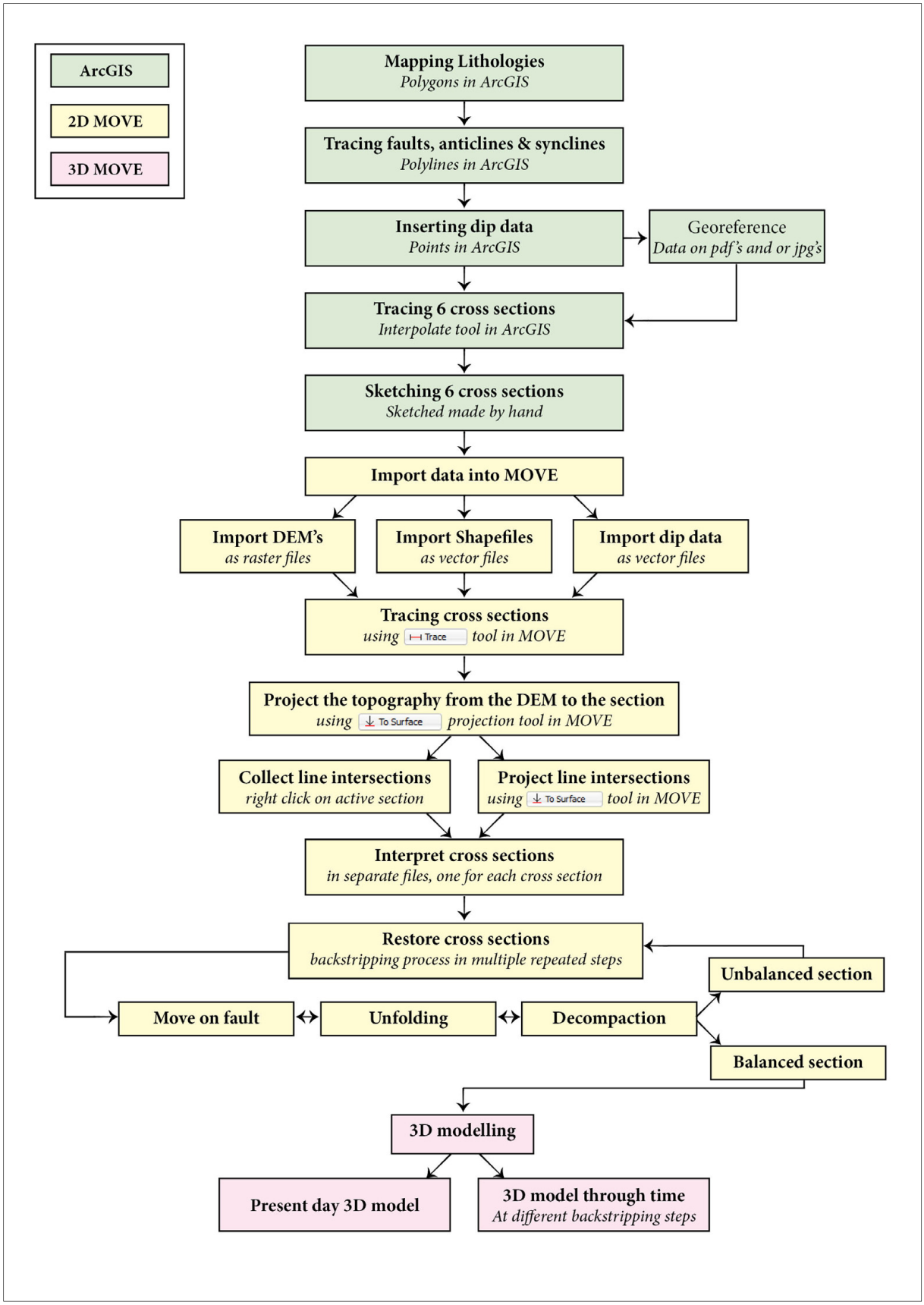

Figure 3-1: Flowchart of the work-process from start to finish, see Figure 3-15 for a more detailed flowchart of last part, the 3D modelling.

3.2 Methods

3.2.1 Google Earth and ArcGIS Map 10.1

Lithology:

Mapping of the study area was partly made in Google Earth and in ArcGIS Map. The 3D view in Google Earth was used in some areas to recognize lithological boundaries, that where not as clear in map view. The polygons mapped in Google Earth where not merged or clipped before imported into ArcGIS Map 10.1 after being converted to KML files (Figure 3-2). The lithological formations where mapped as polygons in different colours based on different formations. The polygons were made with the free-hand construction tool in ArcGIS Map 10.1 in order to contain as many (x, y) coordinates as needed for every polygon. The polygons share the same border, meaning there are no gaps between them and they do not overlap.

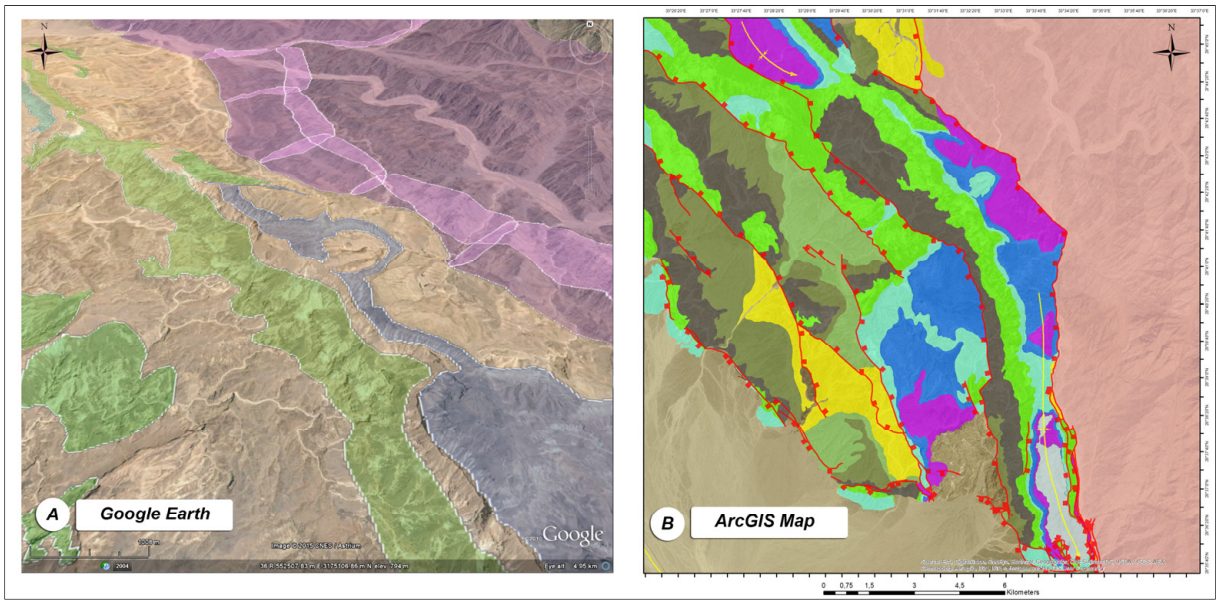

Figure 3-2: (A) mapping in Google Earth, the polygons overlap and are not merged until they are moved into ArcMAP. (B) After importing polygons into ArcGIS they are merged and clipped to represent the correct lithological boundaries.

In some places it was impossible to recognize the boundaries, either because quaternary deposits are on top or due to slides and slumps disturbing the boundaries, (Figure 3-3) then an estimation of the boundary had to be made. The Sudr chalk and Esna shale formations where merged, since the boundary between them was unclear and the Esna shale is relative thin.

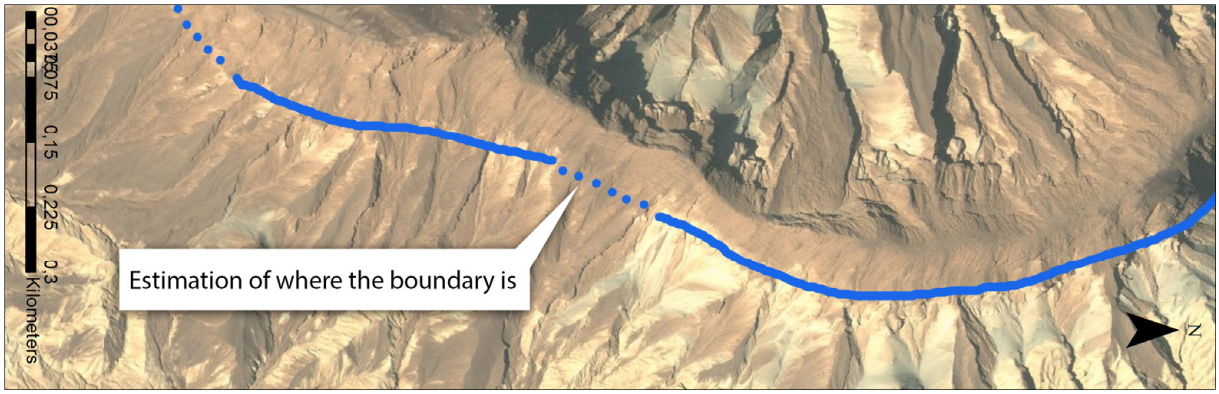

Figure 3-3: Lithological boundaries where not visible at all places and therefor an estimation had to be made.

Faults:

Faults and anticlines/synclines where traced as polylines and the dip direction is shown. Again the Moustafa (2004), M. Muravchik's and Whipp (2011) maps where used as guide for mapping the faults. The faults were used to clip the polygons at the borders to avoid overlap and to ensure that they followed the same path as the faults (Figure 3-4).

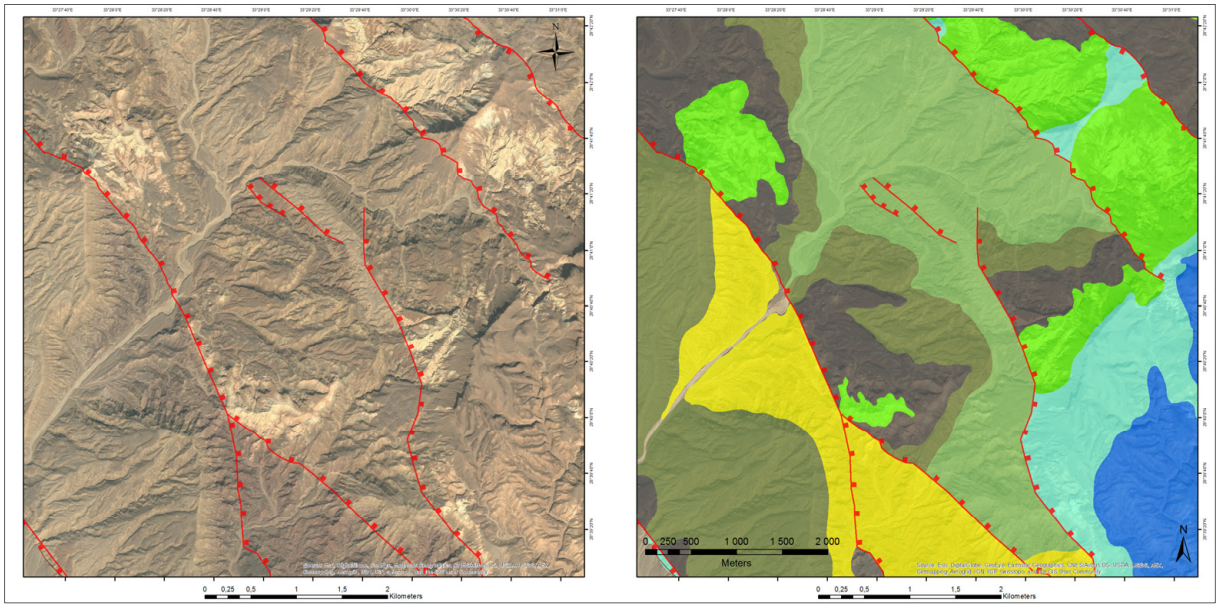

Figure 3-4: Tracing faults and clipping the polygons, to make sure that they share the same boundary.

Dip data:

Dip data was imported directly into ArcGIS from Excel file (From field work by M. Muravchik) and where the dip data only was available on previous maps made by Moustafa (2004) and Whipp (2011) were imported into ArcGIS as pdf´s or jpg´s and georeferenced to the correct location on the map, making it possible to estimate the strike, since only the dip angle is shown as a number on their maps (Figure 3-5).

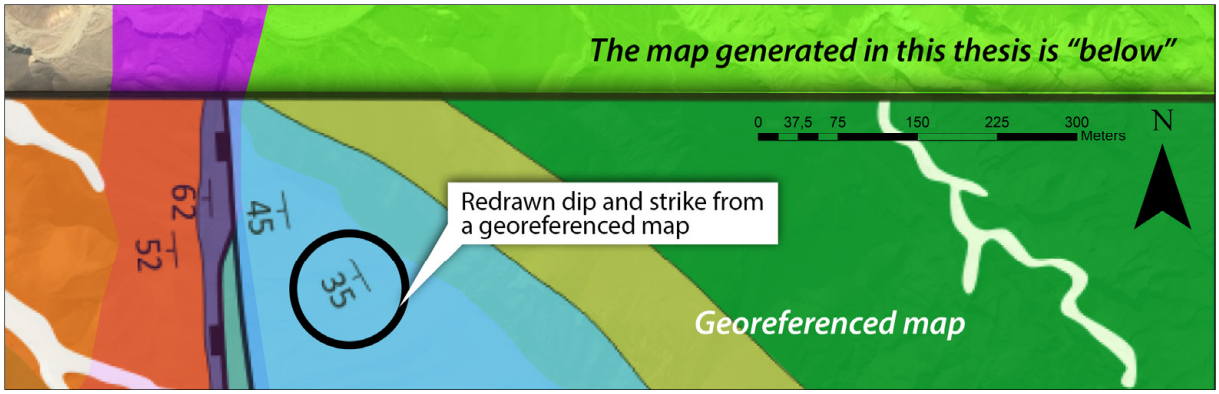

Figure 3-5: Dip/strike redrawn on the map to get the right dip/strike direction.

After mapping the lithological units, faults and dip data, the tool "Interpolate shape module" in ArcGIS Spatial Analyst was used to construct a 3D map of the area. The Interpolate shape modules uses all the data mapped in ArcGIS and by interpolating the z-values from the DEM raster image, a 3D map of the area was generated (Figure 3-6) showing the lithological units and the faults in the study area.

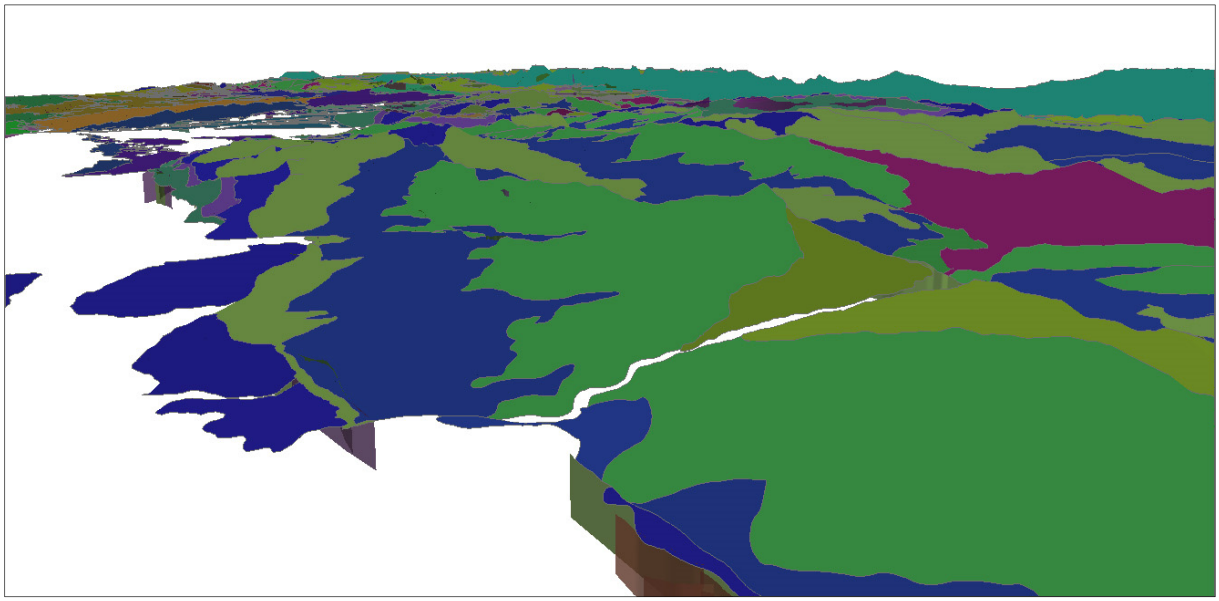

Figure 3-6: 3D map of the study area in ArcSCENE constructed by the "interpolate shape module" in 3D Analyst in ArcMAP.

In the 3D Analyst toolbox in ArcGIS, the tool "interpolate line" generates an elevation profile graph between 2 points (cross section) from the DEM, these where sketched by hand (Figure 3-7), to be used as a guide when moving the data into 2D/3D MOVE.

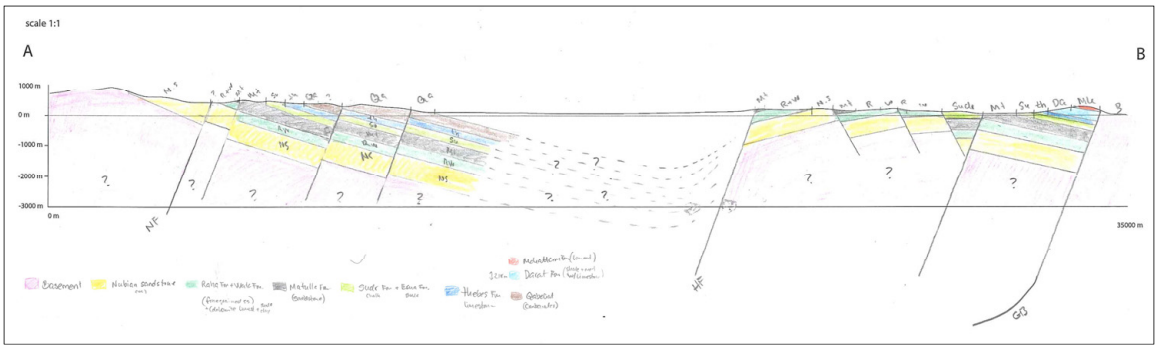

Figure 3-7: A cross-section sketched from ArcGIS interpolate line tool. Notice the cross-section is not to scale.

3.2.2 2D/3D MOVE Midland Valley

After all data was produced in ArcGIS it was imported into the software 2D/3D MOVE Midland Valley, which is a structural modelling and analysis toolkit program used for both 2D and 3D modelling, cross section construction and restoration. In this thesis the workflow in MOVE is divided into 4 categories which are explained in detail below:

1. Import of data (shapefiles and DEM´s)
2. Generating a stratigraphic column
3. Cross section construction/interpretation
4. Cross section restoration (backstripping)
5. 3D models construction for present day structural setting and for different times through the restoration

1. Import of data:

First the DEM file (N28W33) was imported into MOVE as GIS data – raster file, where the elevation data values are represented as a grid and the geographical parameter datum was set to WGS84, the projection type UTM zone 36N. The shapefiles for the mapped lithological units (polygons), faults (polylines) and dip data (points) generated in ArcGIS where imported as GIS data - vector files, using the correct colour table and horizon names, in addition to the same geographical and projection parameters as the DEM file. The dip data was projected onto the DEM surface as red circles representing dip/strike (Figure 3-8).

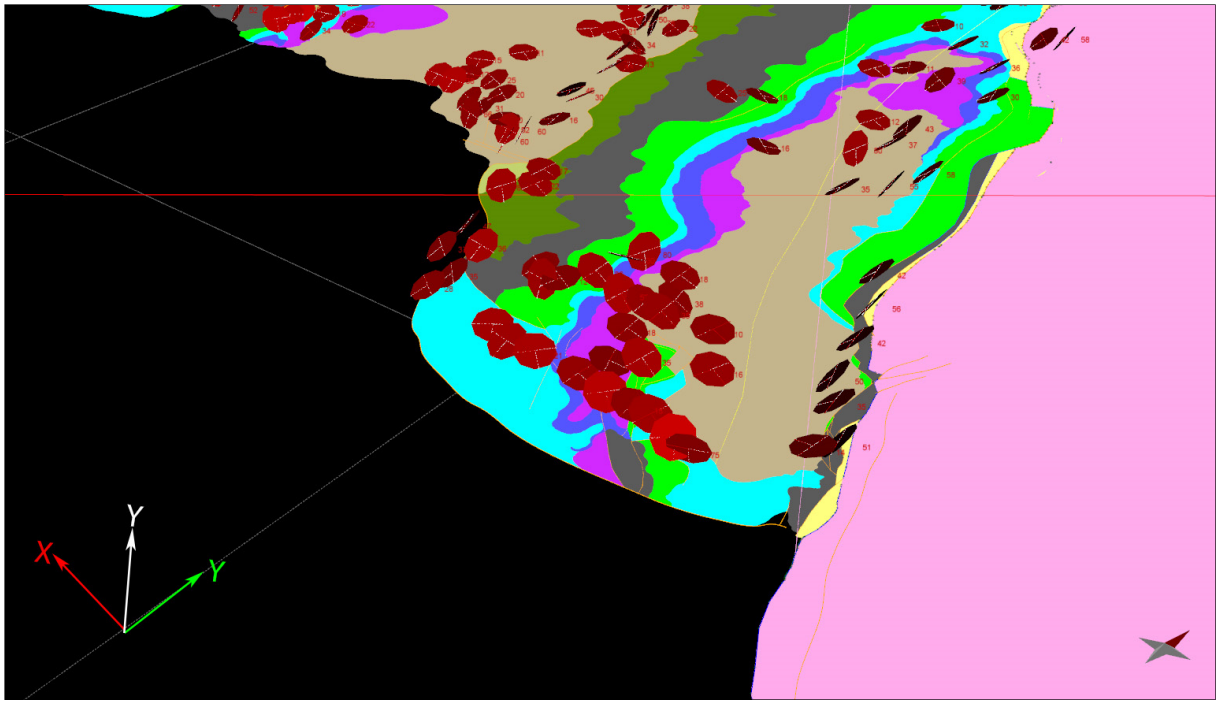

Figure 3-8: Dip/strike represented by red circle plates, projected onto the surface showing dip and strike in the 3D model.

2. Stratigraphic column:

Building the stratigraphic column in MOVE had its limitations due to the complex stratigraphy in the study area. The software stratigraphic column tool in MOVE assumes a layer-cake stratigraphy, but in our case the stratigraphy is complex, due to lateral changes in facies and different lithological formations deposited simultaneously. The stratigraphic column had to be simplified for use in MOVE and when necessary the thicknesses where modified for each section (Figure 3-9). Information on lithology name, colour, rock type, age and thickness is filled into the database created in 2D/3D MOVE under the Data and analyse tool "Stratigraphy". The stratigraphic column is used as a quick way to build the stratigraphy, which is done by drawing one horizon by hand, selecting it, and using the tool “Horizons from template”, where the bed thicknesses can be changed and certain horizons not present in the area can be disabled if necessary, which was used in our case for stratigraphic units deposited simultaneously but not at the same location, such as a lateral change in facies. The order of the stratigraphic units is set by their age, the oldest at the bottom. It does not have to be the exact geological age, just number the stratigraphic units so the oldest has the highest number and will be placed at the bottom and the youngest the lowest number and is placed at the top.

File Edit Table

Stratigraphy | Rock Properties

	1:Horizon	2:Colour	3:Rock Type	4:Age	5:Thickness
1	Conglomerates (Young)		Default	8.0000	100.0
2	Sandstone2		Default	9.0000	100.0
3	Evaporites2		Default	10.0000	100.0
4	DLC3		Default	11.6000	200.0
5	Evaporites+L.mudstone together with DLC2 (Karee...		Default	13.6500	190.0
6	ASL (sandstone) on both sides of syncline		Default	17.0000	80.0
7	Delta Lobe Complex 1 (Abu Alaqa Gr.)		Default	22.0000	150.0
8	Lower Rudeis + Lower mudstone		Default	22.5000	200.0
9	Qabeliat Fm. (maybe eqv. with carbonates nukhul)?		Default	23.0000	80.0
10	Carbonates (Nukhul_Fm)		Default	23.0000	80.0
12	Abu Zenima Fm		Default	28.0000	50.0
11	Prerift-synrift_contact		Default	28.4000	0.0
13	Mokattam_Fm		Default	40.1000	50.0
14	Darat_Fm		Default	40.2000	100.0
15	Thebes_Fm		Default	40.4000	150.0
16	Sudr_Fm		Default	48.6000	225.0
17	Matulla_Fm		Default	83.5000	125.0
18	Wata_Fm		Default	89.3000	100.0
19	Raha_Fm		Default	93.5000	100.0
20	Nubian_Sandstone		Default	145.5000	490.0
21	Basement		Default	542.0000	1000.0

Figure 3-9: Stratigraphic column constructed in MOVE.

3. Cross sections construction/interpretation:

Six cross-sections across the study area where generated using the “Trace” tool, which extracts the topography (z-values) from the DEM’s between 2 chosen points, see Figure 3-11 for location of cross-sections in the study area. Using the projection tool “To Surface”, the newly made flat section is chosen as object to project and the DEM chosen as the target, this generates a new surface that representing the topography in the DEM file. All the line intersections (lithologies, faults and anticlines/synclines) are collected and projected to the surface as well. Dip data within between 400 to 1000 m of the cross-section was projected onto the surface, using the “Project to section” tool (Figure 3-10).

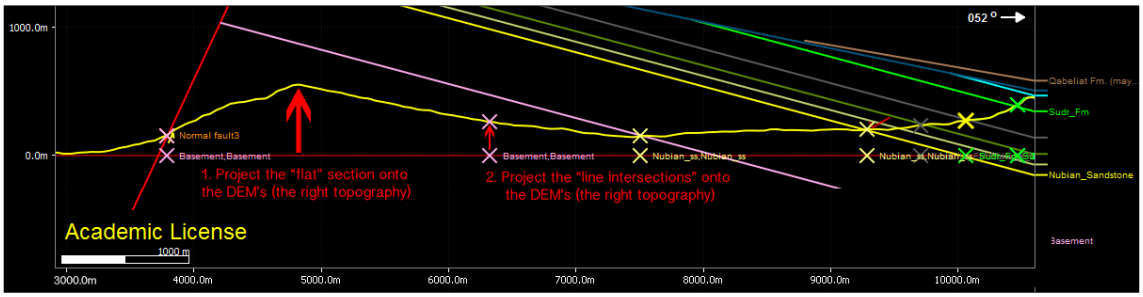

Figure 3-10: (1) Project the flat line section using "to surface", and choose the DEM as the target surface, so the section lines follows the right topography. (2) For the "line intersections", press any one of them and then choose "project to surface, and choose DEM as target, this will move them all to the right topography)

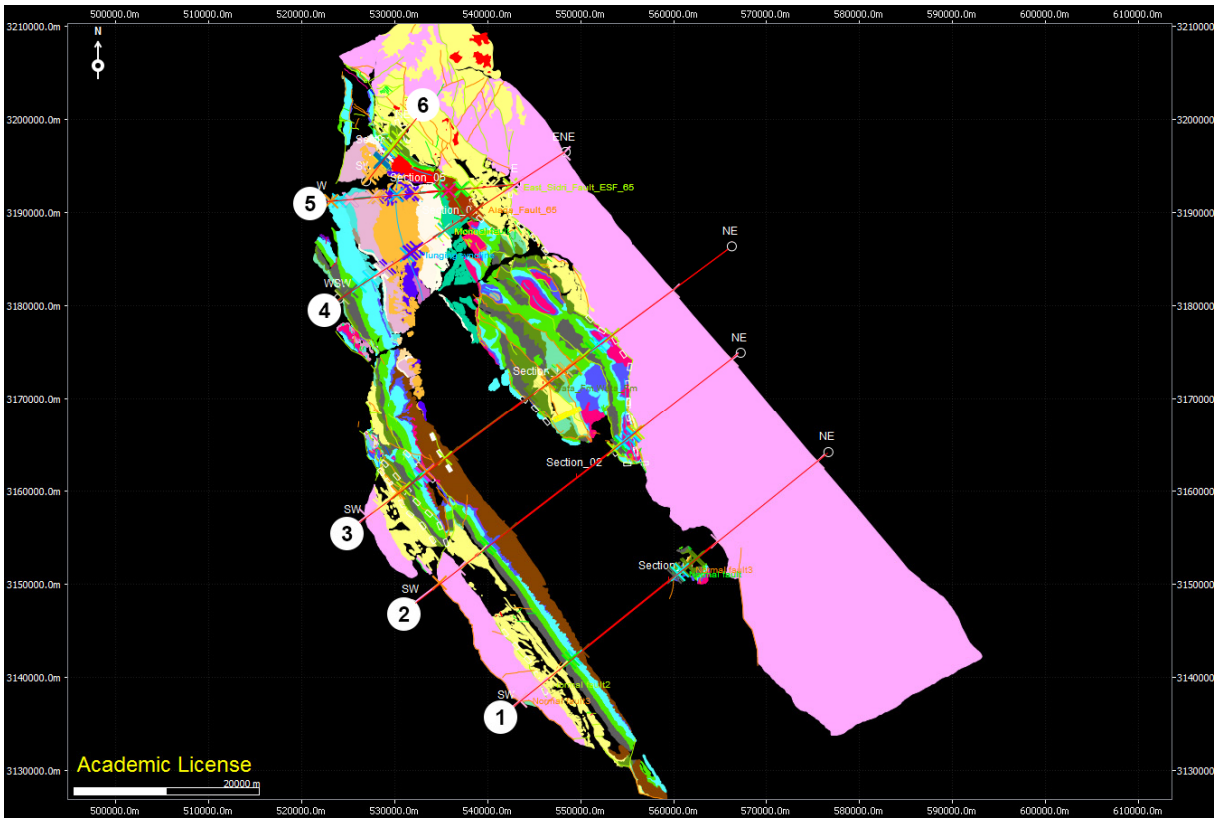

Figure 3-11: Location of cross-sections 1 to 6 in the study area.

The cross sections were interpreted using surface data (lithological boundaries and dip data) in addition to information from previous cross-sections constructed by (Garfunkel and Bartov, 1977; Moustafa, 1993; Whipp, 2011) in the study area. It there was no information on the dip angle of faults, 65° was used as a standard, the faults were projected down from their intersect-point at the topographic surface, in Figure 3-12 three faults are projected (straight red lines).

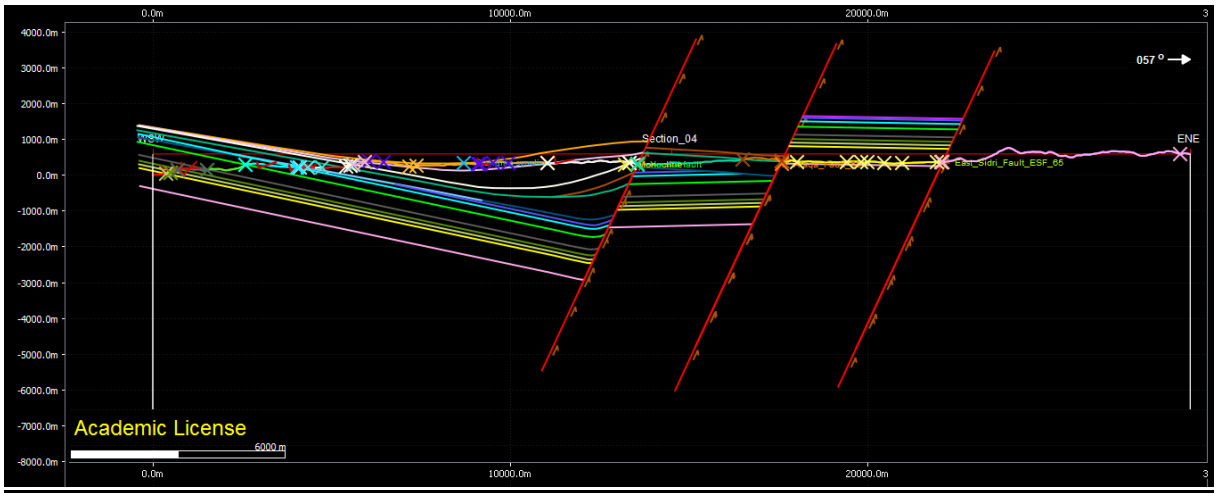

Figure 3-12: An example of the first interpretation of cross-section nr. 4. The red lines are the projected fault the coloured lines are the horizon drawn based on dip data and their surface intersection points.

4. Cross-section restoration:

Before starting on the restoration (backstripping) of the cross-sections the relevant sea-level had to be estimated. To find the proper sea-level at the time, the Global Eustatic Sea-level curve from (Miller et al., 2005) was used, first step was to find the right planktonic foraminifera biozones N(x), based on data from the Amoco Feiran Field notes. Step 2 was to use the found N(x) to read of the Calcareous nannofossils NN(x) biozone from the Neogene timescale made by Harland et al. (1989) and step 3 was to read of the exact sea-level of the Eustatic Sea-level curve made by (Miller et al., 2005), see Figure 3-13 and table 1 (the pictures and curves used in Figure 3-13, can be seen on in high resolution in appendix 1 (Figure 1 to 3) and the result are in table 1.

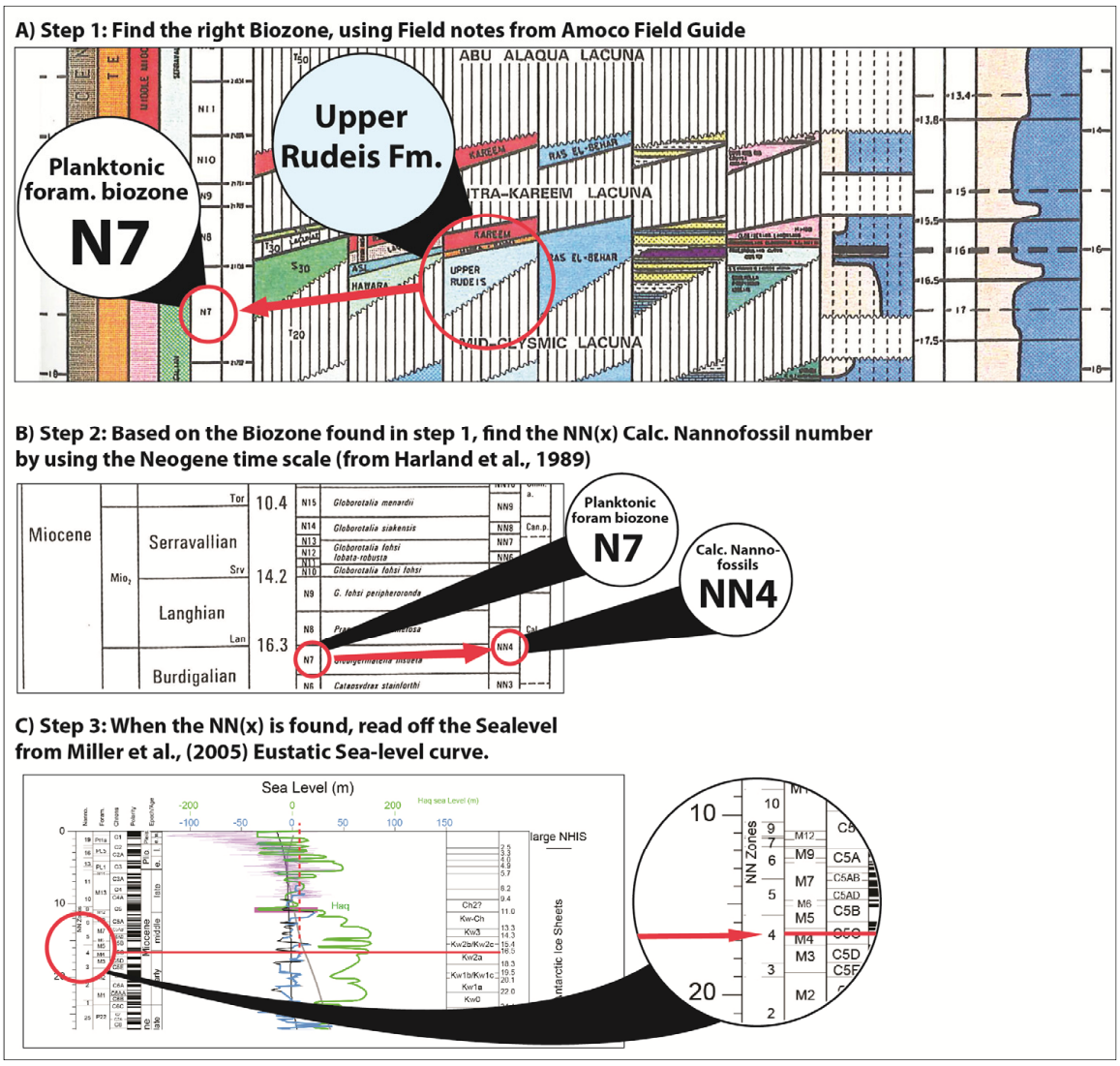

Figure 3-13: The steps made for reading of the Sea level for the stratigraphic unit, based on Biozones. (A) Step 1: finding the right biozones N(x) for the stratigraphic unit. (B) Step 2: Find the NN(x) for the right stratigraphic unit. (C) Step 3: Read of the sea-level based on the biozones found. All the used tables can be found in Appendix1, in figure 1-3. See the results in table 1.

TABLE 1: Sea-level estimated based on Miller et al., 2005 Eustatic Global Sea-level curve.

Rock Unit	Age	Biozones			Water depth (m)	Eustatic Global Sea-level	*Remarks to water depth*
		N	***Foraminifera***	***NN*** *(C. N*.)*		***Miller et al., 2005***	
						Short term	
DCL3 *(S40)*	Late Langhian	N8	*Praeorbulina*	NN5	0	-10 m	*Delta topsets used as top (120m-150m)*
DCL2 *(Evaporite + kareem) (T30/S40)*	Early Langhian	N8	*Praeorbulina*	NN4	0	-20 m	*Delta topsets used as top (120m-150m)*
DCL1/ASL *(S30&T30)*	Late Burdigalian	N7	*Globigerinatella insueta*	NN4	0	0 m	*Delta topsets used as top (120m-150m)*
Lower Rudeis *(S20/T20)*	Burdigalian	N6	*Catapsydrax dissimilis*	NN3	100-200 m	-15 m	*Deep water deposits*
Base Synrift	Aquitanian/ Burdigalian	N5	*Catapsydrax dissimilis*	NN2	~ 30 m	-15 m	*Shallow water*
Mokattam Fm *([(1)]Eqv. Tanka Fm.)*	Late Eocene	P16	*G. Cerroazulensis*	NN19-20	~ 30 m [(2)]	+20 m	*Upper shelf deposits*
Darat Formation	Middle Eocene	P12	*G. Lehneri*	NN16	~ 100 m[(2)]	+20 m	*Middle to outer neritic zone*
Thebes Formation	Early Eocene	P8	*G. Aragonensis*	CP10	~ 100 m	+60 m	*Outer neritic zone to bathyal zone*
Sudr/Esna	Maastrichtian		*G. Contusa*	NC22	~ 100 m	+30 m	
Matulla Formation	Coniacian-Santonian			NC15-16	~ 100 m	+20 m	
Wata Formation	Turonian			NC14	~ 100 m	+15 m	*Moderate shallow shelf or lagoon [(3)]*
Raha Formation	Cenomanian			NC10	~ 100 m		*Shallow marine*
Nubian Sandstone	(Malha Fm top in Nb.ss) Jurassic/ Cretaceous)			NC1	~ 100 m		*Continental passing into shallow marine in the upper part of rift [(3)]*

*Table 1: Table showing Sea level at deposition based on biozones from Miller et al., 2005 Eustatic Global Sea-level curve. *Calc. Nannof. = Calcareous nannofossils. [(1)]*(Jackson, 2008), [(2)](Jackson et al., 2006), [(3)](Alsharhan, 2003). Biozones found in based on the chart in the Amoco Field Guide. Calcareous nannofossils found based on the Neogene time scale from (Harland, 1990), and the Sea-level was read of the Eustatic sea-level curve from (Miller et al., 2005).

The restoration and balancing of interpreted cross sections in MOVE is done in multiple repeated steps (Figure 3-14) After the first interpretations were done, the top of the erosive uppermost bed was reconstructed to its pre-deformed deposition, the delta topsets were sat to 0 meters sea-level (sea-level at that time) and water-depth taken into account regarding the non-delta formations.

A repeated workflow of “unfolding”, “move on fault” and “decompacting” was done for each layer, if there were misfits along the way or at the final restoration step, the first interpretation was changed and all the steps repeated with the new interpretation until the cross-sections balanced, making the interpretation geologically viable (Figure 3-14). The processes of "Unfolding", "Move on fault" and "Decompaction" are explained in detail in part 3.3, 2D kinematic modelling theory on page 40.

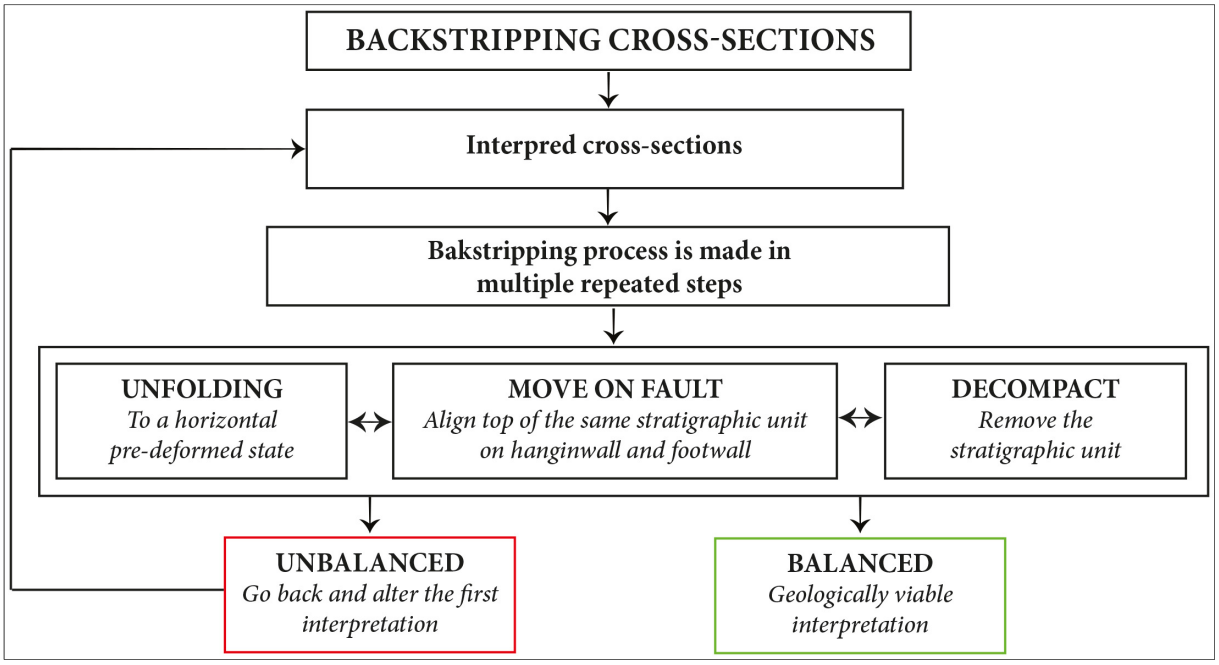

Figure 3-14: Workflow when balancing cross sections.

3D modelling:

To construct the 3D model in 2D/3D MOVE the following data was used, the geological map imported from ArcGIS, the interpreted cross-sections and the needed restoration (backstripping) steps, a 3D models of the present day structural style of the Gulf of Suez was constructed. A flowchart of the work-process for producing 3D models is summarized in Figure 3-15 and explained in more details below.

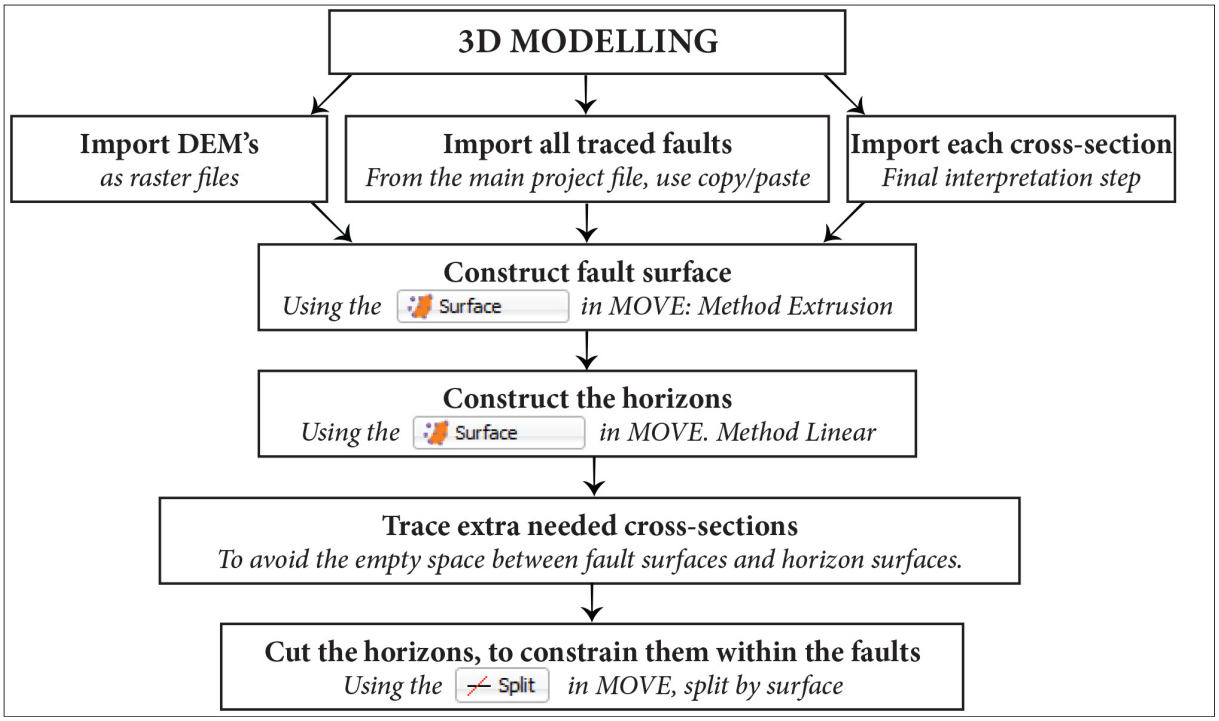

Figure 3-15: Workflow chart on the 3D modelling.

The 3D model is made in a new separate mve-file, the DEM files are imported as raster file and all the needed fault traces from the main project file in MOVE are copied (copy/paste) into the new 3D project file. The fault surfaces are constructed using the Surface tool "Create surface from lines" and method set to "Extrusion" which requires a plunge and plunge azimuth to be chosen for the fault in addition to the length, the surface has to be constructed twice (projected up and down from the fault trace). The "resample lines (interval)" controls the size of the mesh, decreasing the number from for example 140 meters to 50 meters, will produce a tighter spaced mesh, a more accurate surface (Figure 3-16).

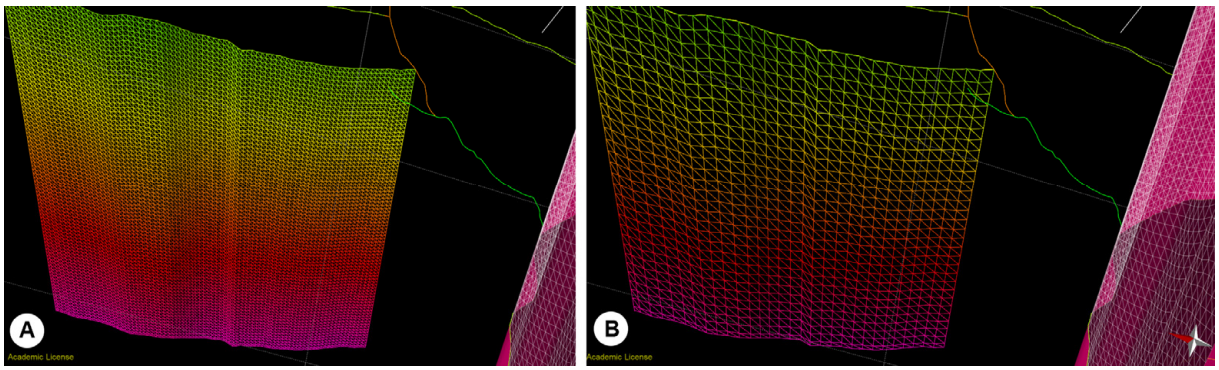

Figure 3-16: (A) Resample lines interval set to 50m, (B) resample lines interval set to 140m, which produces a more spaced mesh.

The horizons are constructed using the “Surface” tool as well, but method is set to “Linear” and multiple horizon surfaces created at once, by sorting lines and choosing the “Separate Surface per set of type: horizon”. Exact data for sample density and Resample lines can be set to control the size of the mesh, for producing a tighter spaced mesh the sample density is increased, which increases the amount of parallel lines. As a standard the sample density and resample lines interval where both set to 100, but when needed, for example to generate the most accurate clinoform in the surface, resample lines interval was decreased to 30m (Figure 3-17).

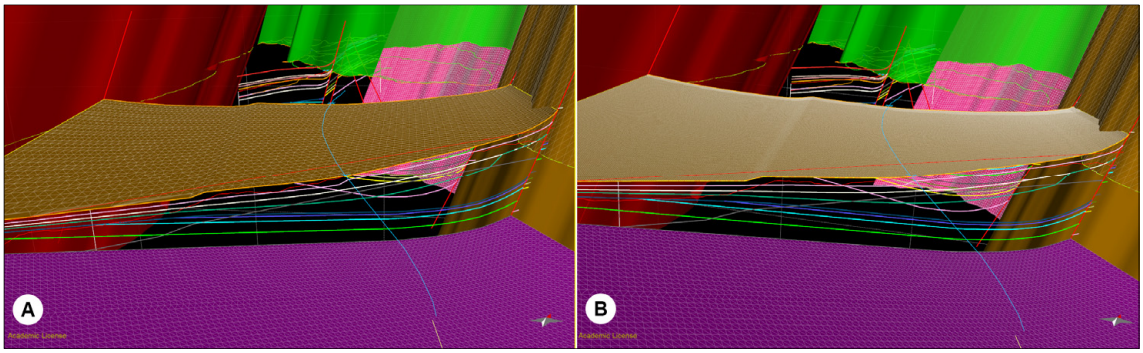

Figure 3-17: (A) Surface generated with standard settings (sample density=100, resample line interval=100 meters), (B) surface generating using sample density=100 and resample line interval=30 meters).

To deal with the problem of empty space between the fault and the constructed horizon surfaces in the 3D model (Figure 3-18), additional cross-sections had to be traced between the original cross-sections, to extend the horizon surfaces beyond the faults, so the faults could be used to cut the horizon surfaces.

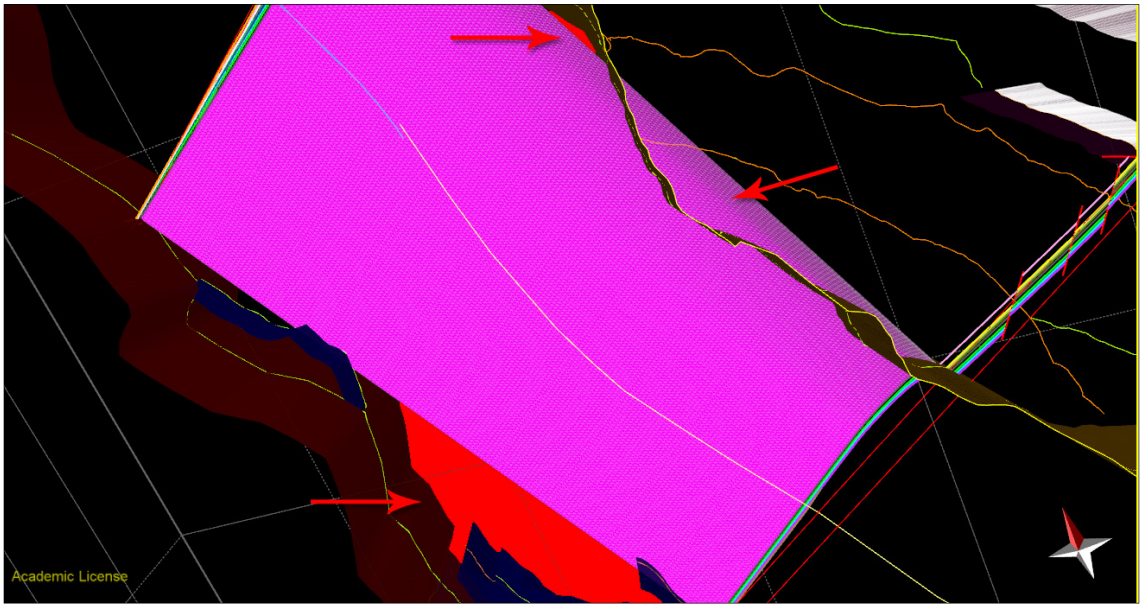

Figure 3-18: Showing the problem in the 3D modelling with the empty space (red) when creating surfaces.

The last step was to cut the horizons so they did not reach above the topography; this was done by making the DEM into a surface (with lower resolution, since the program crashed regularly if using a large high-resolution surface) and then using the new topography surface to cut the horizons (Figure 3-19). By using a lower resolution topography surface some of the smaller details in the topography are lost, but overall the topography is very similar to the original and therefor the low-resolution surface was used in this thesis making the 3D model.

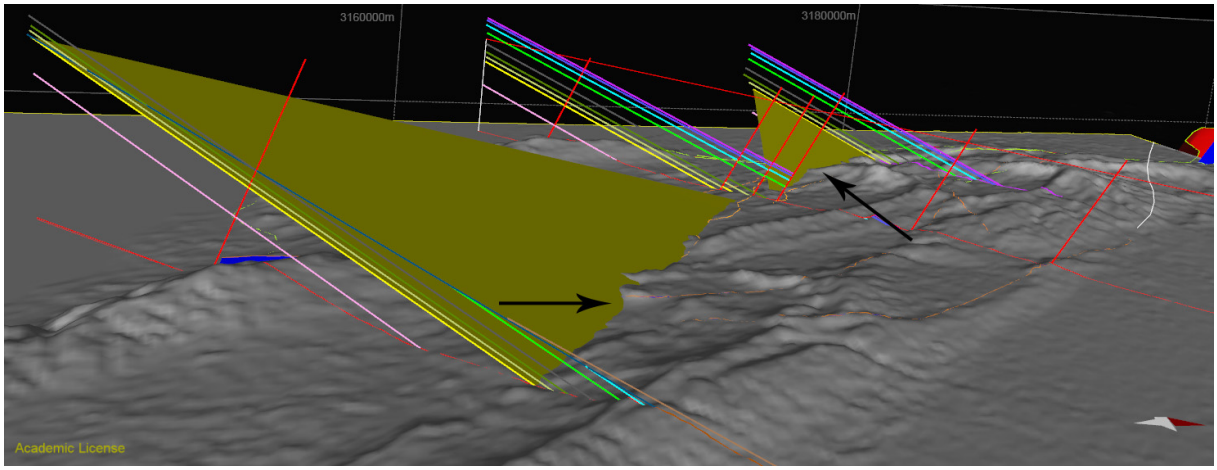

Figure 3-19: Cutting horizons by using the topography surface created, cuts where the green surface meets the grey topography surface.

3.3 2D kinematic modelling theory

A balanced cross section indicates a viable geological interpretation and will give a better understanding of the geological history in the study area. It is not necessary the correct solution, but it can be one possible viable interpretation among many. The theory behind 2D kinematic modelling in MOVE assumes that no rock volume has been created nor destroyed by deformation thereby reassembling should be possible. To restore a section to its depositional pre-deformational state, balancing a section, MOVE has embedded certain geometrical rules into the procedure:

- It removes faults displacements
- It restores eroded rock volume
- It restores rock volume lost in compaction
- It removes fault related folds by simple shear, flexural slip, fault parallel flow or fault bend fold.
- It removes folding, that is related to flexural slip.

2D kinematic modelling includes this workflow:

- Depth conversion (*Not used in this thesis since there is no seismic data*)
- Unfolding (*Vertical/simple shear and flexural slip unfolding*)
- Move on Fault *(removing the displacement)*
- Decompacting *(Backstripping, removing each layer)*

3.3.1 Unfolding:

The "Unfolding" tool restores geological horizons to their pre-deformed target or datum, either by simple/vertical shear or flexural slip, both are shortly explained below:

Simple shear unfolding algorithm:

Figure 3-20 depicts the unfolding of an upper surface (black bed) that is restored to its pre-deformational deposition (green dotted line) by a chosen shear vector, vertical in this example. The restoration can either be done to datum, a horizontal line or to target, any chosen line.

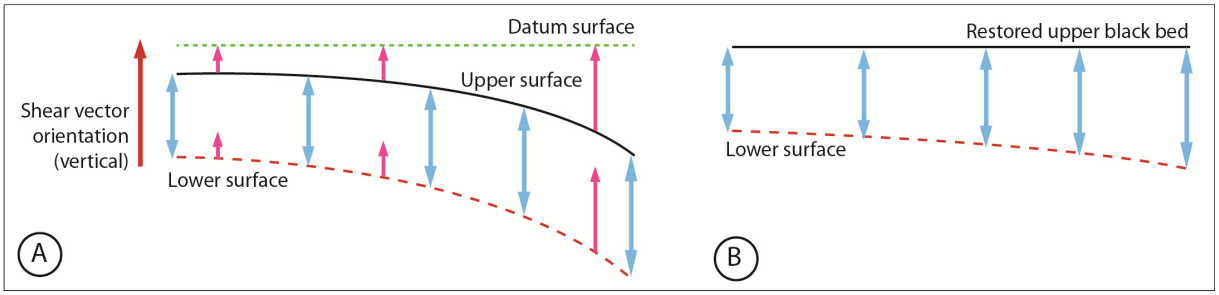

Figure 3-20: (A) Cross sections in a hangingwall before restoration showing the chosen shear vector angle (vertical in this case). (B) Restored upper surface and lower surface has moved upward preserving the thickness, but decreasing the line length (Modified from help pages in MOVE software).

Area volume between the beds is preserved when unfolding, but the line length will be shorter and thereby the surface area decreases, meaning that a steeper dip will increase the loss in line length and surface area in the unfolding process (Figure 3-21). In Map view the surface area will also change, unless when a vertical shear angle is used *(Help page in MOVE)*.

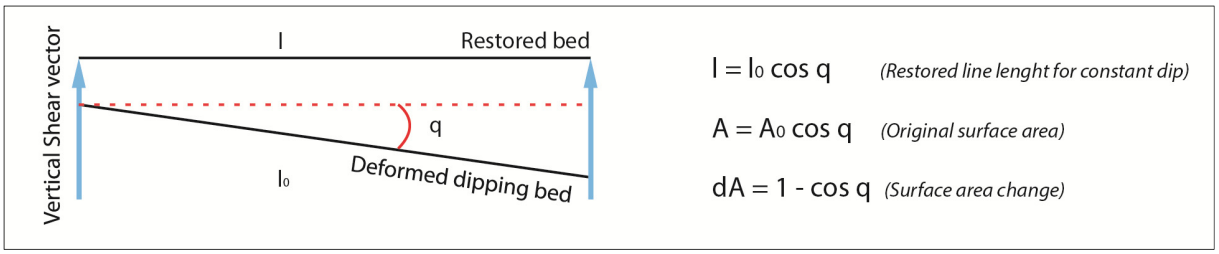

Figure 3-21: Depicts the loss in line length and the Surface area change, during the unfolding process (Modified from the help pages in MOVE).

Flexural slip unfolding algorithm:

When using the flexural slip unfolding tool a pin is set at the fold axis (see Figure 3-22) then the algorithm projects dip domain bisectors, perpendicular to the template bed, and a slip system that follows the template bed is generated. The bed thickness variations are recorded at the point where the slip system and the passive beds intersect and will be preserved after unfolding.

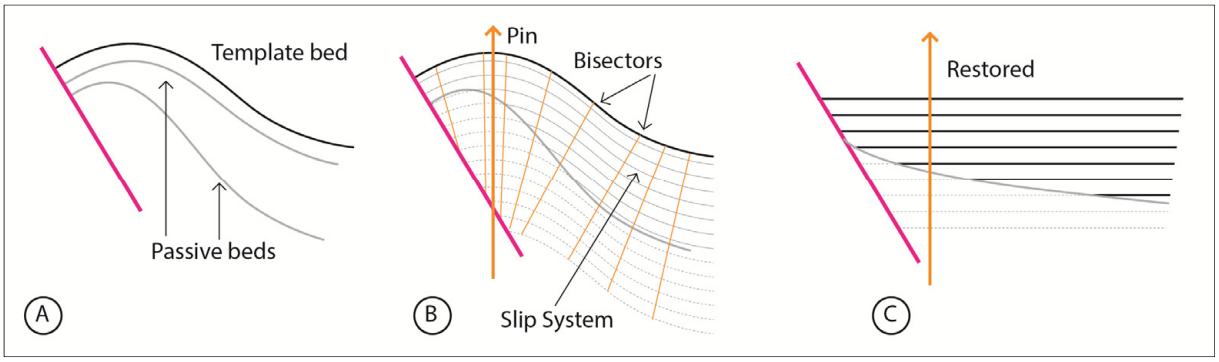

Figure 3-22: Unfolding with flexural slip, A: Original fold with the template bed and the passive beds, B: Depicts where the pin is set and where the bisectors and Slip System is generated, C: depicts the restoration (Modified from the help pages in MOVE).

3.3.2 Move on Fault:

In the tool "Move on Fault " there are six different algorithms controlling the deformation caused by faulting, simple shear, fault parallel flow, fault bend fold, detachment fold, fault propagation fold and trishear. Simple Shear and Fault parallel flow are explained below, since these where relevant for this thesis study area, an extensional environment.

Simple shear algorithm:

This algorithm is used when the deformation is diffused throughout the hangingwall and not discrete slip between beds, as in flexural slip. The principle behind this algorithm is that the extensional area has the same volume as the hypothetical void between the hangingwall and footwall, created by fault displacement and the shear vector angle controls how the hangingwall collapses down on to the footwall (Figure 3-23).

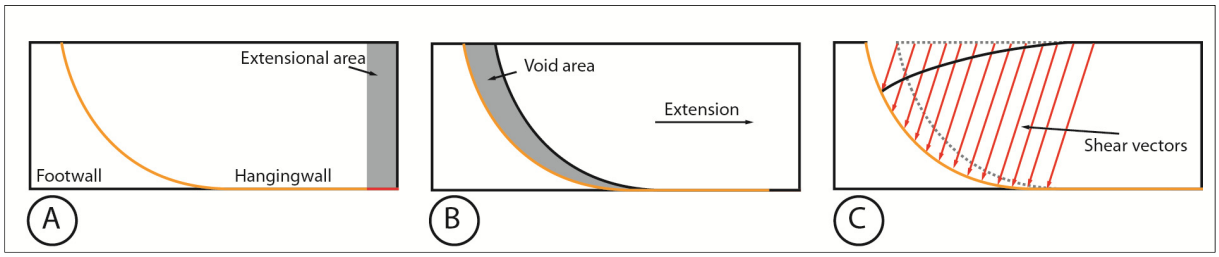

Figure 3-23: (A) Is the before the faulting, (B) show the hypothetical void caused by the faulting, (C) shows how the simple shear algorithm deals with the hangingwall collapse on to the footwall (Modified from Help pages in MOVE).

Fault Parallel flow algorithm:

This algorithm works for models on both extensional and contractional regions and the principles behind the algorithm are that it preserves the line-length of the horizon, the footwall does not deform or translate, no axial plane is calculated and the forelimb is preserved (since the user can use the Layer parallel shear). Figure 3-24 depicts the how this algorithm works, (A) is the present deformed state of a fault, (B) shows how the fault plane is divided by dip bisectors, separating the different dip domains along the fault and flow lines are constructed parallel to the fault plane and (C) depicts the pre-deformed state. This algorithm is mostly used in contractional environment, but can also be used in extensional environments (help pages in MOVE)

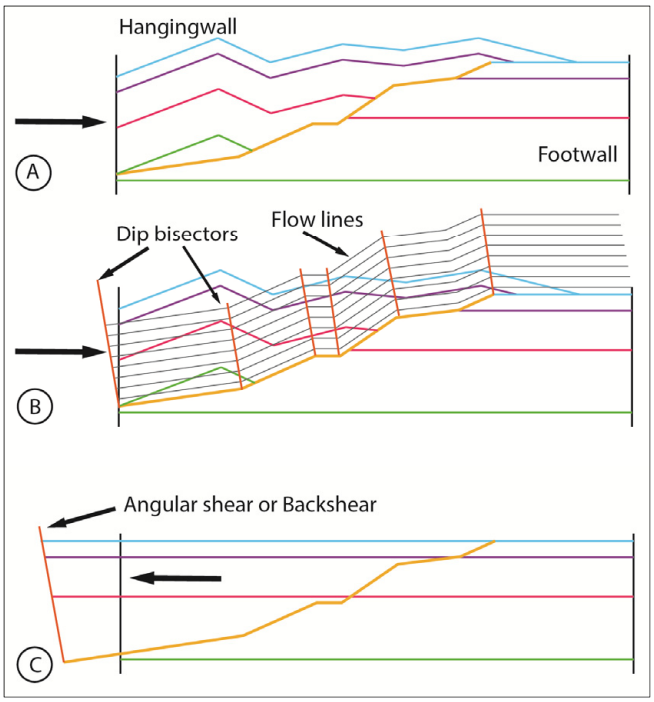

Figure 3-24: (A) Depicts the deformed state, the fold. (B) Depicts how the bisectors divide the fault plane and how to flow lines lie parallel to the fault plane. (C) Is the depositional pre-deformed state of the layers after using Move on Fault with fault parallel flow (Modified from Help pages in MOVE).

3.3.3 Decompaction

Decompaction tool is used when removing a layer in a backstripping process. One method that is supported in this tool is the assumption Sclater & Christie made, which is that the porosity will decrease as a layer is buried and increase as the layer is decompacted, this is represented by this formula:

$$f = f_0 (e^{-cy})$$

f = Present-day porosity at depth

f_0 = Porosity at the surface

c = porosity-depth coefficient (km^{-1}), which is the rate of porosity decay with depth)

y = depth (in meters)

To calculate the porosity decay with depth for a specific rock, an amount of the rock for different depths is needed, and for every depth the porosity is calculated and put in a graph, then a curve is drawn through the results, this should give an exponential curve and the surface porosity (at zero depth) can be estimated as well as the depth coefficient, which is the gradient of the curve. If a unit contains mixed lithologies, the percentage of every lithology included is calculated to get an average surface porosity and a depth coefficient.

The table used here is generated by (Sclater and Christie, 1980) and it is based on typical values from the North Sea (Table 2).

Table 2: Surface porosity, depth coefficient and Sediment grain density values.

Lithology	Surface Porosity (ϕ_0)	C (Km^{-1})	Sediment grain density (P_{sg})
Shale	0,63	0,51	2720
Sandstone	0,49	0,27	2650
Chalk	0,70	0,71	2710
Shaly Sandstone	0,256	0,39	2680

Table 2: Typical values for the North Sea (Table from Sclater and Christie (1980) - *sourced from* (Allen and Allen, 1990) *(Source: Help pages in MOVE).*

Isostasy theory:

In the "Decompaction" tool in MOVE the isostatic deflection (flexural or airy isostasy) of the lithosphere, either due to loading or unloading (erosion) can be taken into account when modelling. Flexural isostasy should only be used for large sections (>10km), since the flexural effect is regional and not constrained to the local area where loading or erosion is taken place. The Airy isostasy is best suited for loads that have a rather constant thickness, and the isostasy is calculated in columns not regionally as in flexural isostasy (Figure 3-25). The formula for readjusting the isostasy used in Airy isostasy is adapted from Rowan, (1993) *(Source: help pages in MOVE).*

$$\mathbf{Z} = \frac{[\boldsymbol{S}-(\boldsymbol{H1}-\boldsymbol{H2})\boldsymbol{\rho c}-\boldsymbol{\rho w}]}{\boldsymbol{\rho m}-\boldsymbol{\rho w}}$$

D1 = Water depth before sediment load

D2 = Water depth after sediment load

S = Thickness of sediment loaded or unloaded

H1 = Crustal thickness before sediment load

H2= Crustal thickness after sediment load

Z = Amount of subsidence relative to a basement reference

ρw = Crustal density

ρw = Water density

ρw = Mantle density

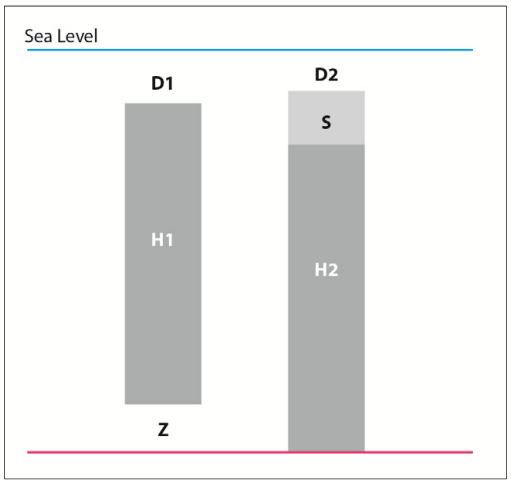

Figure 3-25 A airy isostatic model of a sediment loading. (Modified from HELP pages in MOVE)

3.3.4 Limitations and uncertainties in the data generation and in MOVE software:

- Unclear boundaries between lithological units, either unclear or not visible at all, due to quaternary deposits on top or slides, slumps and erosion
- Pixelated satellite images also making some boundary´s unclear.
- In Google Earth it was necessary to use satellite images taken at different times, to get the best visual of the boundaries, some were taken years apart and therefor had a few mm difference.
- DEM´s where represented by 30x30 m squares, meaning that the topography is average within the 30x30m and therefor smaller topography changes might not be showing in the DEM´s - which causes uncertainties in the topography and hence the lithological boundaries and layer thicknesses.
- The lack of dip data in the study area is also a factor for uncertainties.
- There were certain limitations in the MOVE software, due to the complex stratigraphy in the study area, the synrift sediments where NOT a layer-cake model, which seems to be preferred in MOVE, especially the delta-form (clinoform) is causing troubles during the modelling.

4 Stratigraphy and structural styles of the El Qaa half graben

The purpose of the result chapter is to present the structural and stratigraphic analysis based on the mapped lithologies, traced faults and restoration of six cross-sections throughout the study area. The chapter is divided into 2 main parts. **Part 4.1** shortly describes the nature, thicknesses and distribution of the lithologies mapped in the study area for this thesis, from the oldest to the youngest, divided into prerift and synrift deposits. **Part 4.2** describes the structural style in the study area based on the six constructed cross-sections in the study area.

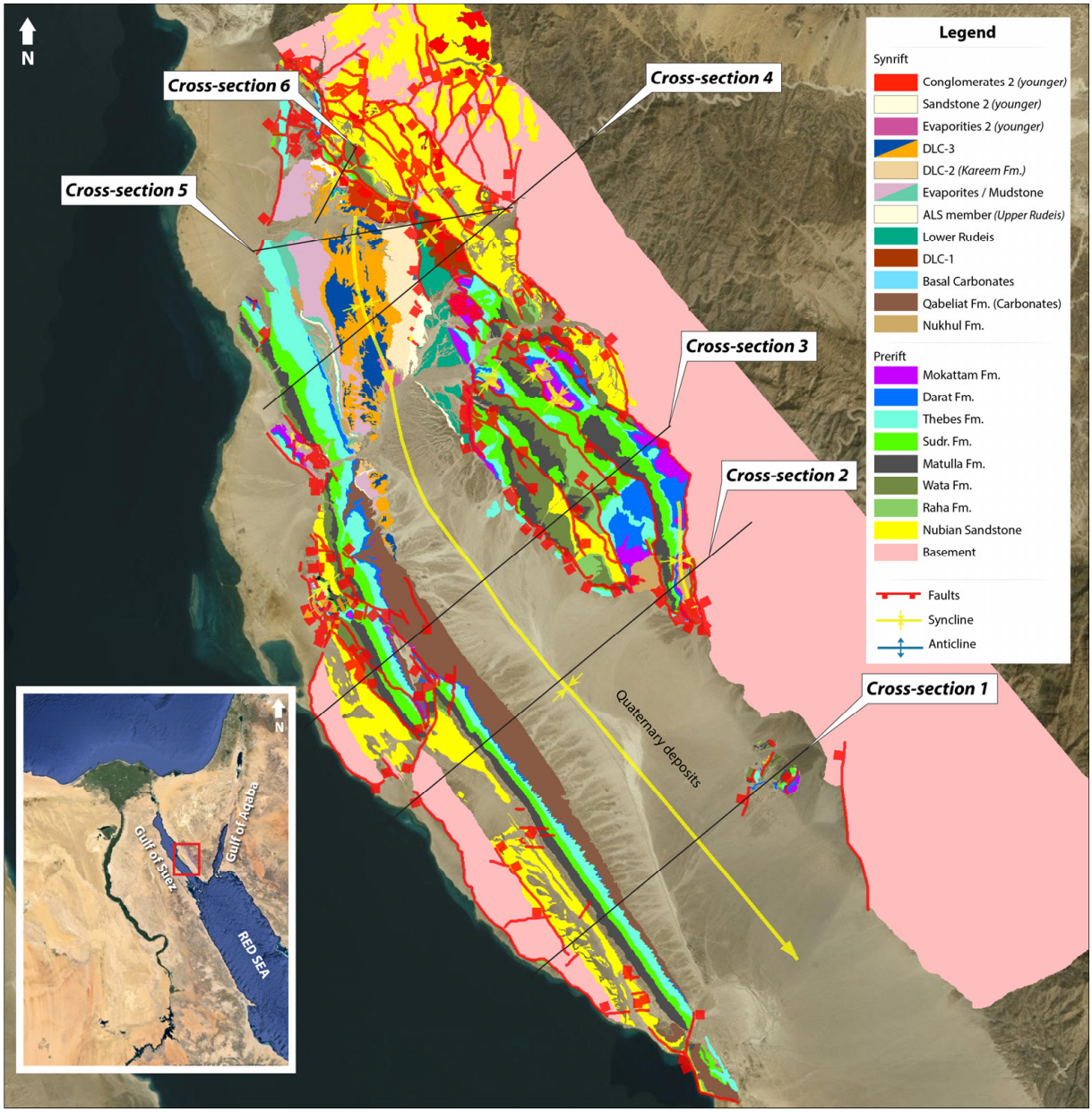

Figure 4-1: Geological map generated in ArcGIS, including legend, location of study area and cross-sections 1-6.

4.1 Stratigraphy of the El Qaa fault block

The stratigraphic units mapped in this thesis are based on the chart made by (Moustafa, 2004). They can be divided into three main packages, the Precambrian basement, prerift units and synrift units. Figure 4-2 is the stratigraphic chart generated for this thesis and differs from Moustafa (2004) in the synrift units, which are subdivided differently from the original chart, for the purpose of this thesis. The synrift units have been divided into three delta lobe complexes DLC-1, DLC-2 and DLC-3, respectively. The delta lobe complexes have different lateral facies that where mapped separately in the geological map generated in ArcGIS, but for the restoration of the cross-sections the lateral changes in facies were considered as one unit for each delta lobe complex, this was done to simplify the restoration of the cross-sections, so an entire delta section (proximal to distal sediments) could be removed in one step. The mapped synrift units are described in detail in part 4.1.2 on page 54. The units in the stratigraphic chart have been given the same colours as used in the geological map generated in ArcGIS. Some of the units where merged, such as the Nubian Sandstone units that have been mapped as one unit and given a yellow colour. The Sudr Chalk and the Esna Shale where also merged into one unit, due to the thin section of Esna shale and the unclear boundary between them. Some of the units in the stratigraphic chart are not present in the study area and are therefore not described in this thesis and have been given a white background in the chart (Figure 4-2). The thicknesses used in the restoration are included in the chart along with the ages representing each unit. The column to the left shows main sequences suggested by Sharp et al. (2000b) and divides the units into three Megasequences. The Prerift units mapped in this thesis are from the oldest.

- **Precambrian Basement**
- **Nubian Sandstone**
- **Raha Formation**
- **Wata Formation**
- **Matulla Formation**
- **Sudr Formation**
- **Thebes Formation**
- **Darat Formation**
- **Mokattam Formation**

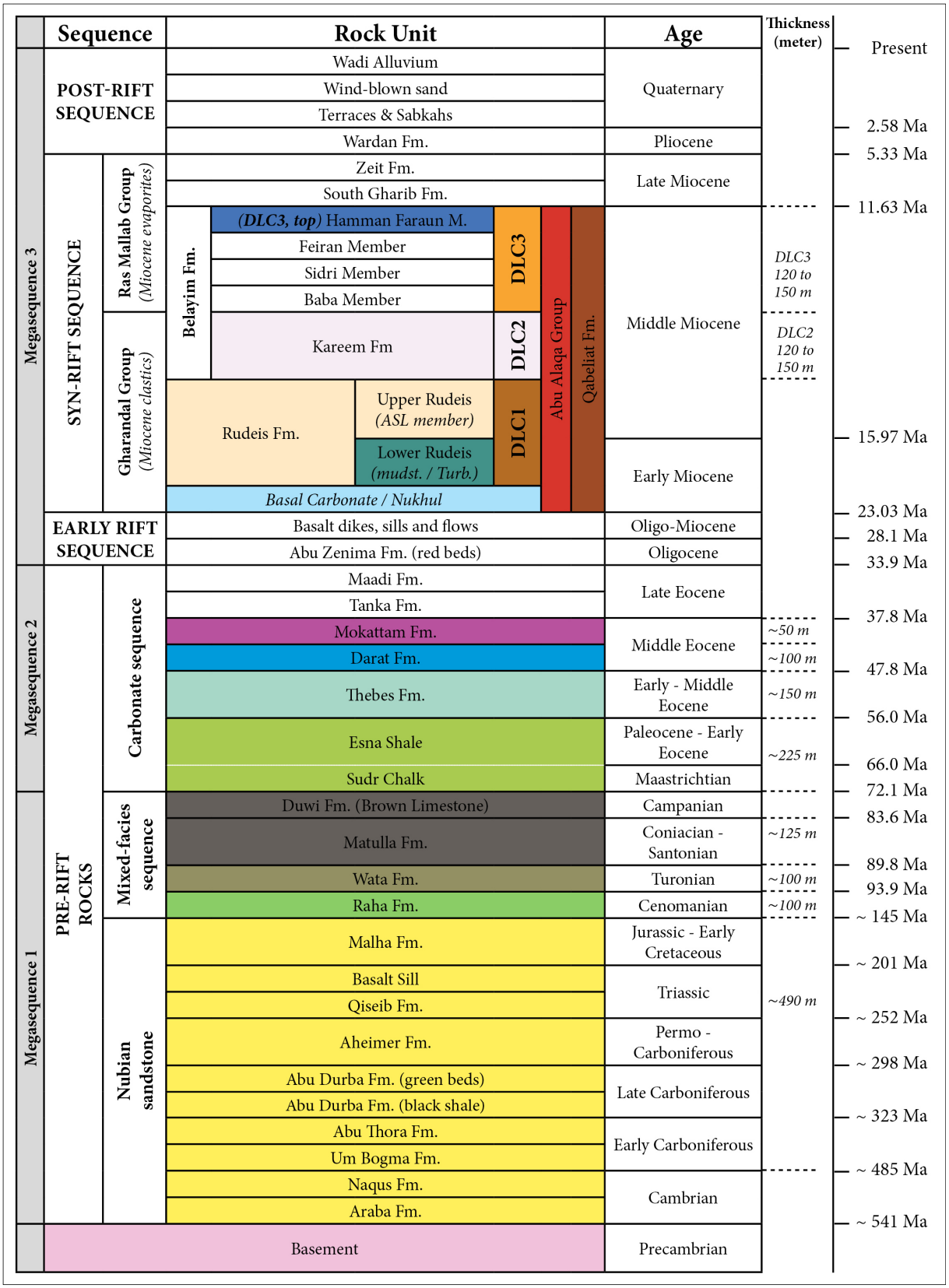

Figure 4-2: Stratigraphic chart and thicknesses of the prerift units in the Gulf of Suez, modified from Moustafa, (2004). All mapped lithologies in this thesis have been coloured. Sequence terminology is based on Sharp et al., (2000b). The ages are based on the ICS International Chronostratigrahpic Chart (Martinsson and Bassett, 2010).

4.1.1 Prerift

A geological map including only the Precambrian Basement and the prerift stratigraphic units can be seen in Figure 4-3. Below is a description of all the units, including their ages, where they are exposed in the study area and the depositional environment.

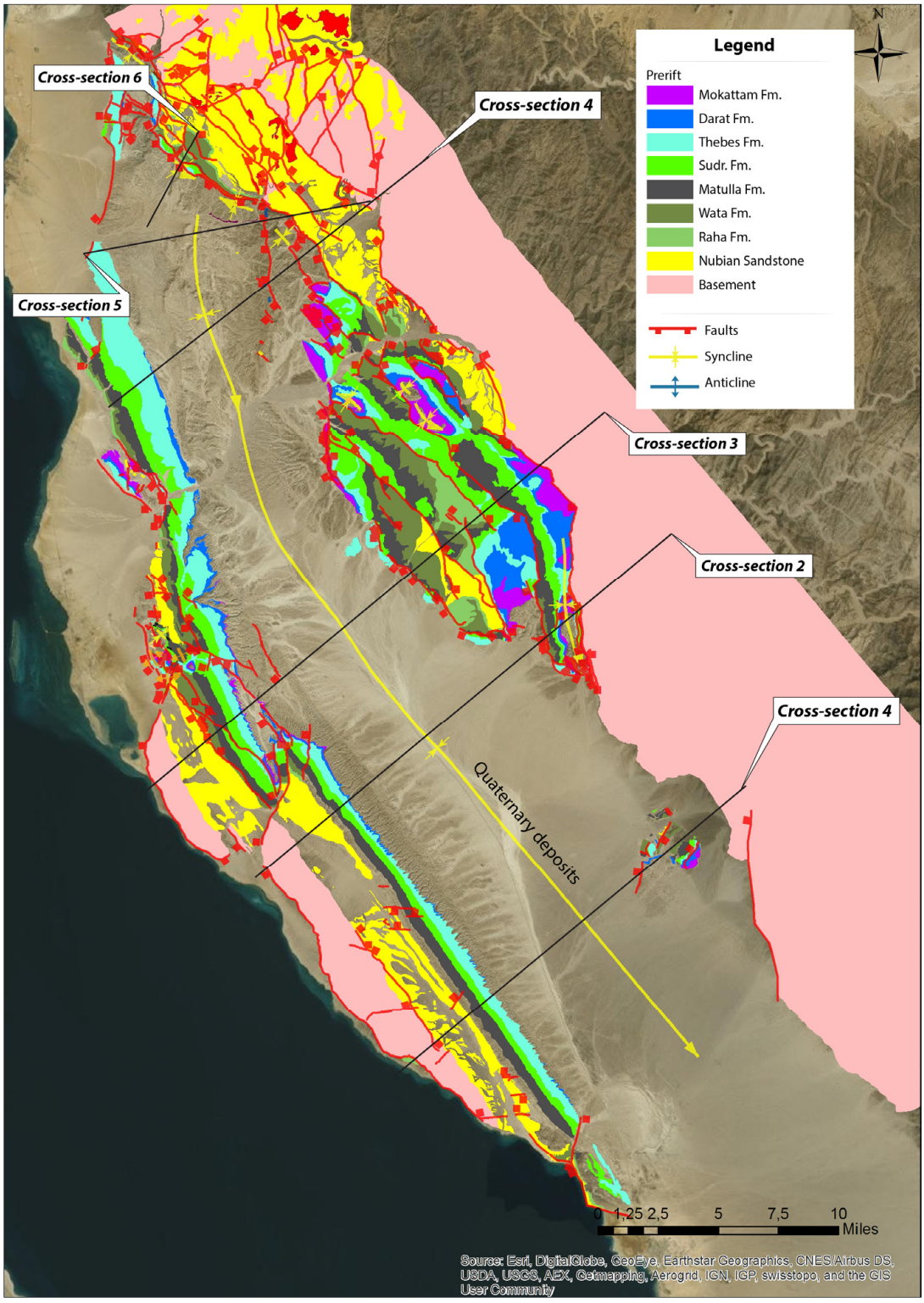

Figure 4-3: Mapped lithologies (with legend), traced faults (red lines) and anticline/synclines (yellow lines). Geological map generated in ArcGIS MAP including Precambrian Basement and the prerift units.

Basement

Precambrian Pan-African basement consists of gneisses, volcanics and metamorphosed rocks, containing strong prerift fabrics that have influenced the rifting in Oligocene (Bosworth and Mcclay, 2001; Moustafa, 2004). The basement is exposed along the greatly uplifted rift shoulder on the EBFB, in the Abu Durba and the Gebel Araba fault blocks located on the western side of the El Qaa half graben and in the immediate Nezzazat fault footwall.

Nubian sandstone

The non-marine Nubian Sandstone consists of multiple formations and lies unconformably above the peneplained basement. It consists mostly of sandstone units, with a few thin carbonate and shale intervals, the formations are from oldest to youngest, Araba, Naqus, Um Bogma, Abu Thora, Abu Durba, Aheimer, Qiseib, Triassic basaltic Sill and the Malha Formations, and the age ranges from Cambrian to Early Cretaceous (Moustafa, 2004). The stratigraphic analysis of the top Basement to the top Nubian Sandstone, gives a thickness between 490-600 m throughout the study area, which is in agreement with the thickness (ca. 500 m) suggested by Moustafa (2004). The Nubian Sandstone is exposed along the footwall of the Nezzazat fault on the western limb of the El Qaa syncline, on the eastern rift shoulders hangingwall where it juxtaposes the Basement of the rift shoulder footwall, on the Hadahid fault block as well on the Baba-Sidri faults footwall from the northern-end and south towards the Feiran Transfer zone, where it is exposed south and north of Wadi Feiran.

Raha Formation

Has a Cenomanian age and is the lowermost part of the mixed carbonate/clastic sequence, consists of shales, sandstone and limestone deposited in a shallow marine environment and has a green and grey colour (Sharp et al., 2000b; Bosworth and Mcclay, 2001; Moustafa, 2004). The stratigraphic analysis of the top Nubian Sandstone to the top of Raha Formation, gives a thickness of ca. 80-100 m, which is in agreement with the thickness (100 m) suggested by Moustafa (2004). The Raha Formation is exposed on both the west and the east side of the El Qaa syncline, along most of the western limb, on the Hadahid fault block, around the Feiran Transfer zone and in the footwall of the Baba-Sidri fault in the northern and southern end.

Wata Formation

Has a Turonian age and consists of a thick limestone with sandstone and shale beds deposited in a shallow marine environment (Sharp et al., 2000b; Moustafa, 2004). The stratigraphic analysis of the top Raha Formation to the top Wata Formation, gives a thickness of ca. 80-100 m thick, which is in agreement with the thickness (100 m) suggested by Moustafa (2004). It has a yellowish brown to grey colour and is exposed on the west and east side of the El Qaa syncline, along most of dipslope, on the Hadahid fault block, around the Feiran Transfer zone and in the footwall of the Baba-Sidri fault in the northern and southern end.

Matulla Formation

Has a Coniacian-Santonian age and is the upper unit of the mixed carbonate/clastic sequence. Is consists of a lower fluvial sandstone unit and a upper shale unit (Sharp et al., 2000b; Moustafa, 2004). The stratigraphic analysis of the top Wata Formation to the top Matulla Formation, gives a thickness of ca. 125-160 m, which is in agreement with the thickness (125 m) suggested by Moustafa (2004). It is dark varicoloured and exposed on along most of the western limb in the El Qaa syncline, on the Hadahid fault block and in the Feiran Transfer zone south and north of Wadi Feiran.

Sudr chalk and Esna shale

The Sudr Chalk and the Esna shale where mapped as one unit in this thesis due to the unclear boundary between them and the thin Esna shale unit. Sudr Chalk has a Maastrichtian age and consists of white chalk. The Esna shale has a Late Paleocene to Early Eocene age and has a blue/grey colour (Sharp et al., 2000b; Moustafa, 2004). The Sudr Chalk and Esna shale together are referred to the Sudr Formation throughout this thesis and the stratigraphic analysis of the top of the Matulla Formation to the top the Sudr Formation, gives a thickness from 200-260 m, it increases northward from ca. 200 m south in cross-section 1 to ca. 260 m northwards in cross-section 5 (Figure 4-3), there is one exception towards the east in a small syncline in cross-section 2 (Figure 4-3) in the Hadahid fault block, there it only is 140 m thick, this could be due to bedding parallel slip and shearing (Whipp, 2011). The thicknesses in this thesis are in agreement with the thickness (225 m) suggested by Moustafa (2004). The formation is exposed along the western limb of the El Qaa syncline,

on the Hadahid fault block, on the Feiran Transfer fault, in places on the Baba-Sidri footwall and in the northernmost end of the study area between the Baba-Sidri fault and the Nezzazat fault, where the two faults link together (Figure 4-3).

Thebes Formation

Consists of grey/white coloured limestone with thick chert bands and has an Early-Middle Eocene age and is deposited shallow water with water depth 100-200 m (Corlett et al.; Bosworth and Mcclay, 2001; Moustafa, 2004). The stratigraphic analysis of the top of the Sudr Formation to the top of the Thebes Formation, gives an increase in thickness from ca. 120 in the southern part to 220 m in the northern part, where it has been eroded by synrift sediments and therefore can be interpreted to have been even thicker northward. This thickness is in agreement within the thickness (150 m) suggested by Moustafa (2004) who also suggested an increase in thickness from 150 m in the south to 350 m near Gebel Musabaa Salama (north of the study area). The Thebes Formation is exposed on the El Qaa dipslope all the way north to the Nezzazat and Baba-Sidri fault linkage, on the Hadahid fault block, Wadi Feiran transfer zone and in the hangingwall of the northern end of the Baba-Sidri fault (Figure 4-3).

Darat Formation

Has an Middle Eocene age and consists of shale, marl and thin limestone beds, deposited in shallow water (Bosworth and Mcclay, 2001; Moustafa, 2004) and the stratigraphic analysis from the top Thebes Formation to the top of Darat Formation, gives a thickness of ca. 100 m, which is in agreement with the thickness (100 m) suggested by Moustafa (2004). The Darat Formation is exposed on the El Qaa dipslope but thins southward until it is completely eroded, on the south, east and north part of the Hadahid fault block and on the Feiran transfer zone north and south of Wadi Feiran (Figure 4-3).

Mokattam Formation

The Mokattam Formation has a Middle Eocene age and is the last prerift unit, it consists of limestone and has a yellowish white colour, deposited in shallow water (Bosworth and Mcclay, 2001; Moustafa, 2004). The stratigraphic analysis of the top Darat Formation to the top Mokattam Formation, gives a thickness of ca. 50 m, which is in agreement with the

thickness (50 m) suggested by Moustafa, (2004). The Mokattam Formation is exposed in places along the El Qaa dipslope mostly on the Durba and Nezzazat block, on south, east and north side of the Hadahid fault block, on the Feiran transfer zone on both sides of the Wadi Feiran and towards the Baba-Sidri fault.

4.1.2 Synrift

The stratigraphic synrift units have been mapped before by others e.g. (Moustafa, 2004; Whipp, 2011) but not divided the same way as they are in this thesis (Figure 4-2). The Synrift sediments in the El Qaa Fault block have a more complex stratigraphy compare to the prerift, especially due to the lateral changes in facies and because of the simultaneously deposition. The Synrift stratigraphic units mapped are from the oldest:

- **Nukhul Formation**
- **DLC-1**
- **The Lower Rudeis Formation**
- **Upper Rudeis Formation (ASL member)**
- **DLC-2 (Kareem Formation, with a distal mudstone and evaporite deposition)**
- **DLC-3**
- **Three younger units Evaporite, Sandstone and Conglomerate area deposited on top of DLC-3.** *(These younger units are only locally exposed in cross-section 6 (Figure 4-3) towards the Baba-Sidri fault, they are not preserved anywhere else in the study area, and area therefor not further described in this thesis).*

Figure 4-4 shows the geological map generated in ArcGIS which only contains the synrift lithologies and the faults in the study area.

Nukhul Formation

Has an Early Burdigalian age, and is considered to be the oldest synrift unit. It is a polymictic conglomerate that includes limestone, chert and basalt pebbles eroded from the prerift strata below at rift initiation. The Nukhul Formation conglomeratic base is deposited in a fluvial environment that gradually changed into shallow marine (Gupta et al., 1999; Moustafa, 2004). The Nukhul is only exposed in the south-end and north-end of the Hadahid

fault block in the center of synclines in the Hadahid sub-blocks. Due to the erosion of the exposed Nukhul Formation the thickness of the Formation could not be estimated.

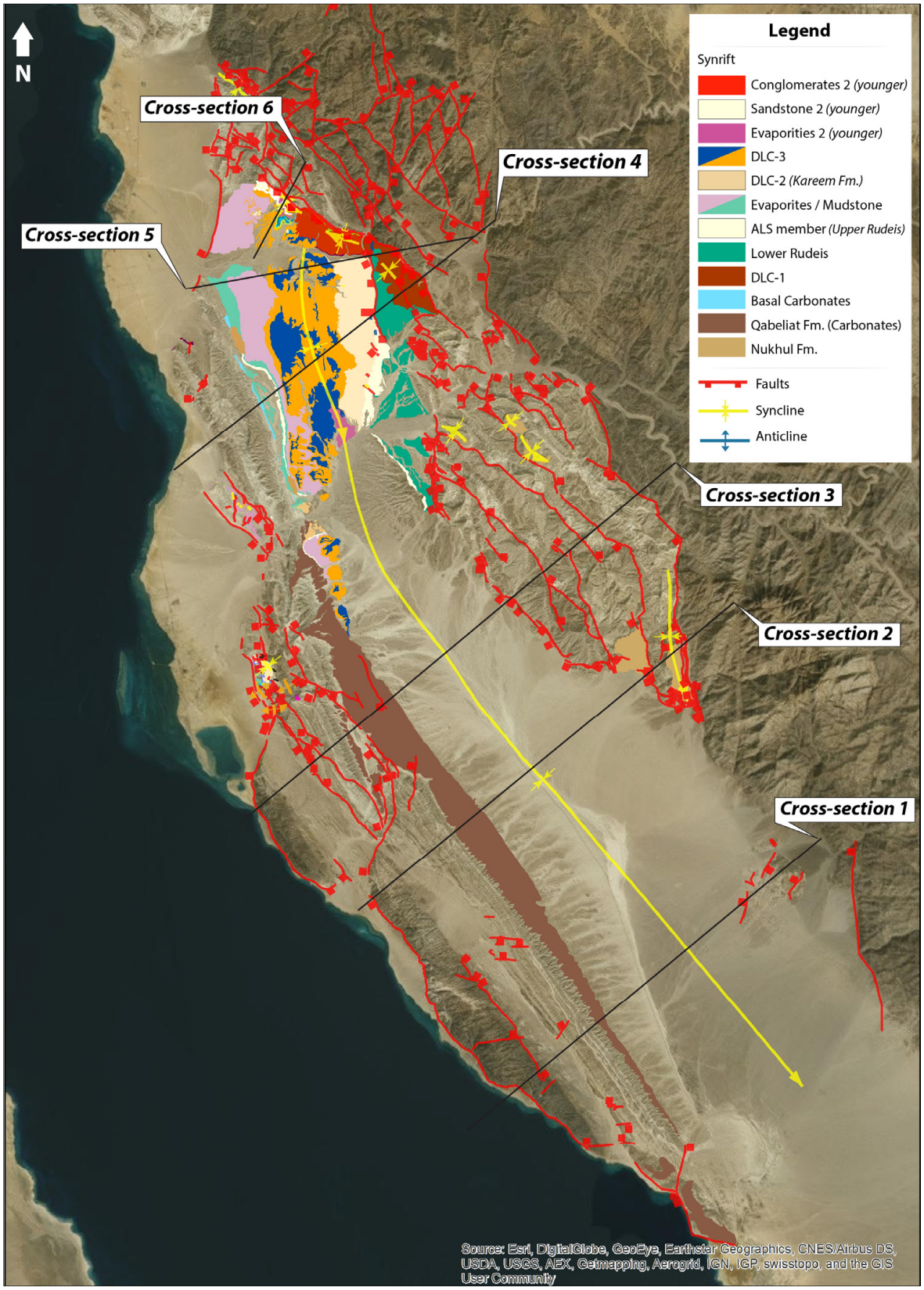

Figure 4-4: Geological map generated in ArcGIS MAP only containing synrift-sediments, along with faults and anticline/synclines and the location of the six cross-sections.

Qabeliat Formation

The Qabeliat Formation is a carbonate platform and has a Early to Middle Miocene age and consists of grey limestone and coralline (Moustafa, 2004). It is interpreted to have been deposited simultaneously as the DLC's and is exposed south of Wadi Feiran on the dip slope of the El Qaa syncline, the stratigraphic analysis show in increase in thickness south towards the Durba block, and then decreases in thickness further south towards the Araba block. Due to the erosion of the Carbonate platform top it is not possible to measure the exact thickness, but a minimum thickness of ca. 500 m was measured in a sub-fault block on cross-section 3 crossing the Durba block (Figure 4-4).

Basal Carbonates

There is a thin section of Basal Carbonates north of Wadi Feiran, which is interpreted to be equivalent with the Carbonate platform south of Wadi Feiran, but had a very restricted dispersal due to the delta deposits coming from the east (Figure 4-4).

Delta deposits

DLC-1, Lower Rudeis and the ASL member have been merged in the restoration process since DLC-1 is interpreted to be deposited simultaneously with both lower Rudeis Formation and the upper Rudeis Formation (ASL member) and therefor there is no clear boundary between them on the eastern side and they were removed as one unit in the restoring process (Figure 4-5).

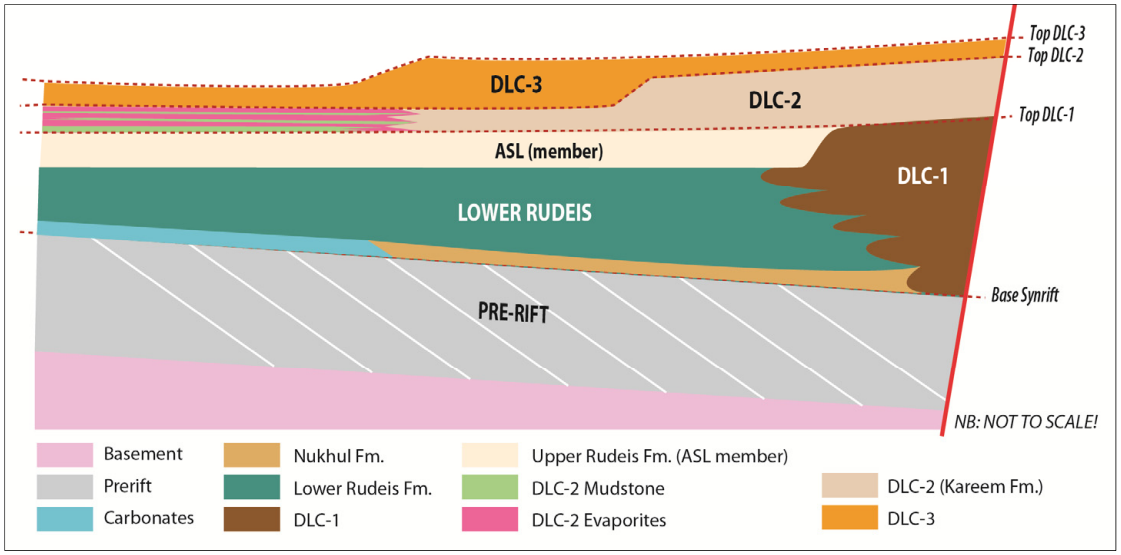

Figure 4-5: The diagram illustrates how the synrift deposits were divided for the backstripping process in this thesis. The figure is not to scale.

The stratigraphic analysis of the top DLC-1 horizon to the base of the synrift gives a maximum thickness of ca. 1000 – 1300 m in cross-section 4 and 5 (Figure 4-4).

DLC-1

Delta Lobe Complex 1, also referred to as a part of the Abu Alaqa Group, has a Burdigalian to Langhian age and consists of coarse-grained delta deposits in the hangingwall of the Baba-Sidri fault. It is made up of multiple fan sequences. The first 3 sequences are coarser, upward-fining, aggradational and only cover an area of up to 2 km^2, the remaining fan sequences are progradational and consist of mixed carbonates/siliciclastics and cover an area of up to 30 km^2 (Gawthorpe et al., 1990). The stratigraphic analysis shows that the foresets beds in the DLC-1 dip at an angle of maximum 20° DLC-1 is only exposed in the immediate hangingwall of the Baba-Sidri fault, south of Wadi Sidri. The Baba-Sidri fault is interpreted to have been active meanwhile DLC-1 was deposited, this is evident in the increased angle of the lower fan sequences, meaning that the older fan-sequences have rotated to an steeper angle compare to the young fan-sequences. The slope break (representing the shoreline at the time) in DLC-1 is located a few 100 m west of the Baba-Sidri fault *(M. Muravchik 2015, pers. Comm.)*. Figure 4-6 is an illustration of the delta reach and includes the interpreted shorelines for DLC-1, DLC-2 and DLC-3.

Lower Rudeis Formation

Has a Burdigalian-Langhian age and marks the change from shallow marine to open marine environment and consists of claystone with sandstone and limestone interbeds (Moustafa, 2004). The Lower Rudeis Formation is exposed from Wadi Sidri, between the Baba-Sidri fault and the Feiran fault southward to the Hadahid monocline, where it onlaps the Mokattam Formation and on the dipslope of the El Qaa syncline a thin section of the Lower Rudeis claystone is exposed. The Lower Rudeis Formation is a thick succession with a large wedge-shape towards the Feiran fault scarp and represent an increase in subsidence rate compare to the Nukhul Formation deposits below, it is present in cross-section 4 to 6 and the thickness was measured to be between 1000-1300 m (See Appendix 2, Figure 8A and Figure 9A).

Upper Rudeis (ASL member)

Has a Burdigalian-Langhian age and marks the boundary between the lower and the upper Rudeis, also representing the "mid-clysmic event" (ca. 17 Ma) which caused a major tectonic rearrangement of the faults to the larger structures seen today. After this event the faults either stopped (died out) or fault activity was remarkable reduced (Moustafa, 1993; Patton et al., 1994). The ASL member consists of sandy limestone and marl and is exposed in the hangingwall of the Feiran fault south past the Wadi Feiran to the Hadahid monocline and there is also a thin section exposed on the dipslope of the El Qaa Syncline (western limb), from south of Wadi Sidri to south of Wadi Feiran.

DLC-2

DLC-2 (Kareem Formation) has a Langhian age and consists of a fine-grained, calcareous sandstone, evaporites and mudstone. The subsidence has diminished remarkable at this time and sediments within the Kareem Formation reflects the unroofing of the prerift units eroded as the footwall was uplifted (Patton et al., 1994; Bosworth and Mcclay, 2001; Moustafa, 2004). The DLC-2 exposed on the eastern limb of the El Qaa half graben is the proximal sandstone unit, towards the western limb, the unit changes into a layered evaporite/mudstone unit. On the eastern limb northwards it is exposed in the immediate hangingwall of the Feiran fault where it juxtaposes Lower Rudeis Formation, the foresets dip at an angle of ca. 15° and the slope break (representing the shoreline at that time) is positioned a few 100 m *(M. Muravchik 2015, pers. Comm.)* west of the Feiran fault (Figure 4-6).

DLC-3

Has a Seravallian age and consists of a lower unit containing mixed carbonates and siliciclastics (Moustafa, 2004). This is the uppermost delta lobe and it is exposed from north of Wadi Sidri to south of Wadi Feiran in the center of the El Qaa half graben and upwards on both the eastern and western limb, south of Wadi Feiran the DLC-3 is only exposed on the western limb. Carbonates formed on the delta front, now represent the top of the DLC-3. The foresets are dipping at an angle of ca. 10° and the slope break (shoreline) is positioned on the western limb of the El Qaa half graben ca. 2-3 km *(M. Muravchik 2015, pers. Comm.)* from the syncline axis (Figure 4-6). There have been found clasts from the Precambrian

Basement within the DLC-3 unit (Garfunkel and Bartov, 1977), these clasts represent the unroofing of the uplifting rift shoulder, seen as a reversal prerift stratigraphy present in the deposited synrift units.

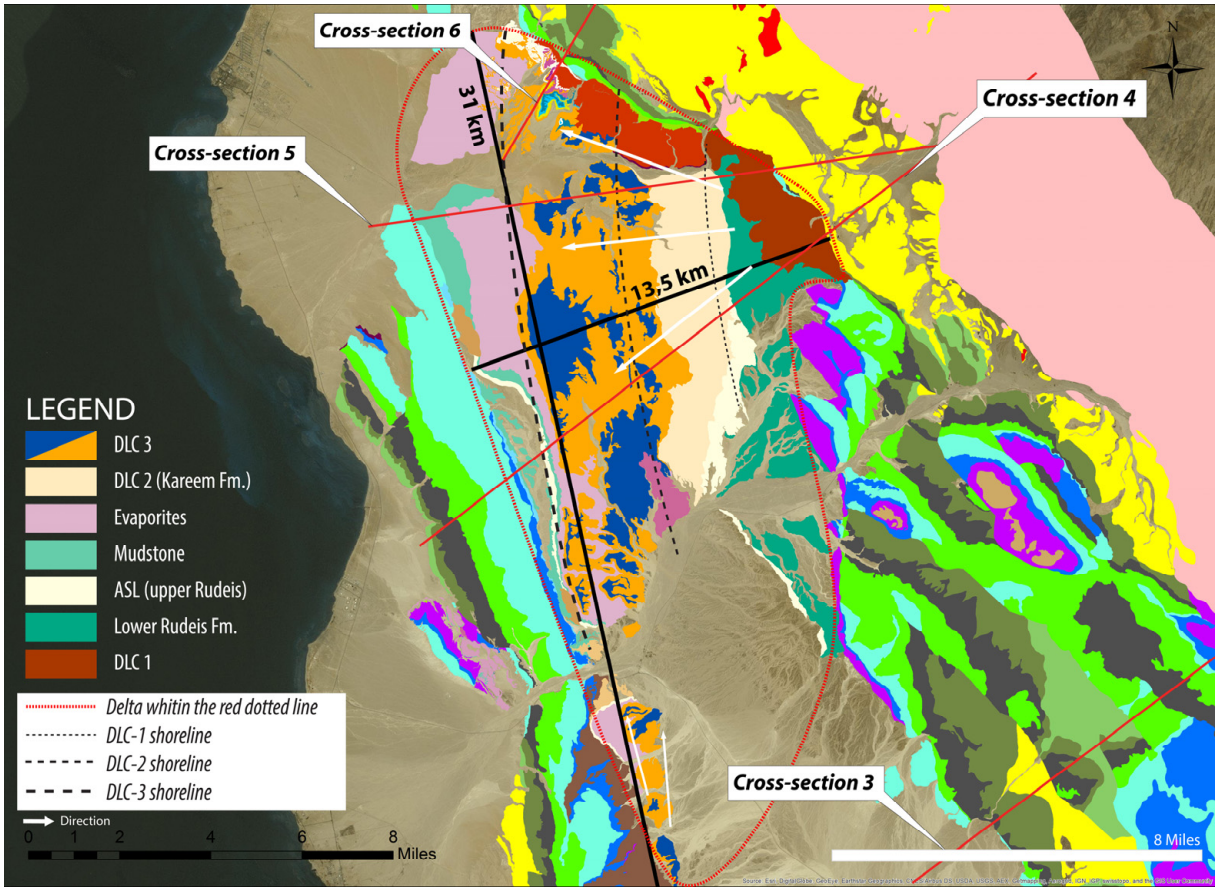

Figure 4-6: Illustrating the deltas, and where the shorelines for DLC-1, DLC-2 and DLC-3 are interpreted to be located (See the dashed lines in the Legend). The Deltas extends approximately 31 km in width and 13,5 km in length towards the Nezzazat fault in the west.

4.2 Present day structural styles of the El Qaa fault block

4.2.1 Rift boundary faults

The El Qaa fault block is bounded by large normal faults striking NW to NNW and dipping 65° down-to-the-west (Figure 4-7). To the west the basin is bound by the CFB (Coastal fault belt)

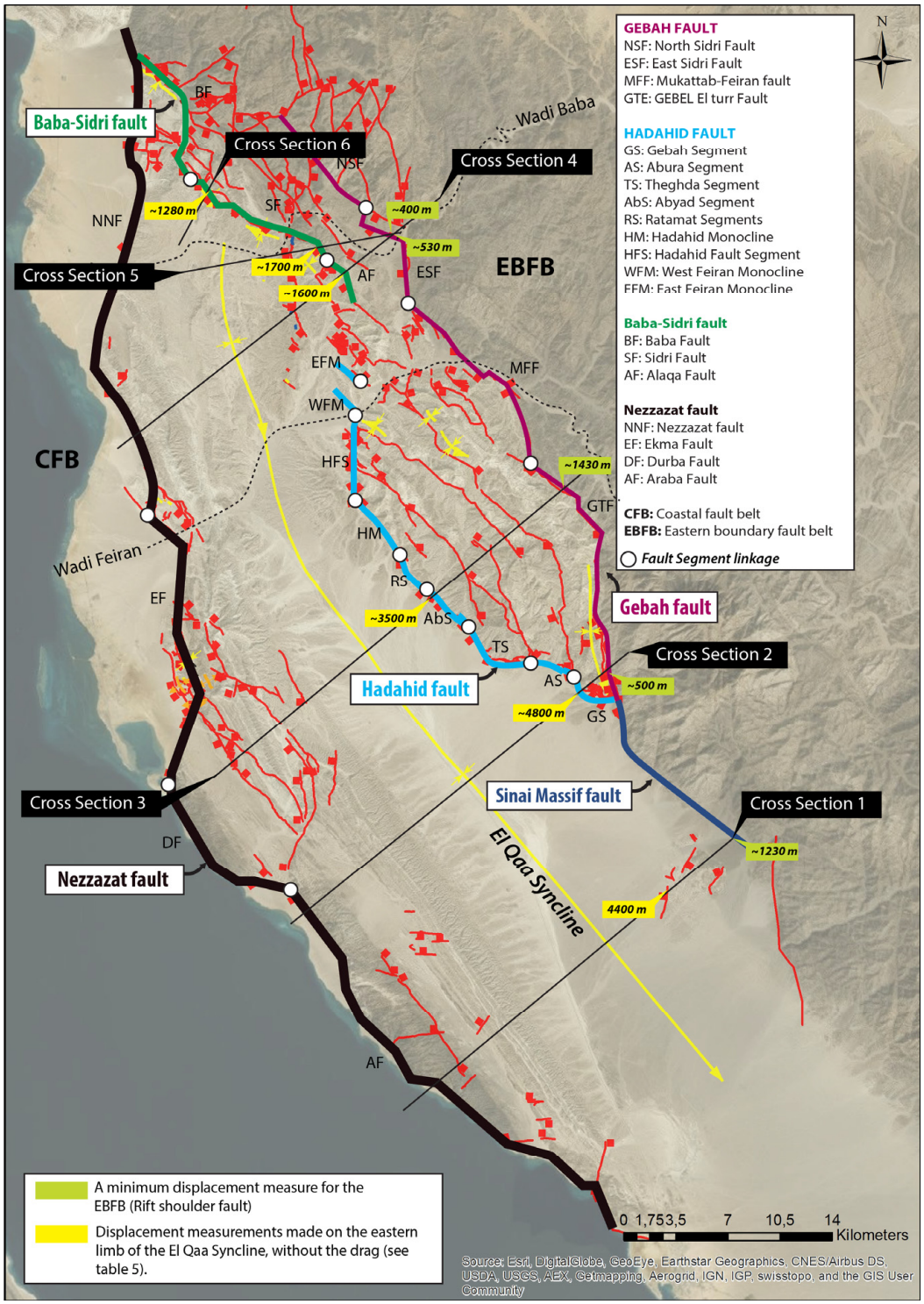

Figure 4-7: Mapped faults in the El Qaa fault block. The faults in the CFB and EBFB are highlighted and given different colours, the fault segments are also included along with the segments boundaries.

which contains the NW-striking Nezzazat fault, which includes the fault segments, from the north, The Nezzazat fault, Ekma fault, Durba fault and the Araba fault, the linkage of these fault is described further in the transect of cross-section 3. For the CFB there are no constrains on the displacement in this thesis due to the lack of offshore data. The eastern boundary is the Eastern Boundary Fault Belt (EBFB), which contains the Baba-Sidri fault, the Gebah fault, Hadahid fault/monocline and the Sinai Massif fault, only Precambrian basement is exposed on the rift shoulder, and the absolute minimum displacement was estimated to between 400 – 1430 m (see table 3). The Hadahid fault contains 8 segments which are from the south: The NNW-SSE to WNW-ESE striking Gebah Segment (GS), WNW-ESE striking Abura Segment (AS), WNW-ESE to NW-SE striking Theghda Segment (TS), NW-SE striking Abyad Segment (AbS), NNW-SSE striking Ratamat Segment (RS), NW-SE striking Hadahid Monocline (HM), N-S striking Hadahid Fault Segment (HFS) and the NW-SE striking Feiran Monoclines FM (west and east), see Figure 4-7 for location of the fault segments.

Table 3: Minimum displacement measurements for the EBFB (rift shoulder)

Cross-sections nr.	1	2	3	4	5	6
Displacement for EBFB (m)	~1230	~500	~1430	~530	~400	~1280

Table 3: Minimum displacement-measurements from the EBFB (rift shoulder). For cross-section1 it is the Sinai Massif fault, for cross-section 2 to 5 it is the Gebah fault and cross-section 6 it is the Baba-Sidri fault.

The main faults that dominate the study area have a NW-SE and NNW-SSE strike orientation and are linked by shorter faults with NNE-SSW, E-W and N-S strike orientation, generating a zig-zag pattern. The El Qaa fault block developed as the CFB and EBFB rotated towards the east, causing a large syncline to develop in the centre of the block, the El Qaa syncline has a very long, low-gradient western limb and a short, steep eastern limb. The dip-angle of the prerift stratigraphic units in the western limb increases southward, in the plunge direction, from ca. 9-10° in cross-section 5 to ca. 17° in cross-section 1. The synclines axis exact position below the Quaternary sediments is not known, but was estimated in the construction of cross-sections in this thesis. In the next section the results based on the 6 constructed cross-sections starting south are described in detail.

4.2.2 Cross-section 1 transect

Cross-section 1 strikes in a SW-NE direction, is ca. 28 km long and crosses the Sinai Massif fault (EBFB) towards the east and the Araba block towards the west. The displacement on

the rift shoulder is estimated to be minimum 1230 m. Due to the burial of strata and lack of data on the easternmost block towards the Sinai Massif fault, the block was simplified for the interpretation of cross-section 1 (Figure 4-9A). Displacement on the fault on the eastern limb in the El Qaa half graben is estimated to be ca. 3000 m with the drag and ca. 4400 without, which is the largest displacement for the six cross-sections. Since the El Qaa syncline is plunging towards the south, the largest displacement was as expected to be in cross-section 1 along with the steepest angle on the prerift stratigraphic units, which are dipping at ca. 17° in cross-section 1. On the dipslope the Qabeliat Formation (carbonate platform) is exposed and lies unconformably over the eroded prerift Thebes Formation, but northward it lies unconformably over younger prerift units, such as the Darat Formation, The Qabeliat Formation thickness increases northward towards the Wadi Feiran. North of Wadi Feiran it is replaces with a thin section of basal Carbonates, which are interpreted to have been deposited simultaneously as the Qabeliat Formation (Figure 4-8). West of the Nezzazat fault there is a small sub-block in the immediate hanging wall, where the Raha Formation is exposed and the minimum displacement was measured to be 800 m. See full restoration of cross-section 1 in Appendix 2, figure 4 A-D.

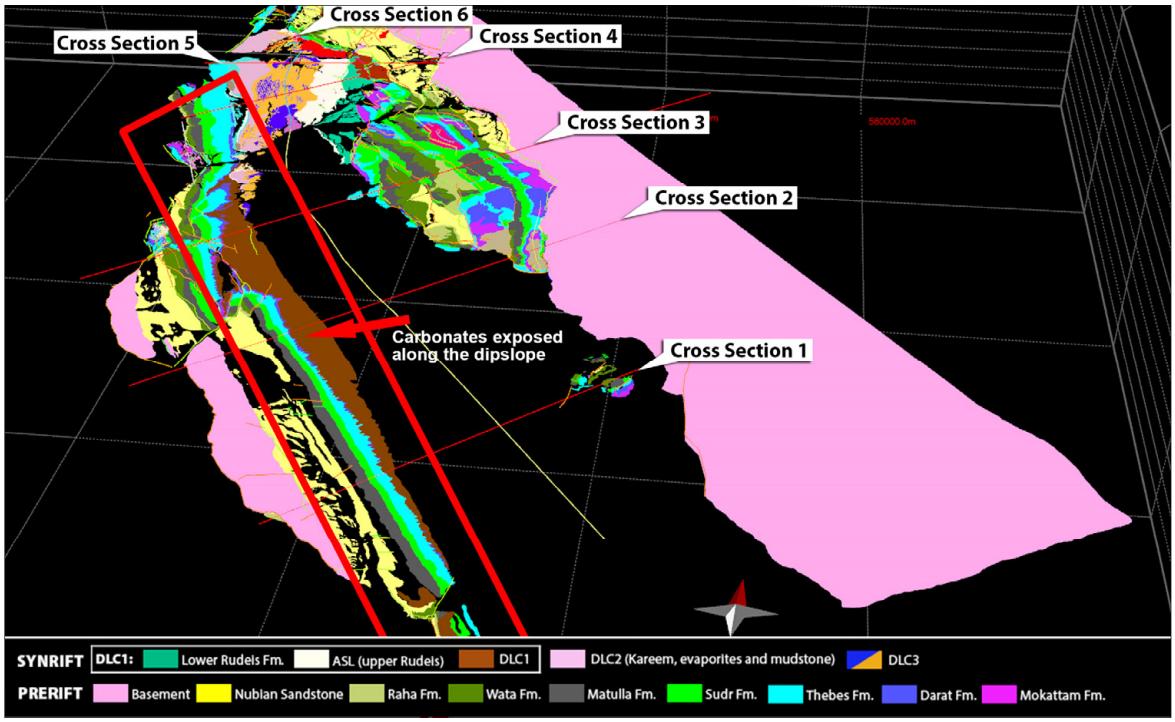

Figure 4-8: Carbonate platform deposited on the dipslope of the El Qaa Half graben, it is thickest south of Wadi Feiran and thins southwards. The red box show where the carbonates are exposed.

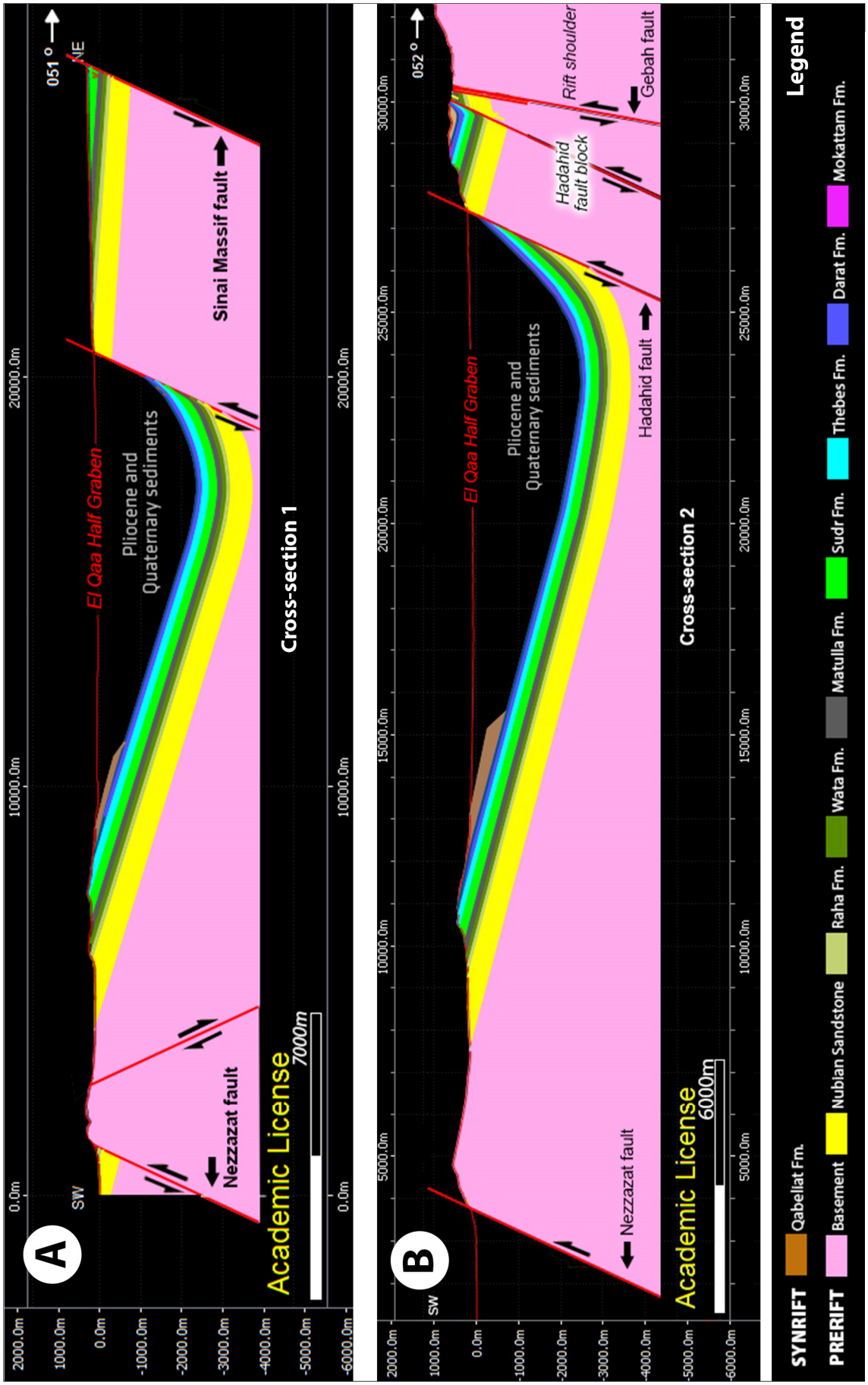

Figure 4-9: (A) Interpreted cross-section 1, Nezzazat fault on the western side and Sinai Massif fault on the eastern side with the El Qaa half graben in the centre. (B) Interpreted cross-section 2 crossing the Hadahid Fault block to the east and the Araba fault block to the west and the El Qaa half graben in the centre. See location for cross-section in Figure 4-7.

4.2.3 Cross-section 2 transect

Cross-section 2 strikes in a SW-NE direction, is ca. 44,8 km long and crosses the southern end of the Hadahid fault block towards the east and the Araba block towards the west (Figure 4-9B). The rift shoulder at this location has a minimum displacement of ca. 500 m (see table 3 on page 61) and the fault juxtaposes the Precambrian Basement in the footwall against the Nubian Sandstone in the hangingwall. The easternmost sub-blocks is dipping 4° towards the west, and the dip increases in the sub-blocks closer to the small syncline up to 14° towards the west, illustrated on the eastern side in Figure 4-10.

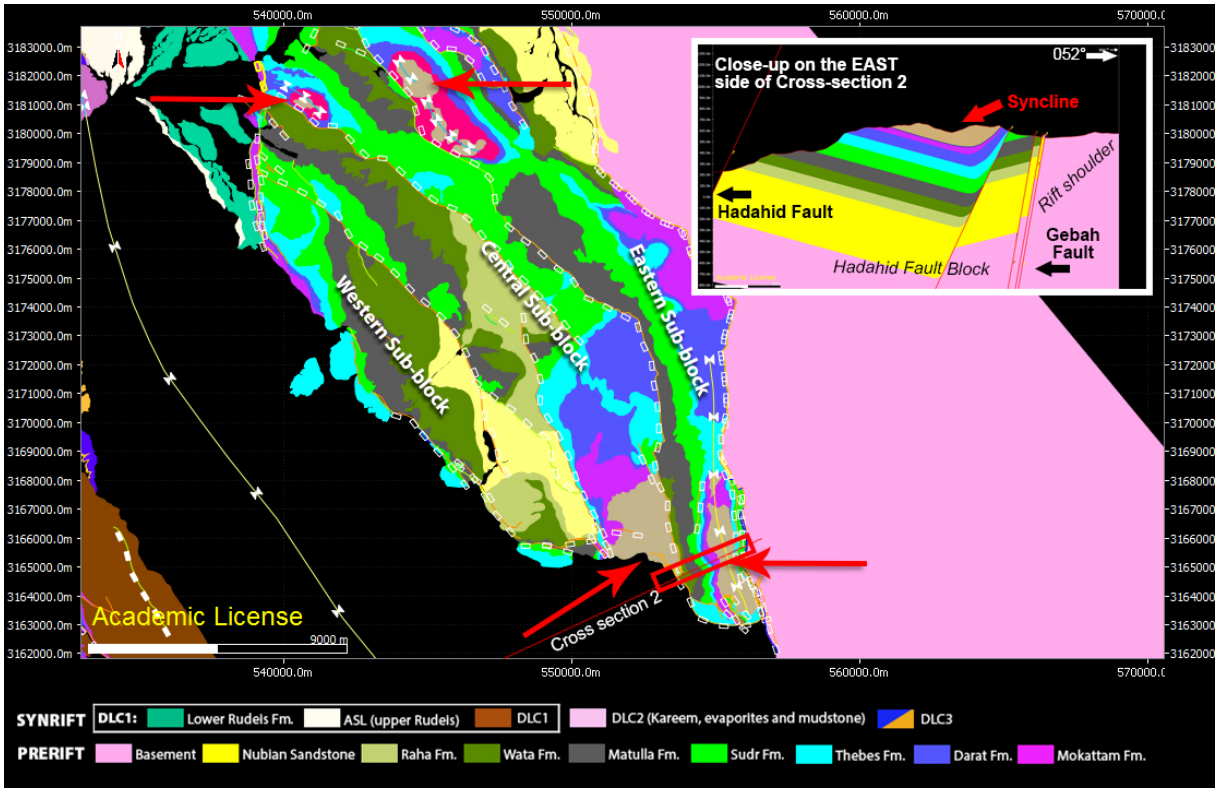

Figure 4-10: Hadahid Fault Block, red arrows point to where the Nukhul Formation is exposed. The syncline shown in the close-up of the west side of cross-section, notice the dragged Nukhul Formation Notice the division of the Hadahid block into 3 main sub-block, the Eastern Sub-block, the Central Sub-block and the Western Sub-block.

The Hadahid fault block has been divided into the 3 main sub-blocks, the Eastern sub-block, the Central sub-block and the Western sub-block (Moustafa and El-Raey, 1993) see Figure 4-10 for the location of the Sub-blocks. Cross-section 2 only crossest the Eastern Sub-block and therefor lacks the large overall monocline structure seen further north in cross-section 3 (which is described in detail in the following section). Instead there is a syncline structure in the western sub-block and a smaller anticline structure towards the rift shoulder (see close-up in Figure 4-10). In the center of the syncline the Nukhul Formation is deposited and

dragged along the eastern limb, which indicates that this fault was active and the displacement increased after the Nukhul Formation was deposited. The displacement in the small syncline is ca. 360 m with the drag and ca. 460 m without (Figure 4-10). There are thickness variation in the Thebes, Sudr and Matulla Formations when comparing the west side with the east side, the largest difference was in the Sudr Formation that was ca. 200 m on the western side and 140 m on the eastern side, located in the syncline, this could be due to parallel slip and shearing within the unit caused by the deformation.

The Nukhul Formation is exposed on 4 different locations on the Hadahid fault block, always right above the Mokattam Formation, which is considered to be the last prerift deposition (Figure 4-10). In all four location it is present in the center of a syncline, indicating that there where small displacement faults present at the rift initiation phase at this location and that the Nukhul Formation was deposited in small isolated basins in shallow water. For cross-section 2 the restoration for the base of the synrift can be seen in Figure 4-11A. There are no prerift units exposed in the immediate hangingwall of the Hadahid fault in the El Qaa half graben, the displacement was estimated to be 1400 m with the drag and 4850 m without (table 5 on page 75). In the dipslope of cross-section 2 the prerift units are dipping at an angle of ca. 15° and the dip increases southward towards cross-section 1 where it is ca. 17°. On the dipslope the Qabeliat Formation lies unconformable over the prerift units which were rotated to an angle of ca. 4° prior to the deposition of the Qabeliat Formation and causing the angular unconformity between prerift units and the base-synrift (this is described further in part 5.1 Tectonic evolution of the El Qaa fault block on page 80). The prerift units exposed on the dipslope are, a thin section of the eroded Darat Formation, Thebes, Matulla, Raha, Wata Formations, Nubian Sandstone and the Precambrian Basement in the immediate footwall of the Nezzazat fault. See the full restoration for cross-section 2 in Appendix 2, figure 5 A-D.

4.2.4 Cross-section 3 transect

Cross-section 3 strikes nearly SW-NE is ca. 49 km long and crosses the Hadahid Fault Block through all three sub-blocks in the east and the Durba block towards the west (Figure 4-11B).

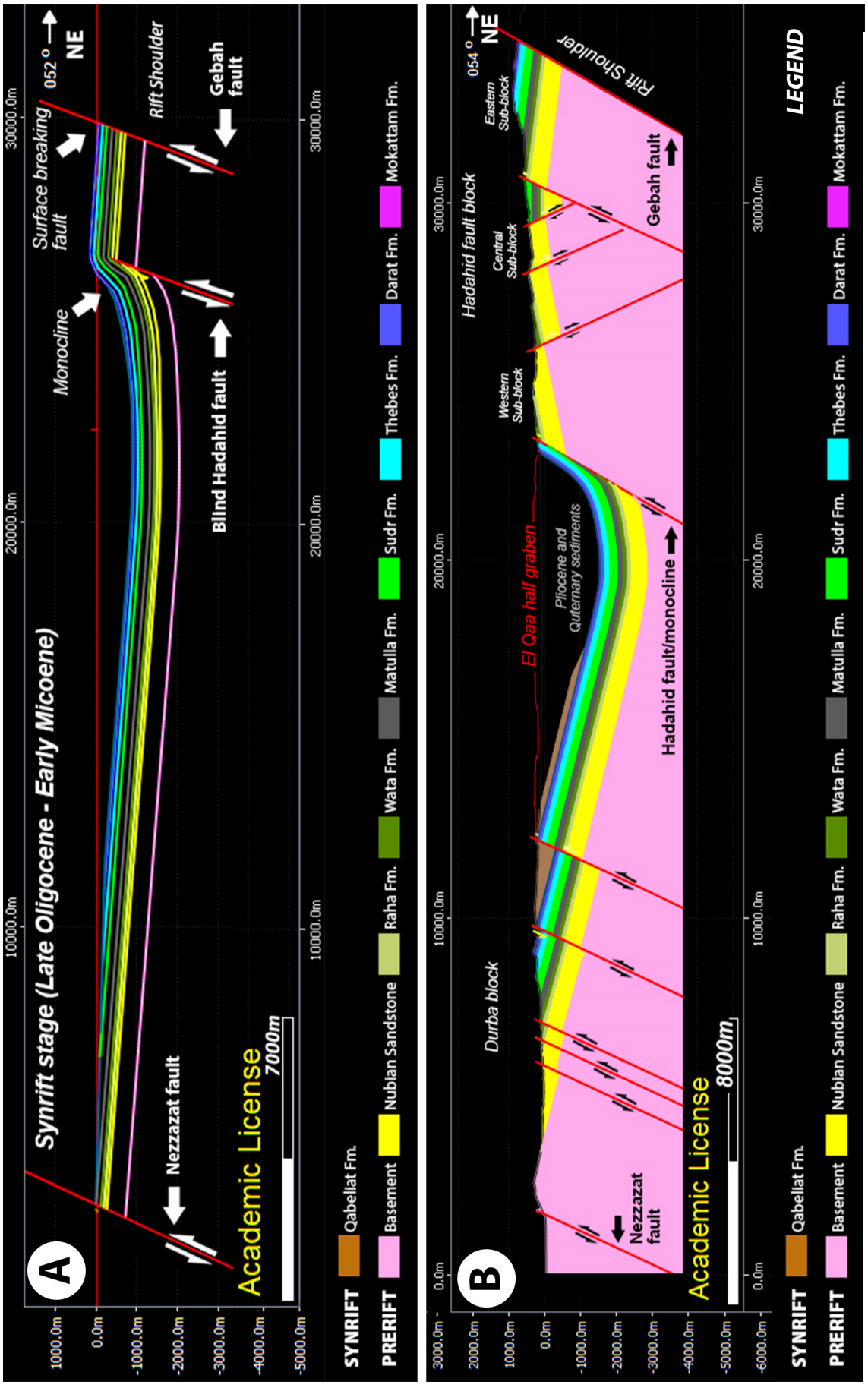

Figure 4-11: (A) Restoration of cross-section 2, backstripping to the base of the synrift sediments, notice the blind Hadahid fault with the monocline above. See the entire restoration for cross-section 2 in the Appendix 2, figure 5 A-D. (B) Interpreted cross-section 3. The Hadahid Fault Block in the eastern side, the El Qaa Half graben in the middle and the Durba block on the western side. See location for cross-section 2 in figure 4-7.

The rift shoulder faults displacement in cross-section 3 is larger compare to cross-section 2, it is estimated to be minimum 1430 m and the fault juxtaposes Precambrian basement in the footwall with Mokattam Formation in the hangingwall. The Hadahid fault block makes up the eastern area in cross-section 3 and it crosses all three Sub-blocks, the Eastern, Central and the Western Sub-blocks which together form large anticline-structure in the Hadahid fault block (Figure 4-12). Displacement in the three Sub-blocks ranges from 120-540 m, the Eastern Sub-block is the only block dipping down towards the east at an angle of ca. 7° in cross-section 3 and ca. 14° in cross-section 2, this dip is likely related to the movement (increased displacement) on the Rift Shoulder fault, causing the easternmost block to rotate towards the east as a result to the fault block rotation. The Central Sub-block starts in the east with an almost horizontal block that lays ca. 428-460 m lower than the surrounding blocks, the following blocks show an increased westerly tilt angle towards the Hadahid fault from 8° to 12° in the Western Sub-block (Figure 4-12).

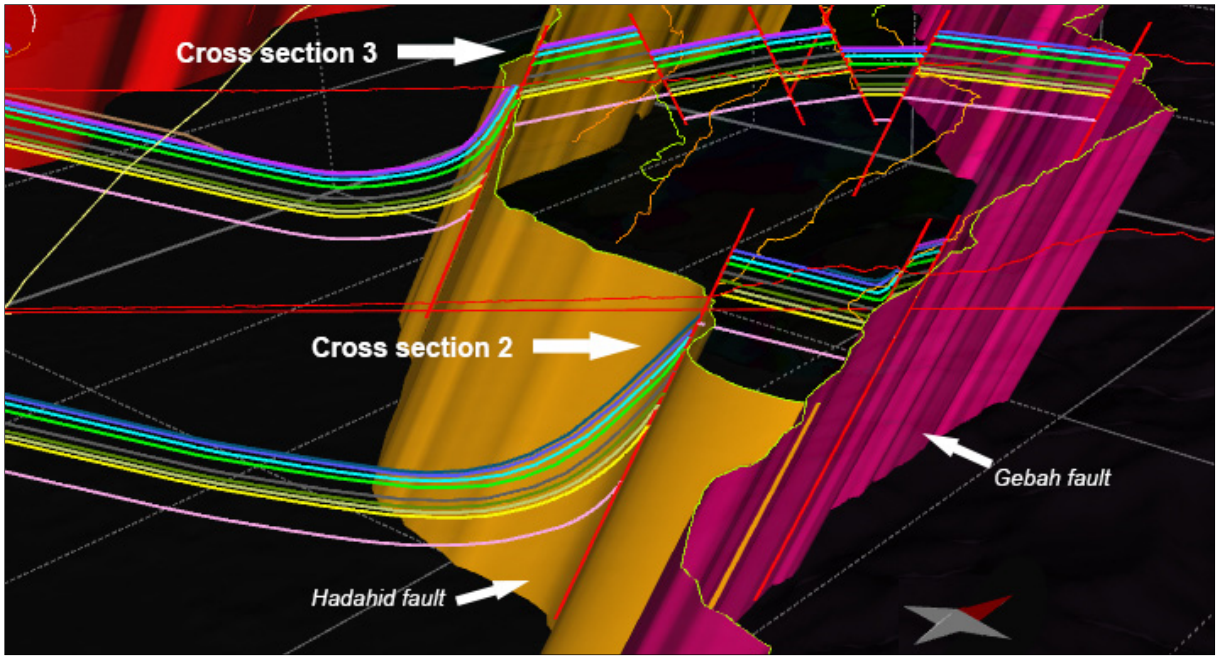

Figure 4-12: The Hadahid block in 3D, The Gebah fault (pink), Hadahid fault/monocline (orange), notice the anticline shape of the smaller blocks in the Hadahid fault block in cross-section nr. 3.

The large anticline structure seen in the Hadahid fault block originated from the monocline caused by the initial blind Hadahid fault. The upward migration of the blind fault tip caused a monocline to develop in the more ductile sedimentary units above, and as the fault tip migrated upwards the footwall uplift and hangingwall subsidence increased, causing the

monocline to tighten and the limb to rotate to a steeper angle (Sharp et al., 2000b). Figure 4-13 shows a small area of the Hadahid fault/monocline north and south of cross-section 3, the dip data along the Hadahid footwall has an overall increase in dip-angle from 10° to 70-80° and an overall decrease in dip from south to north on the footwall edge, which is expected in the transition from the surface breaking Hadahid fault to the Hadahid monocline. There are displacement variations along the Hadahid fault/monocline, due to the displacement variations on each of the segments present before linkage, but from south to north along the Hadahid fault/monocline there is an overall decrease in dip angle of the stratigraphic units, interpreted as the transition from a surface breaking faults towards a monocline in the north.

The El Qaa half graben is located in the area west of the Hadahid block. The eastern short and steep limb of the El Qaa syncline is located in the hangingwall of the EBFB. Figure 4-14 shows a 3D model, containing the interpreted cross-sections 1 to 6 and the four main border faults, the Nezzazat fault (red), Gebah fault (pink), Hadahid fault/monocline (orange) and the Baba-Sidri fault (green). The syncline form is clearly visible in the 3D model and in the immediate hangingwall of the Hadahid fault/monocline the Thebes Formation is exposed in some places along the fault, but most of the sediment on the east side of the El Qaa half graben is buried under Quaternary sediments. The strata is expected to be dragged along the fault scarp as a result of the increased displacement on the EBFB, this prevents the exact displacement value for the Hadahid fault from being measured, but from the interpreted cross-sections, the displacement has been estimated, both with dragged strata up the footwall scarp and without (the horizons were straightened out towards the footwall-scarp with the same angle as the dipslope), this does not give a correct value, but can give a maximum displacement possible, all measurements were made for the top of Sudr Formation and are presented in table 5 on page 75 and show an overall decrease in displacement northward from 3000 m for cross section 1 to only 700 m in cross section 5, which is located south of Wadi Sidri. Without the drag the displacement decreases from 4400 m in the south to 1200 m in the north. This data also fits the trend in the dipping-angle of the prerift units on the dipslope, which decreases northward from 17° in cross-section 1 to ca. 10° in the cross-section nr. 5 (see table 4 on page 74).

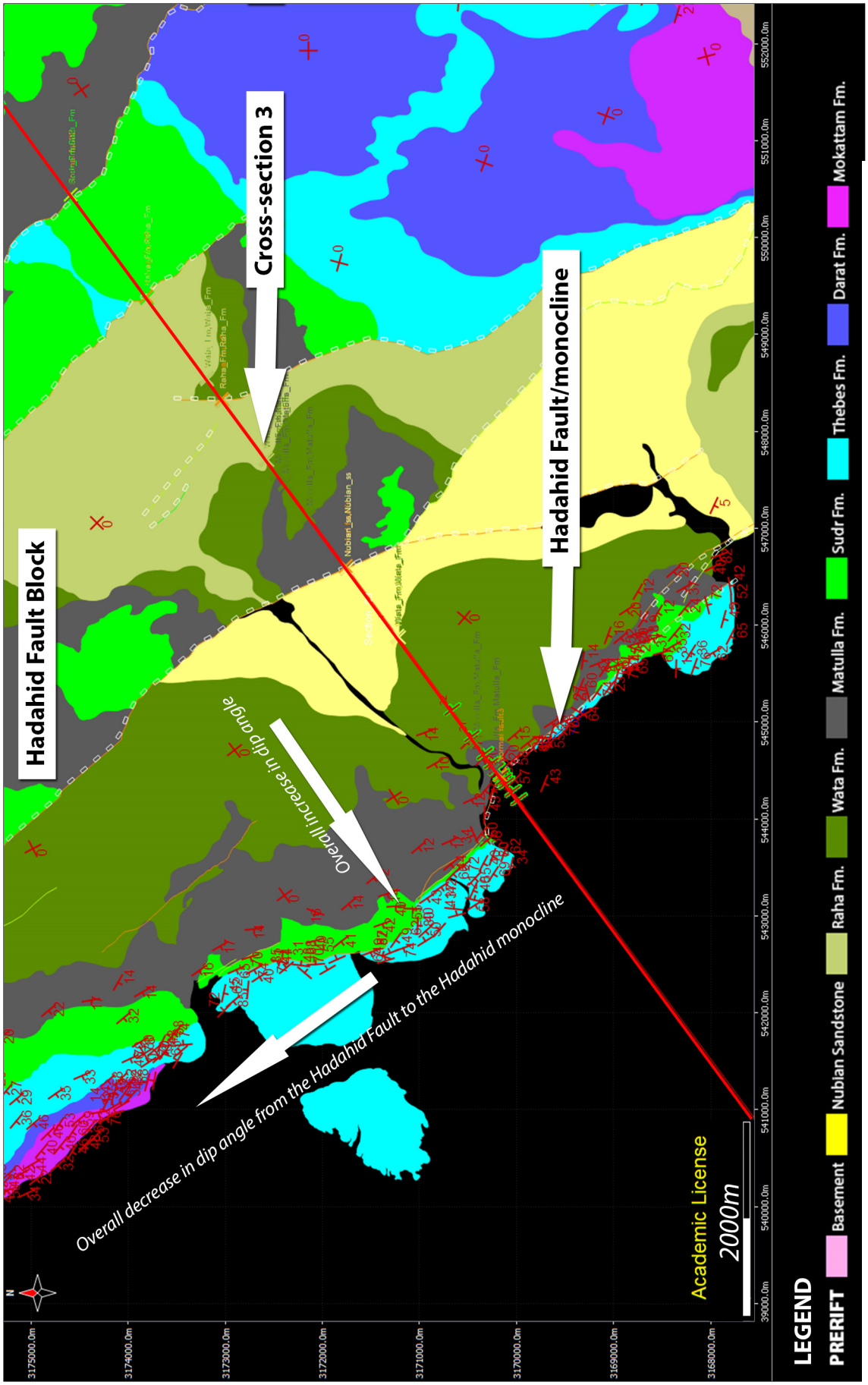

Figure 4-13: Dip data near cross-section 3 (red line). The dip varies along the fault segments in the Hadahid fault/monocline, but overall it increases from 0-10° to as much as 70-80° and an overall decrease is seen from south to north on the Hadahid fault.

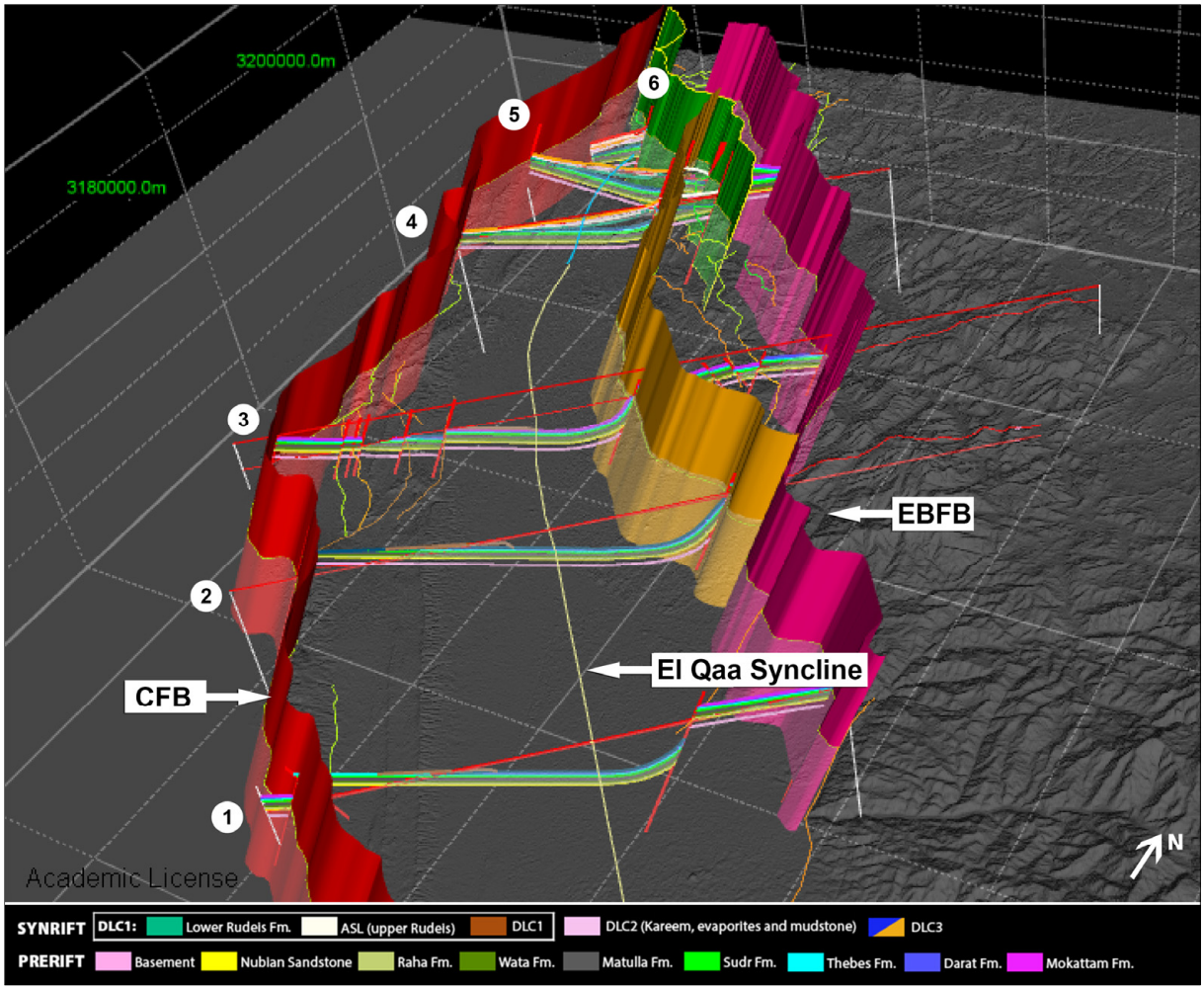

Figure 4-14: 3D model including all the interpreted cross-sections 1 to 6 and the 4 main border faults, red: Nezzazat fault, Pink: Gebah fault, Orange: Hadahid fault/monocline and the green: Baba-Sidri fault. Notice the large syncline developed in the immediate hangingwall EBFB. Numbers 1 to 6 are the cross-sections.

Towards the Nezzazat fault, cross-section 3 goes through a more complex structural area located in the Ekma and Durba blocks. The Durba block lies south of the Ekma block and north of the Araba block and the blocks are divided by NNE striking transfer fault, which splays into numerous smaller faults with dip angles ranging from 55° to 76° (these where constructed in this thesis with an angle of 65°). These faults start out as transfer faults but eventually change direction and become rift-parallel faults and is also referred to as a "horsetail splay" (McClay and Khalil, 1998). The same is seen for the division of the Durba block and the Ekma block, the transfer fault shows the same horsetail splay (Figure 4-15). To the west the Qabeliat Formation is found in several fault blocks, indicating that these faults where active after the Qabeliat Formation was deposited. South of cross-section 3 in the western part past the Durba block is the less complex Araba block, where cross-section 2 transects. On the eastern side, in the Hadahid fault block, the Gebah fault and the Hadahid

fault merge into the Sinai Massif fault, south of cross-section 2. See the restoration steps for cross-section 3 in Appendix 2, figure 6 A-D.

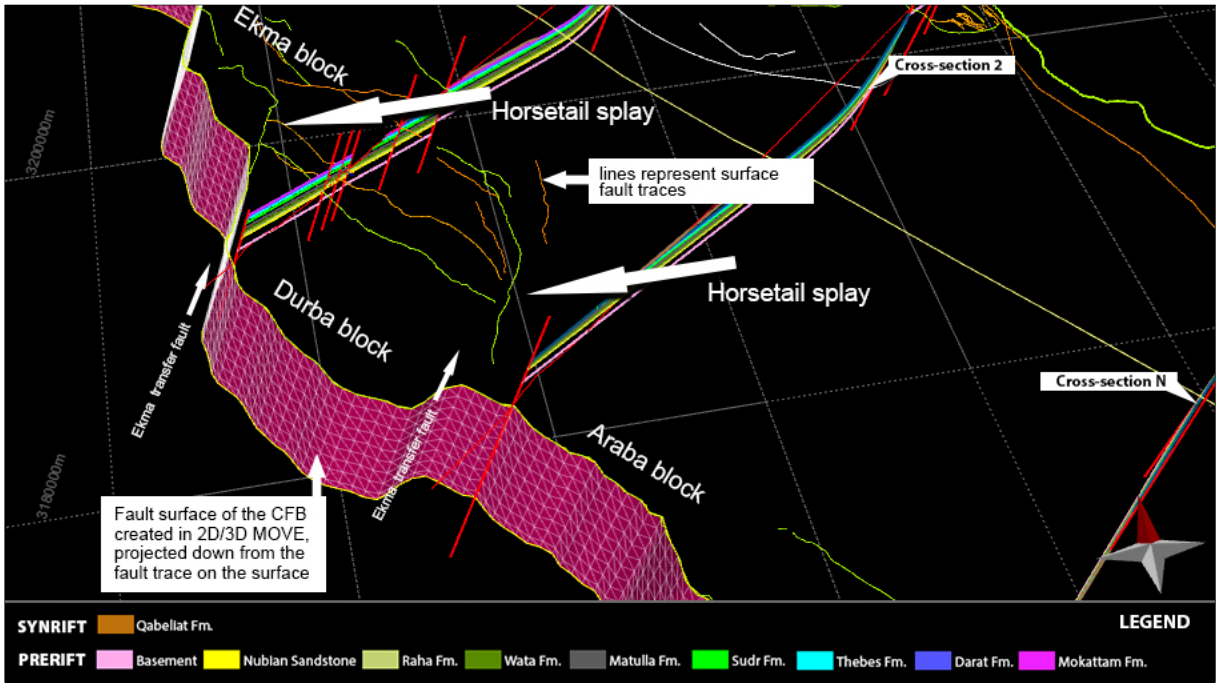

Figure 4-15: CFB, horsetail splay from the Transfer faults diving the Araba block, Durba block and the Ekma block on the western border.

4.2.5 Cross-section 4 transect

Cross-section 4 strikes in a SW-NE direction, is ca. 29 km long and crosses both the Baba-Sidri fault and the Feiran fault. The strata in the rift shoulder dips at an angle of ca. 1° towards the east (Figure 4-16A). Only Nubian sandstone is exposed in the Baba-Sidri footwall and is juxtaposed against the DLC-1 in the Baba-Sidri hangingwall. The displacement at this location is 1070 m. Southward along the Baba-Sidri fault the overall displacement is decreasing towards the Wadi Feiran transfer zone. Due to the lack of exposure of the prerift strata between the Baba-Sidri fault and the Feiran fault below the delta deposits, the dip of the prerift units have been interpreted based on previous cross-sections constructed by (Garfunkel and Bartov, 1977; Moustafa, 1993; Moustafa, 2004) and the prerift bedding-dip was set to dip ca. 6-7° towards the west. This westerly dip is interpreted to be caused by the monocline generated in the early rifting phase. The displacement on the Feiran fault is estimated to be 1000 m with the drag and 1630 m without (see table 3 on page 61), and it juxtaposes Lower Rudeis Formation in the footwall against DLC-1 in the hangingwall, which indicates that Feiran fault was active during and possibly after the delta lobes where deposited.

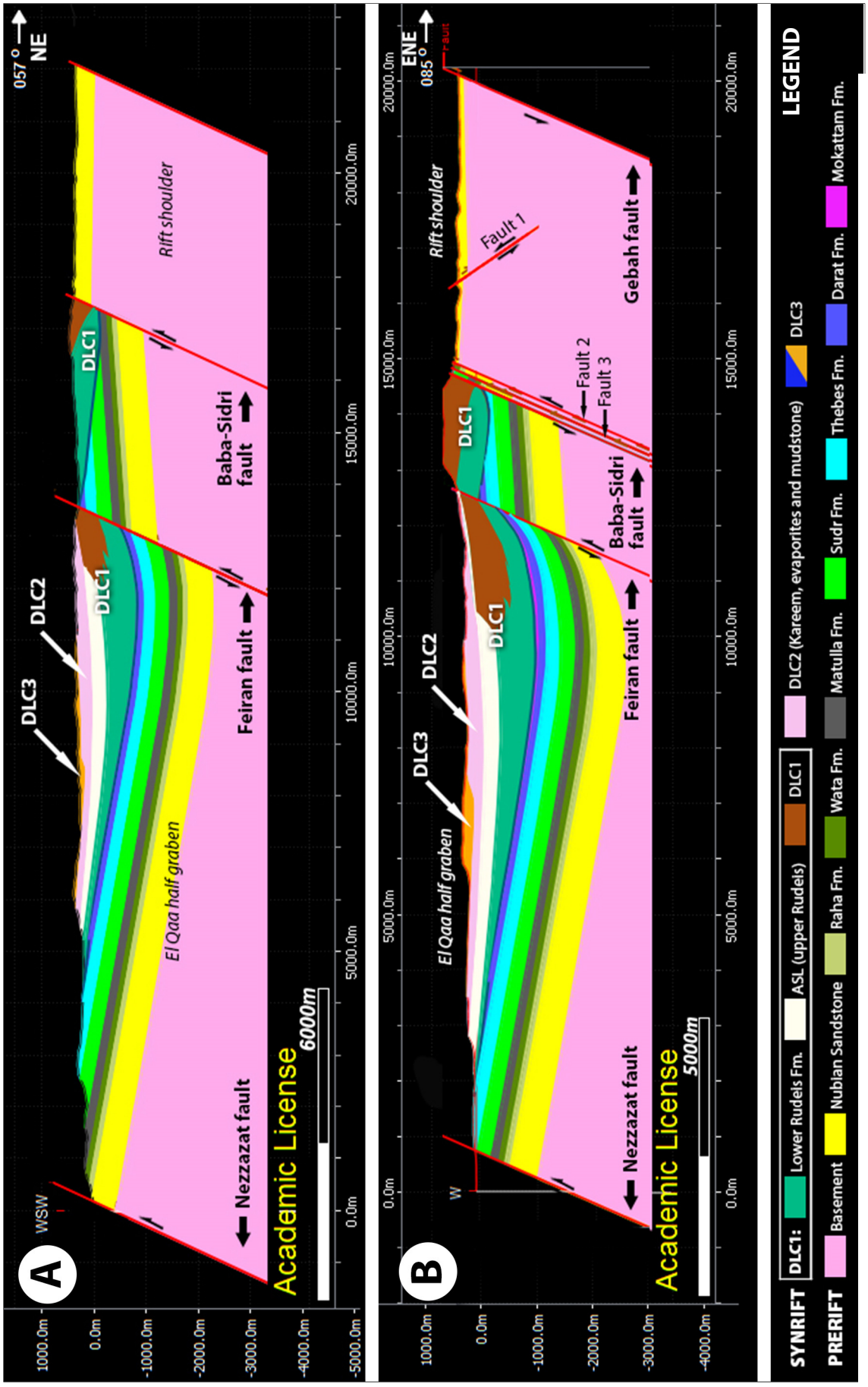

Figure 4-16: (A) Interpreted cross-section 4, Nezzazat fault towards the west and the rift shoulder to the east.(B) Interpreted cross-section 5, Nezzazat fault towards the west and the rift shoulder to the east. Legend applies to both A and B. See location for cross-section 4 in figure 4-7.

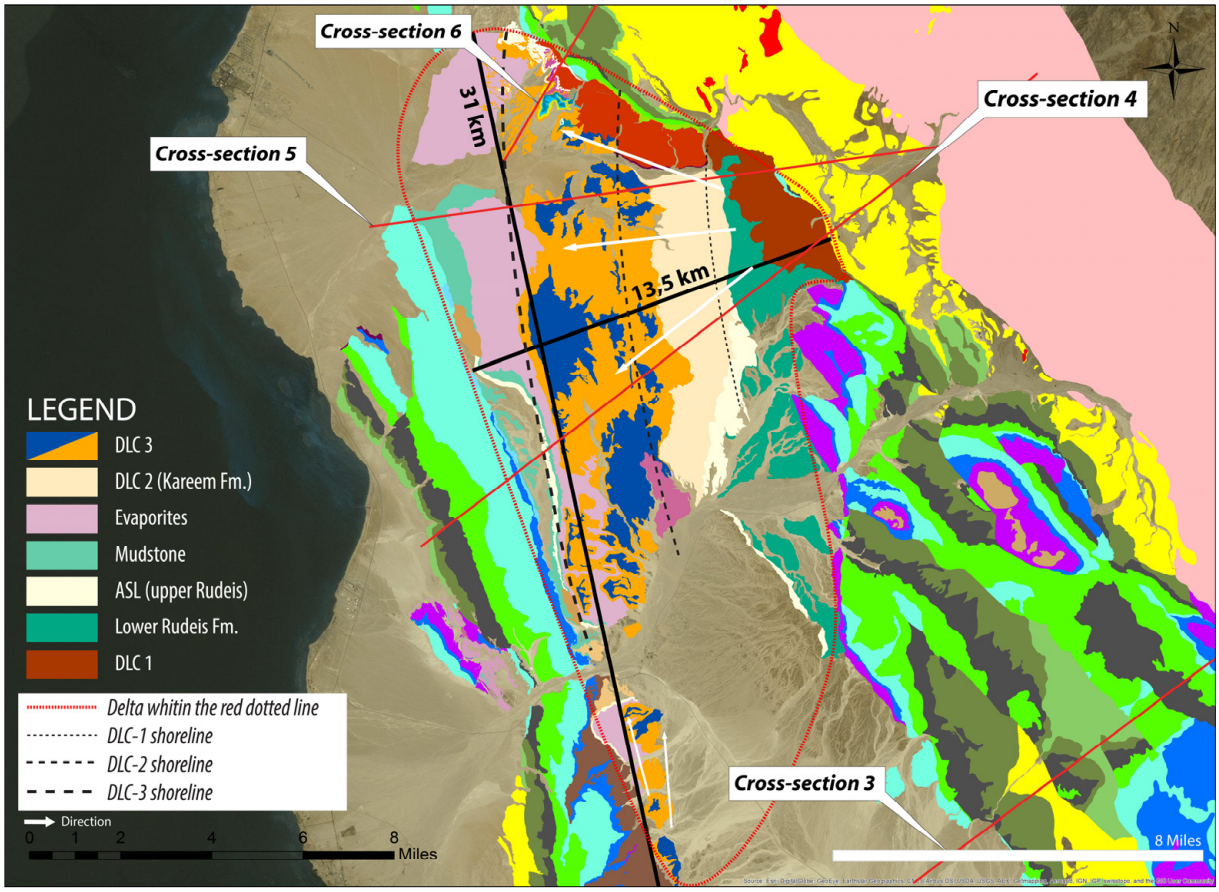

Figure 4-17: Map view of the Delta deposits, red dotted line shows the minimum extend of the delta and the black dotted line shows the extend of the delta minimum length and width.

In the El Qaa half graben the delta deposits are exposed on the eastern limb and partly up the dipslope on the western limb. In the immediate hangingwall of the Feiran fault the exposed units are the DLC-1 whose foresets dip at an angle of max. 20°, the DLC-2 whose foresets dip at an angle of ca. 15° and DLC-3 which lies in the center of the syncline reaching north of Wadi Sidri and south of Wadi Feiran, where it can be found on the dipslope towards the Carbonate platform. The foresets in DLC-3 are dipping between 10-12° and the top is recognized as carbonates that formed on the delta front *(M. Muravchik 2015, Pers. Comm.).* Further up the dipslope a thin section of the Basal Carbonates are exposed before the prerift units, it has been interpreted to be deposited simultaneously as both the delta deposits (DLC-1, 2 and 3) and also Qabeliat Formation which is exposed south of Wadi Feiran and present in cross-sections 1, 2 and 3. West of the Basal Carbonate unit prerift stratigraphic units are exposed, first the partly eroded Darat Formation, then the Thebes, Sudr, Wata, Matulla, Raha and the Nubian Sandstone Formations. Prerift units at this location are dipping ca. 10-11° towards the east (see table 4 on page 74).

Table 4: Dip angle of the prerift sediments on the dipslope in cross-section 1 to 5.

Cross-sections nr.	1	2	3	4	5
Dip-angle (east)	~17°	~15°	~14°	~14°	~10°

Table 4: Dipping angles of the prerift stratigraphic units exposed on the El Qaa dipslope. Notice the decrease from south in cross-section 1 northward to cross-section 5.

The large delta recognized in cross-section 4, 5 and 6 reaches minimum 31 km from north of Wadi Sidri to south of Wadi Feiran and minimum 13,5 km from the Baba-Sidri fault towards the Nezzazat fault (Figure 4-17). The drainage system derived from the uplifting rift shoulder fed the delta and the sedimentary entry point is interpreted to be located near the linkage of two fault segments within the Baba-Sidri fault, the Sidri fault and the Alaqa fault, respectively. The area between where the Gebah fault and the Baba-Sidri fault overlap is interpreted to be a low-gradient transfer zone, which typically form large catchment areas and thereby also larger fans entering the basin (Gawthorpe et al., 1990). See restoration steps for cross-sections 4 in Appendix 2, figure 7 A-F.

4.2.6 Cross-section 5 transect

Cross section 5 strikes in a nearly W-E direction, is ca. 21 km long and crosses both the Baba-Sidri fault and the Feiran fault, the latter being splayed off the Baba-Sidri fault (Figure 4-16B). Towards the east the Gebah fault has a minimum displacement of ca. 400 m. Bedding in the hangingwall of the rift shoulder is relative horizontal, tilting at an angle of ca. 1° towards the west, the second sub-block tilts at 3° towards the east and the displacement between these two blocks is ca. 120 m. There are 2 close faults (Figure 4-16B) in the immediate footwall of the Baba-Sidri fault, fault 2 juxtaposes Nubian Sandstone in the footwall against Matulla Formation in the hangingwall, has a displacement of ca. 670 m and the bedding in its hangingwall is tilted 12° towards the east. Fault 3 juxtaposes the Matulla Formation in the footwall against the Thebes Formation in the hangingwall, has a displacement of ca. 420 m and the bedding in its hangingwall is tilted 28° towards the east. The Baba-Sidri fault juxtaposes the Thebes Formation in the footwall against the DLC-1 in the hangingwall and has a ca. 820 m displacement. The exposed deposits in the area between the Baba-Sidri fault and the Feiran fault only contains delta deposits (DLC-1), the prerift units are not exposed and are interpreted based on previous cross-sections constructed by Garfunkel and Bartov (1977); Moustafa (1993); Moustafa (2004) and the prerift bedding-dip

was set to dip ca. 6-7° towards the west. The immediate hangingwall of the Feiran fault forms the steep, short eastern limb of the El Qaa half graben and due to the westerly dipping strata in the Feiran fault footwall, the fault is interpreted to have started as a blind fault with a monocline developed above its upward migrating fault tip. The stratigraphic units in the eastern limb of the El Qaa half graben are expected to be dragged up the fault scarp due to increasing displacement and rotation of the main border faults. Lack of data on the dragged prerift sediments makes it impossible to measure an exact displacement, but the displacement was estimation both with the drag and without as in the other cross-sections (see table 5) which shows an overall decrease in displacement northward from 3000 m for cross section 1 to only 700 m in cross section 5, which is located south of Wadi Sidri. Without the drag the displacement decreases from 4400 m in the south to 1280 m in the north. This data also fits the trend in the angle of strata in the dipslope, which decreases northward from 17° in cross-section 1 to ca. 9-10° in cross-section nr. 5 (see table 4 on page 74). The Feiran fault displacement was estimated with and without the drag to be ca. 500 m and ca. 1580 m without.

Table 5: Displacement measurements made on the eastern limb of the El Qaa Syncline

Cross-sections nr.	1	2	3	4	5	6*
With drag (m)	~3000	~1400	~900	~1000	~700	-
Without drag (m)	~4400	~4800	~3500	~1600	~1700	~1280

*Table 5: Displacement-measurements taken from the EBFB hangingwall. *cross-section 6 is in another direction and much shorter than the other five and therefor there is no noticeable drag of strata in cross-section 6.*

The Feiran fault juxtaposes Lower Rudeis Formation in the footwall against the DLC-2 (Kareem Formation) in the hangingwall. The stratigraphic units exposed in the El Qaa half graben are, from the east, the proximal deposits of DLC-2 (Kareem Formation), the DLC-3 which is exposed around the center of the syncline, the distal deposits of DLC-2 (evaporite and mudstone), the distal deposits of DLC-1 (ASL and Lower Rudeis Formation) and the last unit before the Nezzazat fault is the eroded prerift Thebes Formation, which is dipping ca. 9-10° towards the east. Cross-section 5 is very similar to cross-section 4 since the delta is deposited across both of them and they both cross the same location on the EBFB to the east, but they have different striking direction, cross-section 5 strikes nearly W-E and cross-section 4 strike SW-NE. See the restoration steps for cross-section 5 in Appendix 2, figure 8 A-F.

4.2.7 Cross-section 6 transect

Cross-section 6 is the northernmost section striking SSW-NNE it is ca. 7 km long, starts in the eastern Budra fault block and crosses the Baba-Sidri fault (Figure 4-18A). The sub-blocks in the Budra fault form an overall large anticline structure, similar to the anticline structure present in the Hadahid fault block. The bedding in the sub-blocks is tilted towards the west and the dipping angle is increasing from ca. 8° towards ca. 22° in the sub-block closest to the Baba-Sidri fault. The displacement for fault 1, 2 and 3 are ca. 50 m, ca. 40 m and ca. 300 m, respectively. The increase tilting of the sub-blocks in the rift shoulder towards the large basin-bounding fault (Baba-Sidri fault), indicates that the fault at this location started as a blind fault migrating upwards creating a monocline in the softer sediment above, and by further upward migration the fault eventually breached the surface and the large anticline-structure seen today is the result of this breached monocline. The Baba-Sidri fault displacement at this location is ca. 1280 m and the fault juxtaposes Sudr Formation in the footwall against a young evaporite deposit in the hangingwall. The three youngest stratigraphic units found in the immediate hangingwall of the Baba-Sidri fault are only found locally at this point, they are not preserved anywhere else in the study area and are therefore not described further in this thesis.

Northward along the Baba-Sidri fault from the intersection with cross-section 6 there is a clear increase in displacement, since the exposed stratigraphic units in the hangingwall are getting younger, meanwhile the stratigraphic units juxtaposed in the respective footwall gets older northward (Figure 4-3). Southward along the Baba-Sidri fault the displacement seems to vary, but eventually the footwall strata gets younger toward the Wadi Feiran transfer zone, leaving an overall decreasing displacement from the north towards the south in the Baba-Sidri fault. In the Immediate hangingwall of the Baba-Sidri fault (El Qaa half graben) in cross-section 6, a small syncline has developed and causes the hangingwall beds to be dragged up the fault scarp (Figure 4-18B). Within the syncline the older stratigraphic units have rotated to a steeper angle then the younger units, the dip-angle is decreasing upwards from 54° to 38° on the NE limb and the dip angle is ca. 17° on the SW limb.

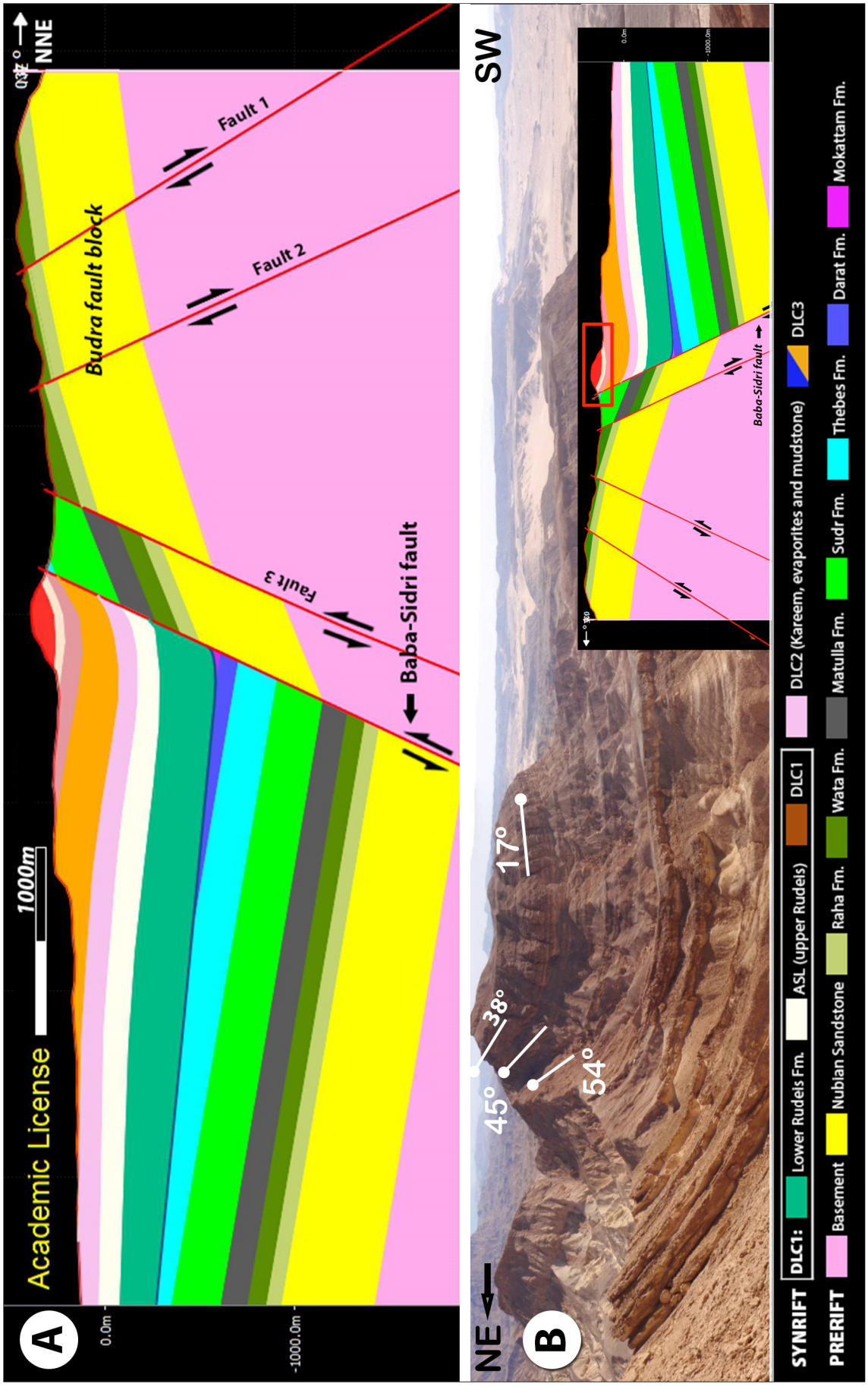

Figure 4-18: (A) Interpreted cross-section 6, which is northernmost section, crossing the Baba-Sidri fault.(B) Bedding dip angles from the small syncline formed in the immediate hangingwall of the Baba-Sidri fault. Notice that the cross-section is flipped to show where the dipping layers are. Location of the cross-section can be seen in figure 4-7. Field picture is from Martin Muravchik.

Figure 4-18B shows a field-picture along with the location on the cross-section, notice that the cross-section was flipped to illustrate where the dipping layers are located. Cross-section 6 is nearly perpendicular to the delta deposits in the El Qaa half graben and only synrift stratigraphic units are exposed SSW of the Baba-Sidri fault. The restoration steps for cross-section 6 can be seen in Appendix 2, figure 9 A-F.

4.2.8 Summary of cross-section 1 to 6

A summary of the main features described in cross-sections 1 to 6. The El Qaa syncline is plunging southward and the prerift units angle on the dipslope increases southward from ca. 9-10° in cross-section 5 to ca. 17° in cross-section 6. The minimum displacement measured on the EBFB decreases northwards from ca. 4400 m in cross-section 1 to ca. 1280 m in cross-section 6 (Figure 4-7). Anticline structures present in both the Hadahid fault block and the Budra fault block are evident for some of the main border faults starting out as blind faults, with monoclines above, before turning into surface breaking faults. Delta deposits are only present in the northern part of the study area in cross-sections 4-6 (Figure 4-17), in the southern part the Qabeliat Formation (Carbonate platform) located on the dipslope was building simultaneously as the delta was deposited in northern part. The Hadahid fault block is interpreted to have small displacement faults active at rift initiation, due to the deposition of the Nukhul Formation in several synclines located in the Hadahid fault block. The faults in the Durba block have been active after the Qabeliat Formation was deposited and have caused displacement to occur within the Qabeliat Formation

5 Synthesis and Discussion

Figure 5-1 shows the map generated by this study, including the mapped prerift and synrift units, the faults and the location for the six cross-sections. The map and cross-sections form the basis for analysing the stratigraphy of the study and its structural style and evolution.

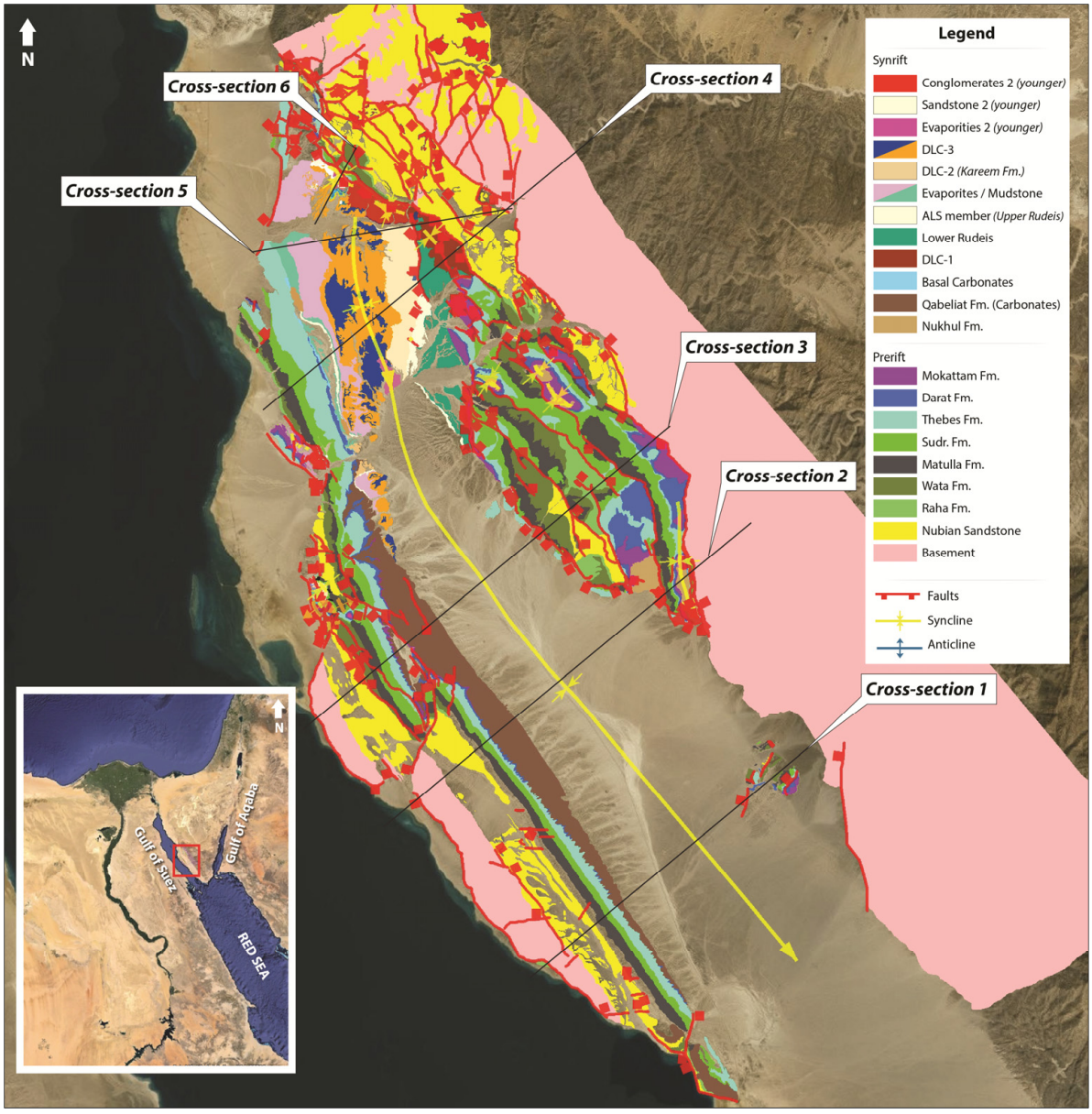

Figure 5-1: Geological map generated in ArcGIS, including legend, location of study area and the location of cross-sections 1-6. Satelliteimages

This chapter discusses the tectonic evolution of the El Qaa fault block and the implications the study has for the structural development of normal fault network and synrift stratigraphy and sedimentology. The chapter concludes with discussing and outlining limitations of restoration using 2D/3D MOVE software and directions of possible future work.

5.1 Tectonic evolution of the El Qaa fault block

The tectonic evolution of the El Qaa fault block presented in this thesis, is the result of the structural and stratigraphic analysis of the prerift and synrift sediments in the study area and described in chapter 4. The temporal evolution has been divided into four main synrift stages based on main events observed in the restoration process and mapped data. Figure 5-2 is a simple illustration of the four stages, which are described in detail below.

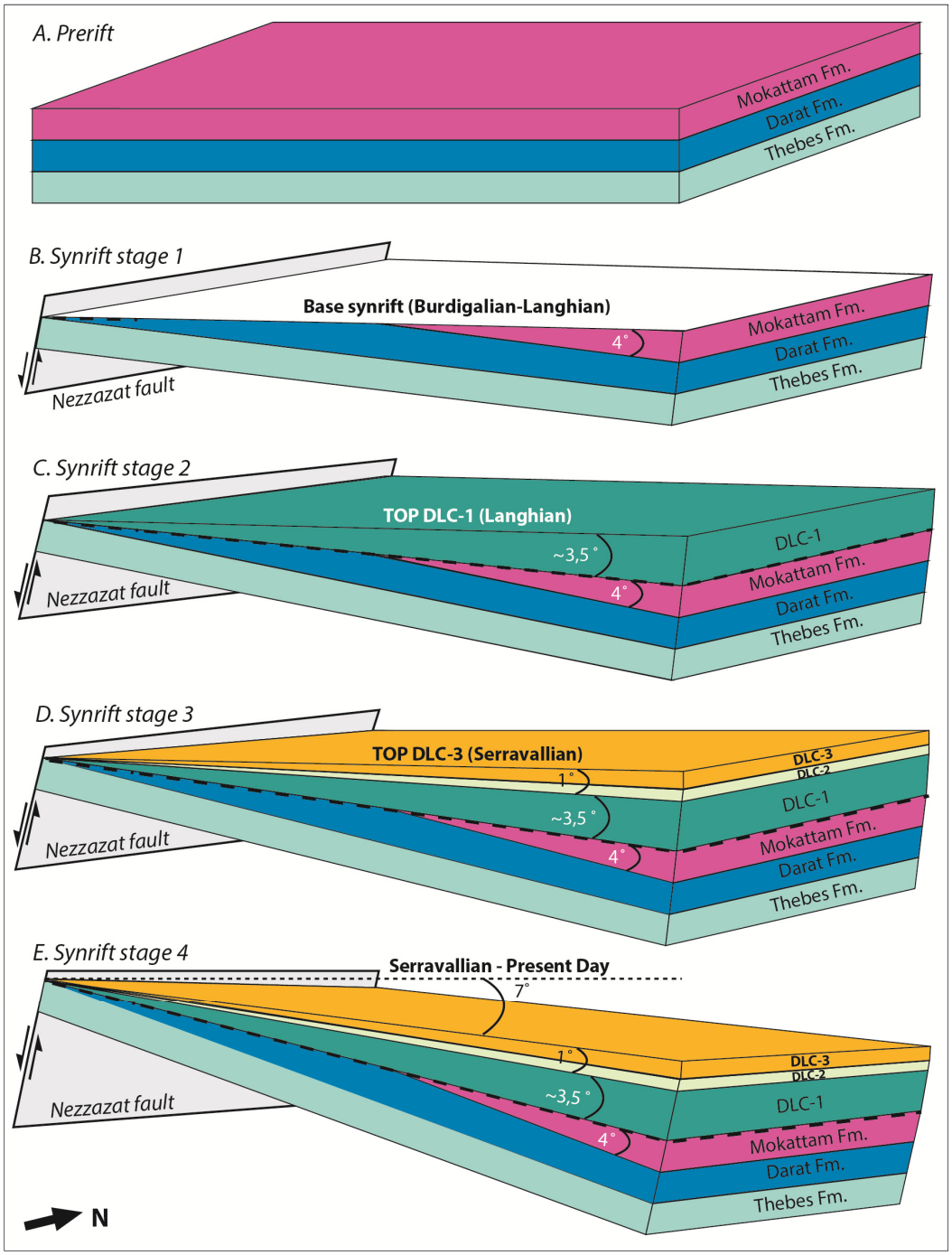

Figure 5-2: A diagram illustrating the four synrift stages for the El Qaa Half graben. (A) the horizontal prerift units, (B) Stage 1, a ca. 4 rotation°, (C) stage 2, a ca. 3,5° rotation, (D) stage 3, a ca. 1° rotation as the delta was deposited and (E) the last stage, a further rotation of ca. 7° rotation towards today's structures.

5.1.1 Prerift

In the restoration process the last step was the unfolding of the top of prerift unit Thebes Formation to the depositional level at that time (see TABLE 1, on page 36). The Darat Formation and Mokattam Formation were also unfolded back to their depositional levels. The Mokattam Formation was the last prerift unit to be deposited prior to rift initiation (Figure 5-2A).

5.1.2 Synrift stage 1 (Burdigalian - Langhian)

The first sign of fault movement is in the rift initiation phase in the Late Oligocene - Early Miocene when both blind faults with monoclines above and surface breaking faults are present in the restoration (Figure 5-3). Figure 5-3 shows the synrift initiation (Base synrift) step in the restoration process in MOVE for cross-sections 2, 3 and 5. At this stage there has developed a southward increase in dipping-angle of prerift stratigraphic units on the dipslope from ca. 3,5° in cross-section 5 to ca. 4,5° in cross-section 2, this created an angular unconformity between the prerift and the synrift units on the western limb in the southward plunging El Qaa syncline.

The oldest synrift depositional unit in the study area is the Nukhul Formation which is exposed on four different locations on the Hadahid fault block. The proto-Hadahid fault block was active at rift initiation and contained isolated faults (both blind and surface breaking faults), at this time the subsidence rate was slow and limited accommodation space was created. The restorations show the fault displacement ranging from 70-120 m. The initial Hadahid fault started out as a blind fault with a developing monocline above the fault tip, creating a large syncline in the hangingwall and an overall anticline-structure in the footwall, consisting of multiple small displacement faults, the majority are east-dipping faults and one west-dipping fault. The Nukhul Formation is also expected to be present below the Pliocene/Quaternary sediments in the El Qaa half graben (Figure 4-5).

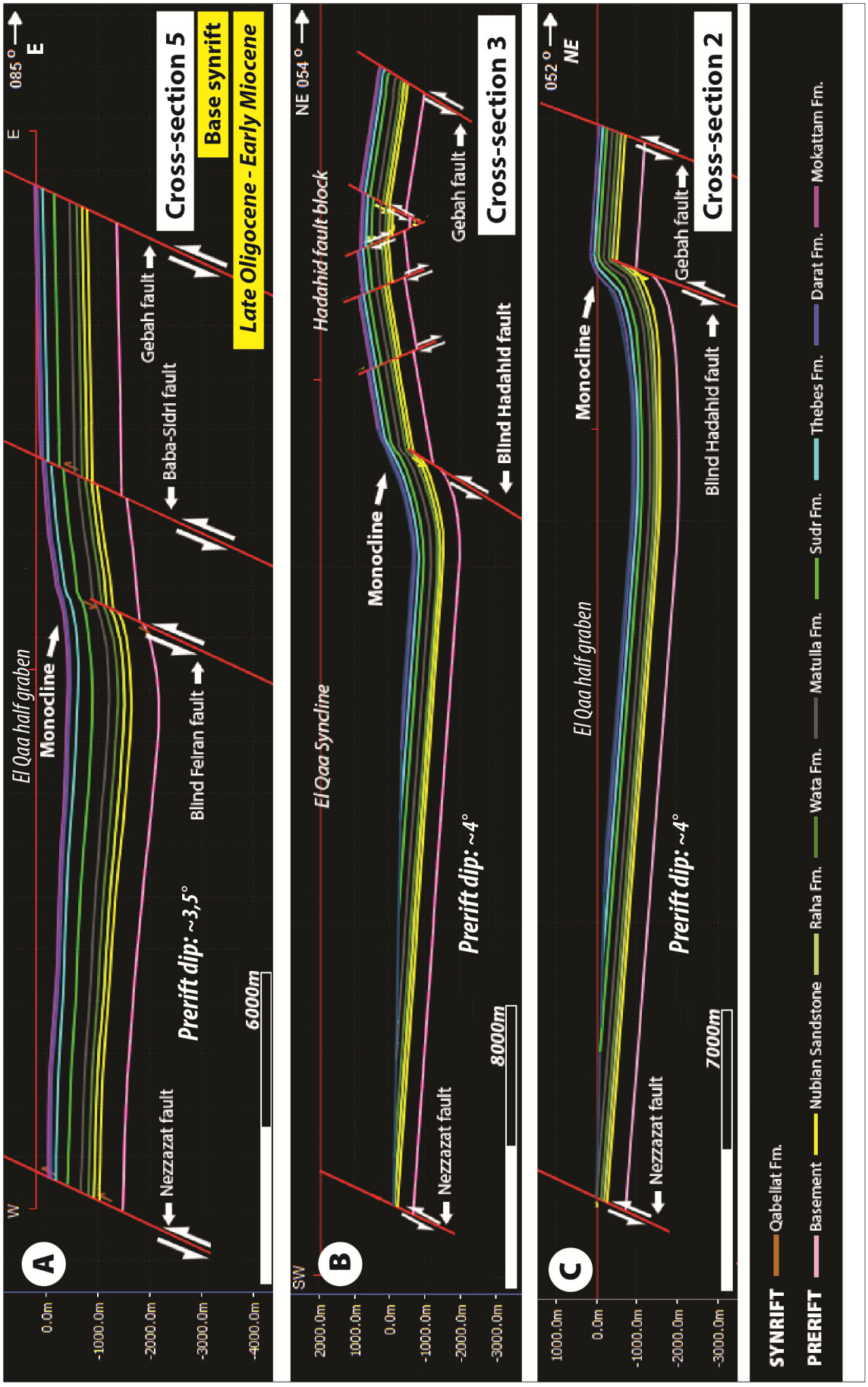

Figure 5-3: Restoration step for the Base-synrift in cross-sections 2, 3 and 5. Notice the difference in the rift initiation stage between monoclines and surface breaking faults and the increase in prerift dipping-angle on the western limb of the El Qaa Syncline. (A) cross-section 5, (B) cross-section 3 and (C) cross-section 2. Legend applies to A, B and C. See figure 4-7 for location of cross-sections. Complete restoration for cross-section 2,3 and 5 can be seen in Appendix 2.

On the western side of the El Qaa half graben there is no fault activity in the study area, except for the Coastal Fault Belt at this stage. The synrift stage 1 can be compared to the first step in the fault growth model (Figure 2-4 A) suggested by Gawthorpe and Leeder (2000), which includes numerous small isolated faults both blind and surface breaking faults with small depocentres developing adjacent to the faults.

5.1.3 Synrift stage 2 (Langhian)

The second synrift stage is represented by a further rotation of the stratigraphic units on the dipslope at an angle of ca. 3,5° from the base-synrift to the top of DLC-1, measured on the dipslope in the Wadi Feiran area (Figure 5-4), shows this stage in the restoration process for cross-sections 4, 5 and 6). The thickness of the DCL-1 unit is ca. 1000-1300 m in cross-section 4 and 5 and it has a large wedge-shape towards the fault scarp (Figure 5-4), which has led to the interpretation, that the subsidence rate and thereby the amount of created accommodation space must have been high at this stage. In addition, the Lower Rudeis Formation is interpreted to have been deposition in a deep water environment, indicating a relative sea-level rise at this point. Gawthorpe et al. (1990) describes the lowermost fan sequences in DLC-1 to be aggradational and coarse grained, and furthermore they describe the increasing tilt-angle of the lower fan sequences to be caused by synsedimentary faulting. The backstripping for cross-section 4 and 5, clearly shows that the Baba-Sidri fault was active as the DLC-1 was deposited, evident in the wedge shape growth succession towards the Baba-Sidri footwall scarp (see Appendix 2, Figure 7D and Figur 8D). At this stage the fault segments are interpreted to have linked to form longer master faults with increasing displacement. During synrift stage 2 the Feiran fault, parts of the Baba-Sidri fault and the southern part of the Hadahid fault are interpreted to have changed from being blind faults with developing monoclines above, to surface breaking faults breaching through the monoclines, since they in synrift stage 3 have broken through the surface. The sedimentary response to the evolution of the Feiran faults breaching through the monocline is expected to be present in the lower part of the DLC-1 by changing from a thinning of synrift sediments towards the monocline, to thickening towards the fault scarp after the fault breached the monocline, see illustration in Figure 5-5.

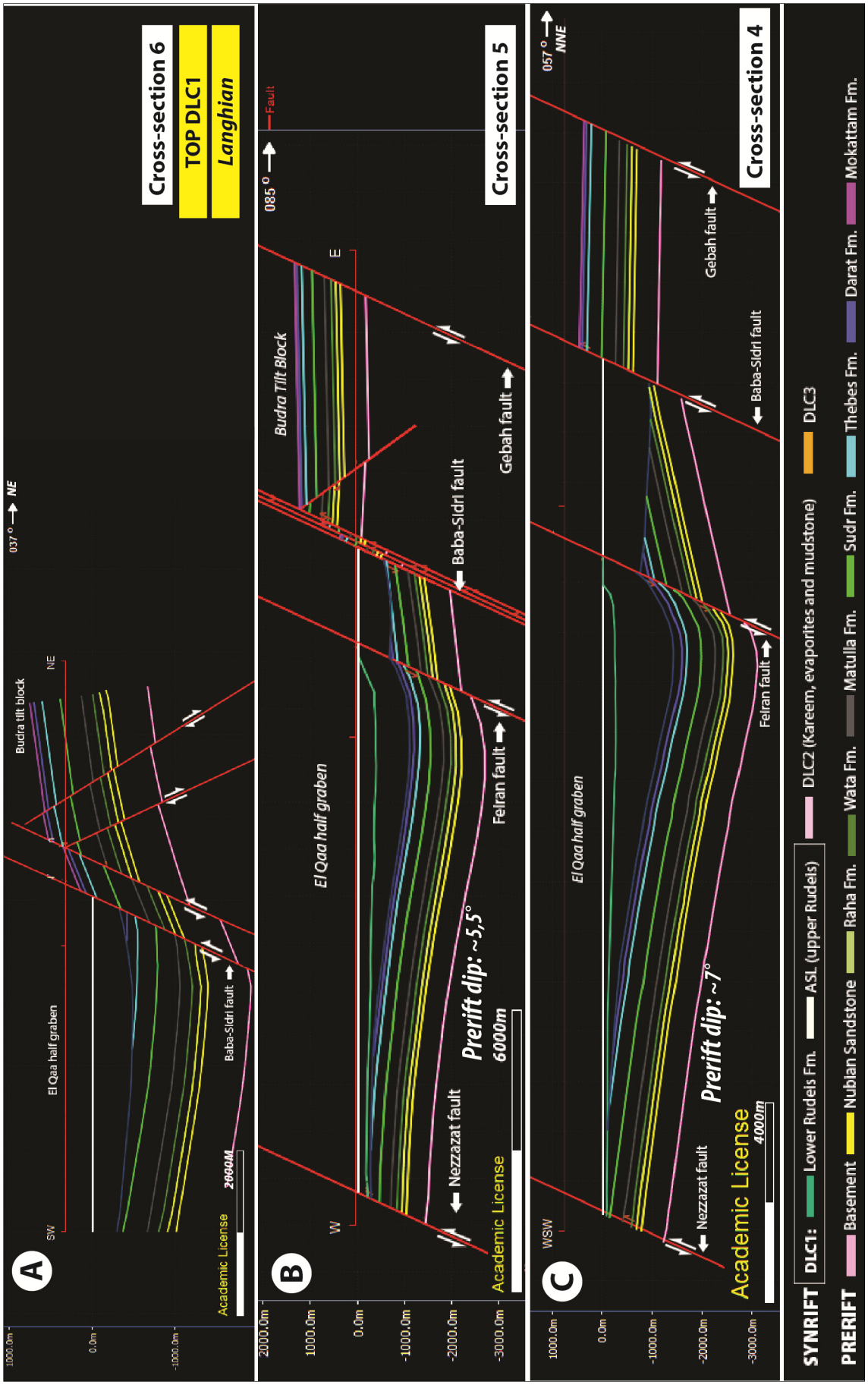

Figure 5-4: Rotational phase 2, a further rotation of ca. 3,5° from the Rift initiation to the top of the DLC1 (which includes the Lower Rudeis Formation and the upper Rudeis Formation (ASL member) in the backstripping process.(A) Cross-section 6, (B) cross-section 5, (C) cross-section 4. Legend applies to A, B and C.

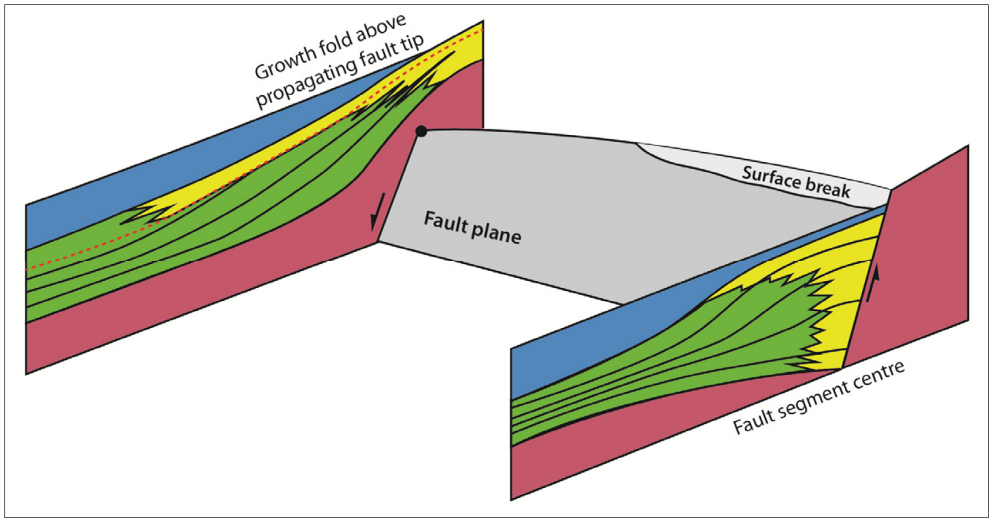

Figure 5-5: Illustrates the sediment response to the change from a monocline towards a surface breaking fault. Modified from Gawthorpe et al. (1997)

In cross-section 2, the Nukhul Formation has been dragged in the eastern limb of the small syncline in the easternmost block, which indicates that further displacement was on the smaller faults in the Hadahid fault block after the Nukhul Formation was deposited (Figure 4-18). In the southern part of the El Qaa syncline, carbonate platforms and reefs where developed on top of the tilted prerift stratigraphic units, therefore the second stage is not seen as a boundary in the backstripping process for southern cross-sections 1, 2 and 3, which all instead have the Qabeliat Formation present on the western side and no delta deposits (see Figure 5-6B, cross-section 3 has the Qabeliat Formation on top).

The sediment entry point for the delta is interpreted to have been near the linkage between the Sidri fault and the Alaqa fault located west of the large Feiran Transfer zone (Gawthorpe et al., 1990) (Figure 4-7). The Feiran Transfer zone is a low-gradient relay ramp formed between the overlapping EBFB faults, the Gebah fault, Baba-Sidri fault and the Hadahid fault. Gawthorpe et al., (1990) argued that the low-gradient Feiran Transfer zone functioned as a conduit for the drainage system in the uplifting rift-shoulder and since drainage tends to find its way towards topographic lows, a large catchments area is produced with time feeding the delta and controlling the size of the delta. The synrift units in the delta deposits contain clasts derived from the eroded prerift units, representing the erosion "unroofing" of the uplifted rift shoulder and the increasing fault displacement at this stage. Wescot et al., (1996) describe the increase of clasts eroded from the Precambrian Basement present in the

delta units deposited after the "Clysmic-event" which in this thesis corresponds to the upper Rudeis Formation (ASL member) which is located in the upper part of the DLC-1 unit. Gawthorpe et al., (1990); McClay et al., (1998); Bosworth and Mcclay, (2001) have also described the unroofing effect of prerift units present in the delta deposits, such as the erosion of the Thebes Formation which produces chert pebble-cobble in the oldest delta deposits and then older Nubian sandstone and Precambrian Basement in the younger delta deposits (the younger delta deposits corresponds to DLC-2 and DLC-3 in this thesis).

5.1.4 Synrift stage 3 (Serravallian)

Synrift stage 3 shows an additional rotation of ca. 1° from the top of DCL-1 to the top of DLC-3, measured on the dipslope in the Wadi Feiran area (Figure 5-6). At this stage, the subsidence/uplift rate and accommodation development have slowed down compare to the earlier stages and the sediment supply outpaces relative sea-level rise, causing progradation of the delta. Increased deltaic progradation may also be a result of a well-developed catchment-area being established by synrift stage 3 in the rift shoulder. It is difficult to isolate out the controls that led to the suggested increase in catchment-area at this point, but there are a few observations that could lead to this conclusion, such as, the increase in delta reach, from 1,5 km across in DLC-1 to 13,5 km across in DLC-2 and 3, the upper deltas are relative thin in thickness only 120-150 m each up to the point of the slope break after which they are thinner and they have a progradational stacking pattern, which suggests that there was a constant supply of sediments, even after the decrease in fault activity. The decrease in fault activity can be suggested from the decrease in the angle of climb from DLC-2 to DLC-3 (from ca. 15° to 10°), the shoreline for DLC-2 is interpreted to be located near the El Qaa syncline axis (Figure 4-17) and the shoreline for DLC-3 is interpreted to be located ca. 2-3 km west of the syncline axis (Figure 5-6). In the southern part of the El Qaa Syncline the Qabeliat Formation (carbonate platform) is expected to have been continuously building up on the dipslope south of Wadi Feiran simultaneously with the delta building out in the northern and central part of the El Qaa half graben. Due to the burial of the Qabeliat Formation below Pliocene/Quaternary sediments, there are no constrains to how far down the dipslope the platform reaches, but it is estimated to be somewhere between where it is exposed and the syncline axis (Figure 5-6B).

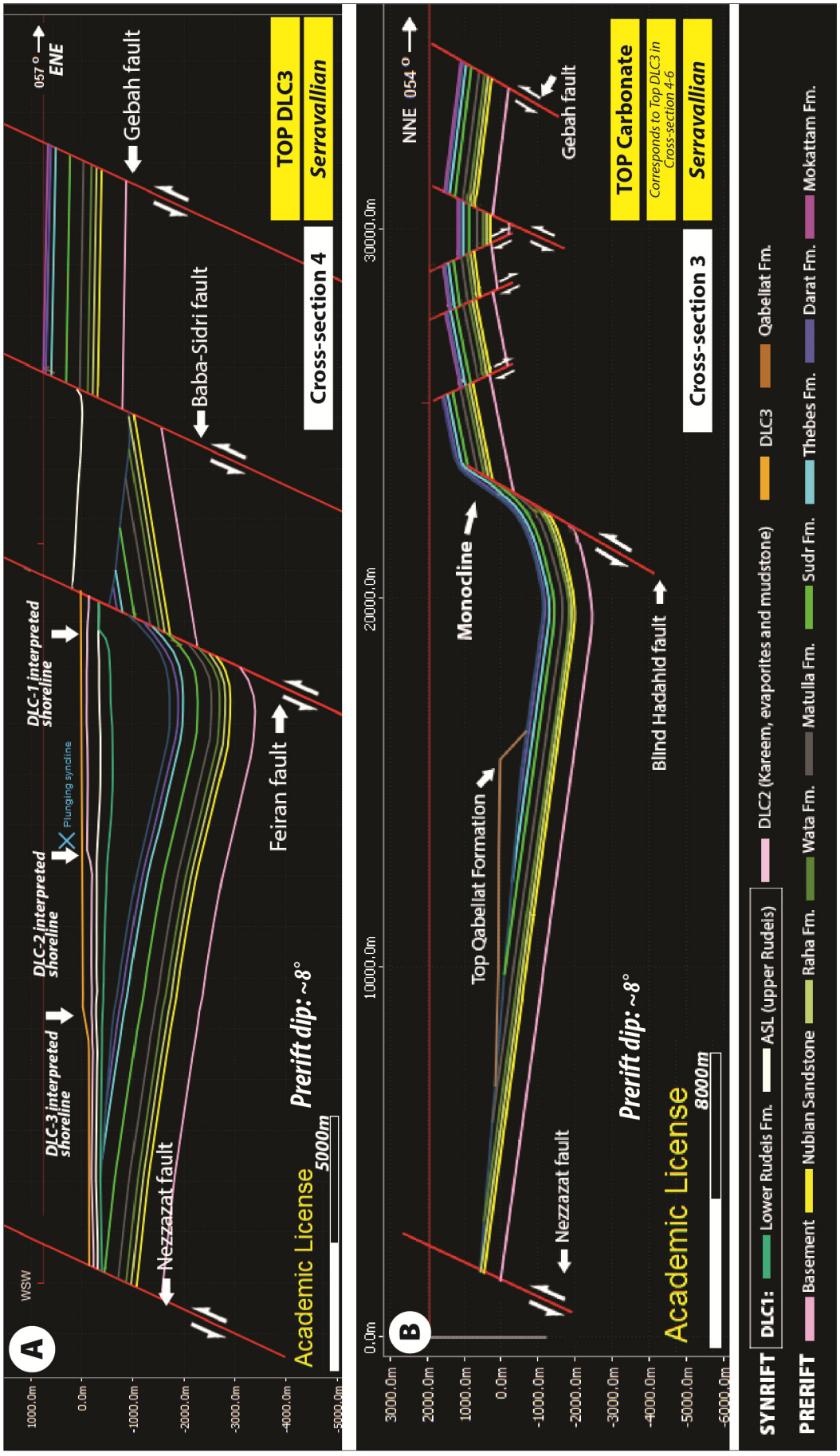

Figure 5-6: (A) Shows the backstripping step of top DLC-3 for the southern cross-section 4 where DLC-3 is on top. (B) Shows the backstripping step of cross-section 3, where Qalibet Formation is on top. The legend applies to both A and B. See location of the cross-section in fiaure 4-7.

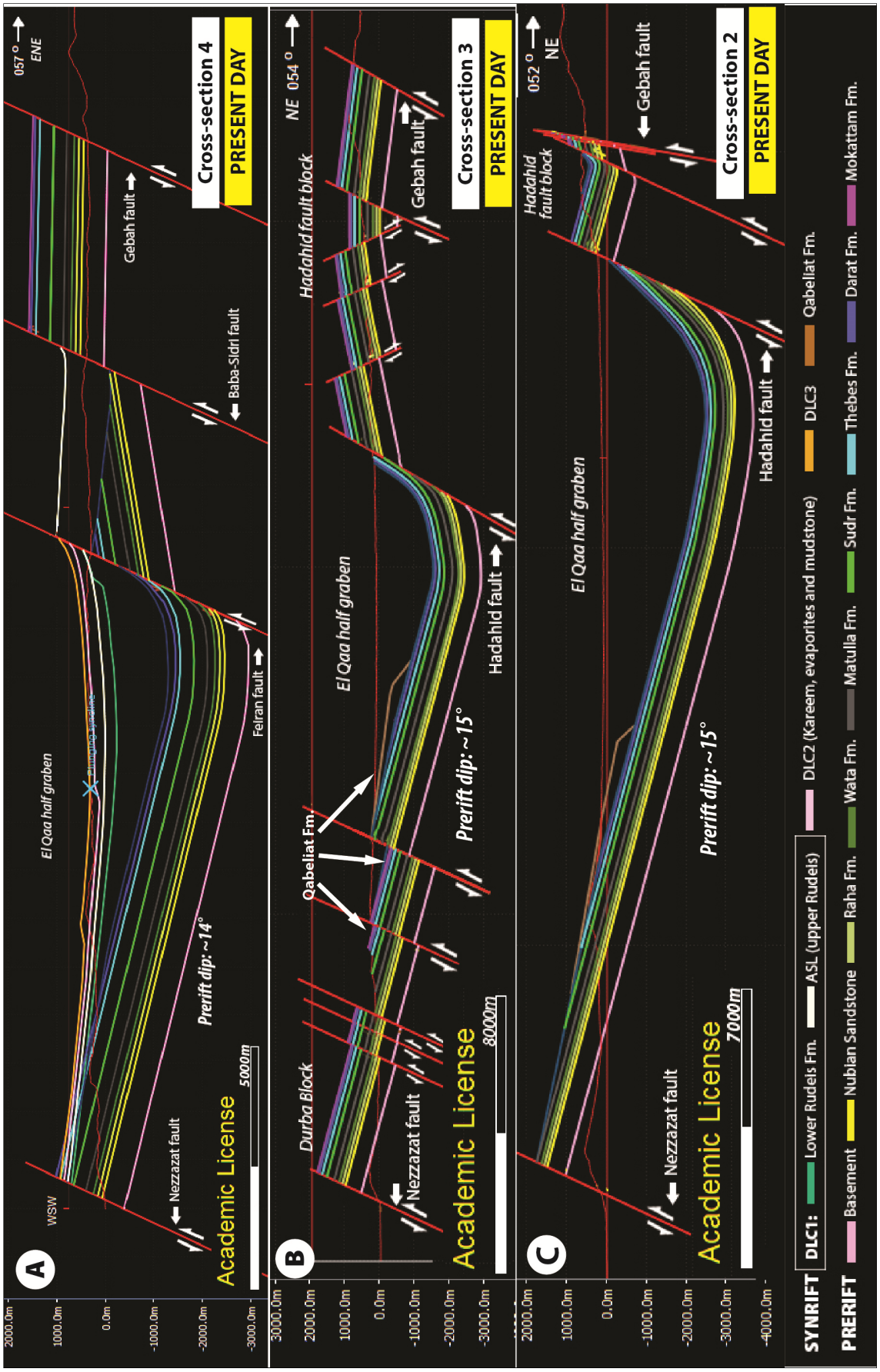

Figure 5-7: The present day interpreted cross-sections 2, 3 and 4. (A) Cross-section 4. (B) Cross-section 3. (C) Cross-section 2. Legends applies to A, B and C.

The Feiran fault juxtaposes DLC-2 in the hangingwall against DLC-1 in the footwall, indicating that the Feiran fault was still active after the deposition of DLC-1 (Figure 5-8). Otherwise this stage represents a more tectonically quiet period, evident in both the prograding delta deposits due to low accommodation development and also in the small variations in fault displacement observed in the restoration, when decompacting both DLC-3 and DLC-2, there was no too little displacement change in the faults in the study area, see Appendix 2, Figure 7C and D and Figur 8C and D.

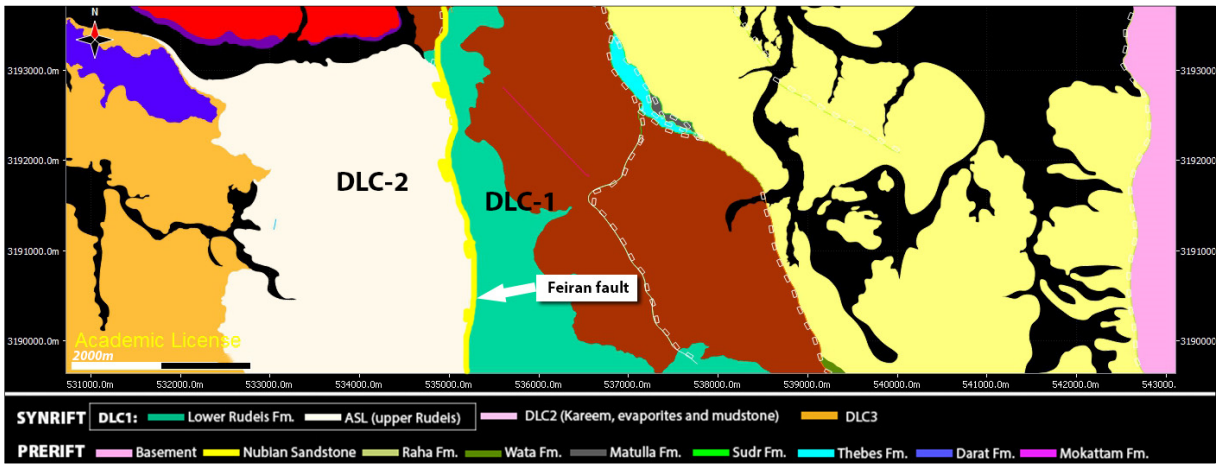

Figure 5-8: Shows the Feiran fault juxtaposes the DLC-2 in the hangingwall against DLC-1 in the footwall.

5.1.5 Synrift stage 4 (Seravallian - Present day)

Synrift stage 4 is the last stage up to present day structural settings in the El Qaa half graben (Figure 5-7). This shows an eastward rotation of ca. 7° measured in the topsets of DLC-3 on the dipslope (the western limb of the El Qaa syncline). In the center of the El Qaa syncline the DLC-3 topsets are horizontal and on the eastern limb they area dipping towards the west. This final rotation is interpreted do have been caused by increasing fault displacement on the large Nezzazat fault located to the west on the CFB (Figure 5-7B). In cross-section 3 there is evidence for fault activity on the western side of the El Qaa half graben in the Ekma and Durba blocks, where the Qabeliat Formation has been faulted after being deposited and is now exposed in three of the sub-blocks on the upper western limb located in the Durba block (Figure 5-7B). The displacement on these fault ranges from 15 - 800 m, and the bedding dip has not changed from prior to these faults (ca. 14°easterly dip). The faults seen in cross-section 3 on the western side are interpreted to be the result of the increase displacement on the Nezzazat fault (Figure 5-7B). On the eastern side, in the sub-blocks

located in the Hadahid fault block and the Budra tilt block do not show noticeable displacement at this last stage, it seems like the fault activity is more concentrated on the western side of the El Qaa half graben and most likely has caused the final rotation of the topsets in DLC-3 to present day structural settings.

5.2 Implications for structural development of normal fault networks

5.2.1 Fault evolution

The structural analysis from the backstripping of the six cross-sections gave a good indication of the fault evolution in the El Qaa fault block and can be partly compared to the model suggested by Gawthorpe and Leeder (2000) and Sharp et al. (2000b) illustrated in Figure 2-4 in chapter two. Starting with small isolated fault segments in Late Oligocene - Early Miocene and through the Langhian the fault segments have linked to form larger faults, such as the Hadahid fault and the Baba-Sidri fault, and towards the end of the DLC-1 deposition in the Langhian, the rift climax occurs and the Clysmic-event rearranges the structures into the larger structures seen today and the smaller faults on the Hadahid fault block are interpreted to have no further displacement after the Langhian. In the Langhian-Seravallian, after the rift climax, there seems to be a change in fault activity towards the rift axis, since small faults are forming on the western limb after the deposition of DLC-3, this indicates an increase in displacement on the CFB (Nezzazat fault), which causes the Delta deposition to rotate, seen in the DLC-3 which is tilted towards the east on the western limb and towards the west on the eastern limb (Figure 5-7A).

The fault activity migration observed in the results of this thesis are consistent with the study made by Cowie et al. (2005) in the Northern North Sea on the Horda platform located east of the Viking graben, see (Figure 5-9).

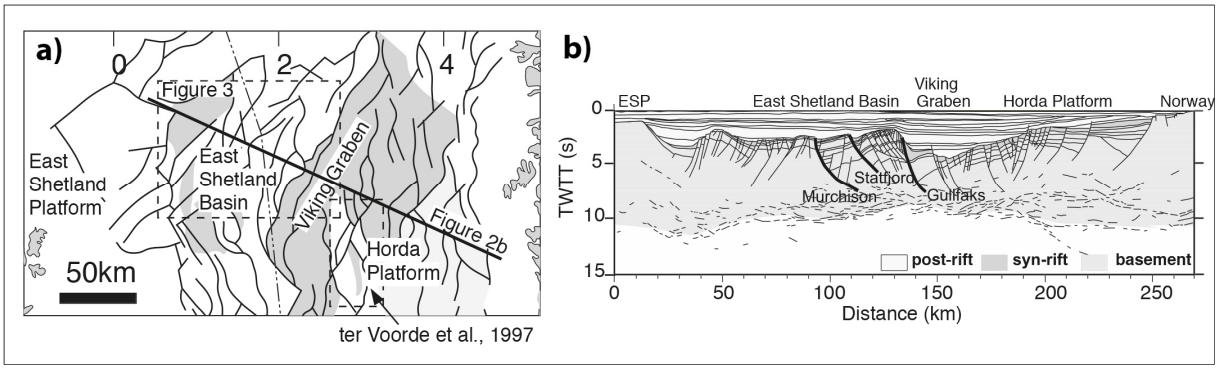

Figure 5-9: (a) Map of the Northern Viking Graben. (b) Cross-section of the North Sea Basin, see location on (a). Modified from Cowie et al. (2005)

They concluded from the study that the fault activity was migrating towards the rift axis, due to the increasing temperature gradient, strain rate and viscosity structure towards the rift center, caused by the thinning of the lithosphere (Figure 2-5 in chapter two). They divided the evolution into 3 stages. The first step included the formation of isolated faults, dipping in both directions with low slip rates. Step two was the formation of half grabens and increasing slip rates and the third step has the highest slip rates located closest to the rift axis whilst the faults located further away from the axis switched off. The 3 stage model of Cowie et al. (2005) could also explain the results of the fault evolution in this thesis. In particular how the Hadahid fault block and Budra tilt block (located further away from the rift axis), were active in the Early Miocene to Langhian, and then after the Seravallian, faults formed in the immediate footwall of the Nezzazat fault as a results of the migration of fault activity towards the rift axis. In addition to the migrating fault activity, Cowie et al. (2005) suggested that the displacement was greatest for the faults closest to the rift axis, this also could explain the large displacement on the Nezzazat fault (ca. 5 km (McClay and Khalil, 1998)) compare to the EBFB (which in this thesis is measured to be max. 4400 m, see table 5 on page 75), which is located further away from the rift axis and show a decrease in displacement activity after the deposition of DLC-1. The faults formed due to increased activity on the Nezzazat fault on the eastern limb, are all dipping towards the rift axis, which can be compared to stage 2 in the model made by Cowie et al. (2005) where inward dipping faults area favored later in the rifting stage (Figure 2-5B).

5.2.2 Comparison of DLC1-3, to synrift deltas in the Corinth rift and the North Sea rift

The large delta deposits filling up the El Qaa half graben in the northern part of the study area, reaches north of Wadi Sidri and south of Wadi Feiran, and is approximately 31 km in width and 13,5 km across the half graben towards the Nezzazat fault (Figure 5-10).

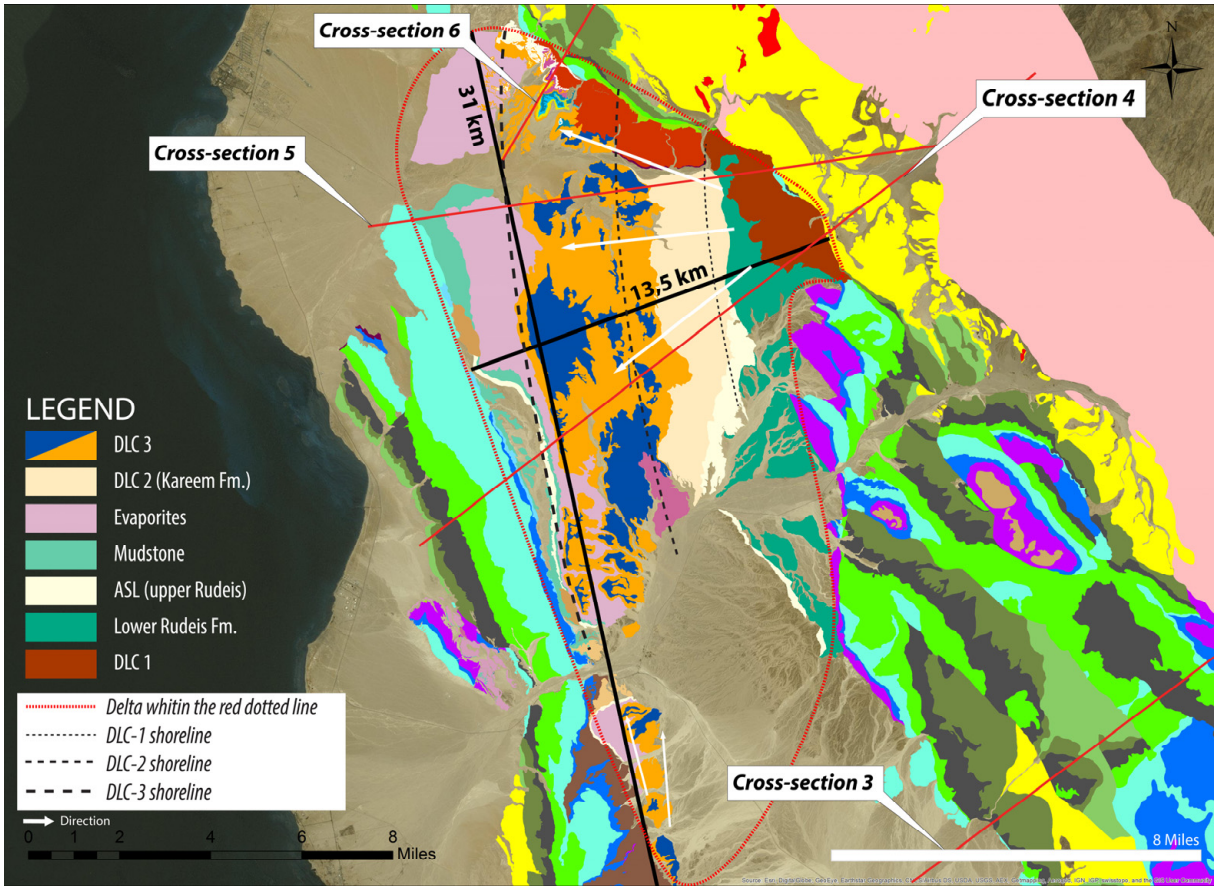

Figure 5-10: Delta deposits in the El Qaa half gra

The DLC-1 delta unit is the lowermost unit consisting of coarse material and is considered to have an aggradational stacking pattern. The upper DLC-2 and DLC-3 have a progradational stacking pattern (Gawthorpe et al., 1990) and extends further towards the west, ca. 13,5 km (Figure 5-10).

DLC-1, the lower part of the deltas, reaches ca. 1,5 km across and 3-3,5 km along strike and is several 100 meters thick (Figure 5-7A). DLC-1 is a steep and short delta complex dominated by coarse material (Gawthorpe et al., 1990). The coarse-grained architecture within the fan sequence, the limited extend and the geometry within the fan sequences, suggests that the catchment area at this time was local and sediments derived from the hangingwall of the Gebah fault (EBFB) (Gawthorpe et al., 1990). Gawthorpe et al. (1990)

describes the initial sediment in DLC-1 to be represented by talus cone, that functioned as a platform for the Gilbert type deltas deposited on top of the talus cone, and the increased fault displacement on the Baba-Sidri fault is evident in the increased rotation of the lower fan-sequences (Figure 5-7A). The structural settings in the Gulf of Suez, as the lower part of the delta was deposited can be compared to the Alkyonides half-graben located in the Gulf of Corinth in Greece. Leeder et al. (2002) describes the delta architecture and the structural settings in the Alkyonides. The Alkyonides islands are part of an uplifted footwall separating the Alkyonides Gulf from the main Gulf of Corinth. An asymmetric half-graben is located between the Alkyonides uplifted footwall and the onshore rift-system, where the Gerania Mountains have developed as a result of the uplifting onshore footwall (Figure 5-11). The southern steep limb consist of the west and east Alkyonides faults, which are located in the hangingwall of the onshore and active Pisia and Skinos fault (W) and the Psatha fault (E). These setting are very similar to the early El Qaa half graben, as the Alkyonides islands could corresponds to the Nezzazat uplifted footwall, and the onshore faults (Pisia, Skinos and Psatha) corresponds the EBFB. The catchment drainage feeding the western deltas in Alkyonides half graben are short and local catchments (Leeder et al., 2002) (Figure 5-11).

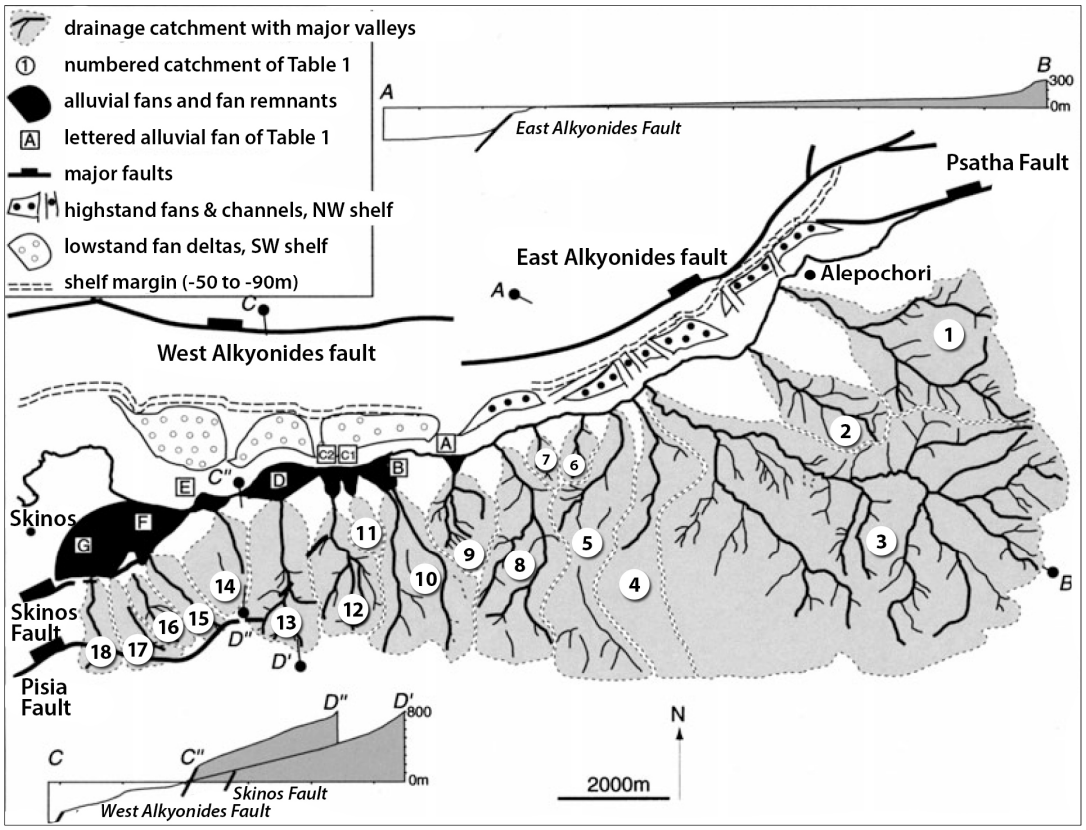

Figure 5-11: A schematic diagram illustrating the structural settings in the Alkyonides half graben (Leeder et al., 2002) *Note the location of the delta towards the west and the small catchments feeding the delta (nr. 9 – 18).*

The scale on the western Alkyonides delta is a few 100 m in thickness and the catchment area ca. 2000 m across (Leeder et al., 2002). The DCL-1 for comparison is ca. 1,5 km across and the catchment area could be 4-6 km, see figure 5-12 for an a rough estimation a possible size of the deltas and the catchment area in the El Qaa fault block.

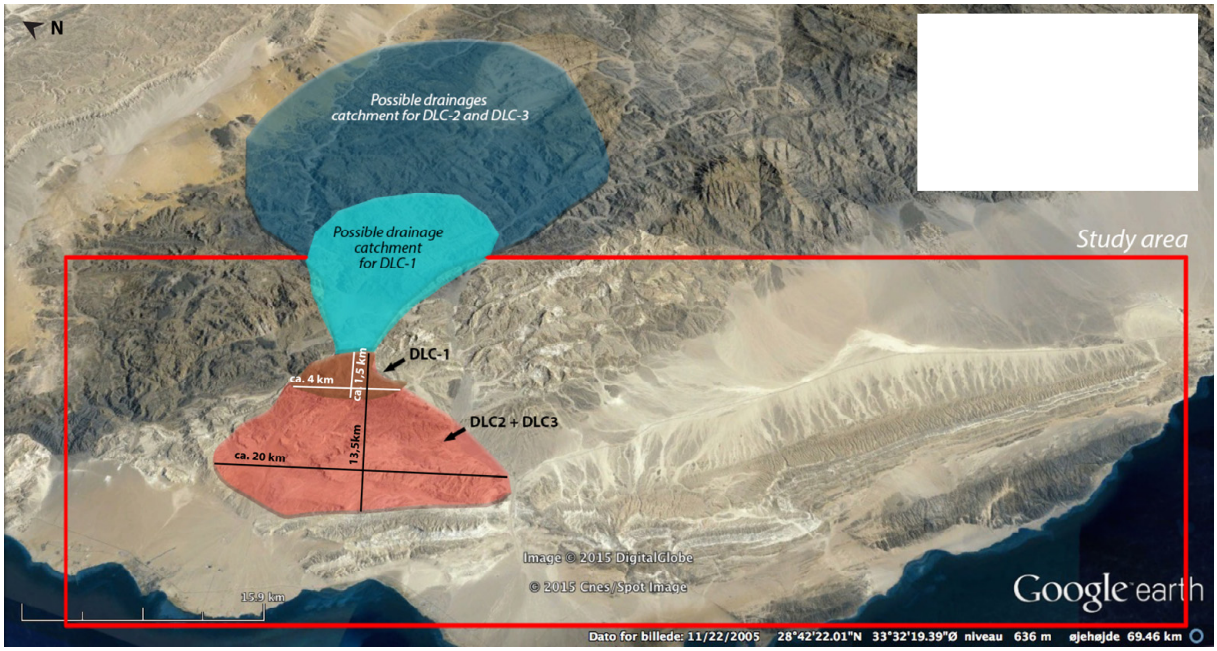

Figure 5-12: A rough estimation of the upper and lower deltas and the catchment-areas. DLC-1 is brown and with the light blue catchment area and DLC-2 and 3 is red with the darker blue catchment-area.

The erodibility of the bedrock present in the rift has a large impact on the slopes created and on the size of the catchment area. Leeder et al. (2002) describes how the slope vary depending on the bedrock lithologies, the erosion of the more resistant units (limestone and serpentinite) creates steeper slopes (ca. 12-22°). In addition to the limestones being karstified and talus cones and debris flows are created in the footwall scarp, see Figure 2-10D (Gawthorpe and Leeder, 2000). The bedrock with less resistant lithologies form shallower slopes (ca. 3-4°) with a larger dendritic drainage network, these changes are seen laterally along the southern border in the Alkynonides half-graben (Figure 5-11). In the El Qaa half graben, the differences in bedrock lithologies is found vertically downwards in the prerift units. The Thebes Formation acted as a more resistant unit and is expected to have caused a "lag" in the deposition of the delta, represented by low erosion rate and sediment supply, as the Gebah footwall was uplifted and eroded. By the time the drainage cut below the Thebes Formation the sediment supply increased (Gupta et al., 1999). The older units the Nubian sandstone would have been easy to erode compare to the granitic Precambrian

basement, that would remarkably harder to erode and one can assume that the sediment supply rate decreased when the rift shoulder eroded down to the basement, Garfunkel and Bartov (1977) described basement clast being present in the top of delta complex (DLC-3).

DLC-2 and DLC-3 are the upper part of the delta deposited in the El Qaa half-graben, these are different from the lower part in that they are prograding instead of aggrading and are much larger in extent (ca. 13,5 km across and ca. 31 km along-strike) then the lower DLC-1. At this time the sediments supply has outpaced the subsidence/uplift rate and is building out towards the Nezzazat fault (prograding) and there may have been established a large catchment area (hinterland) that is feeding the delta from the uplifting rift shoulder. DLC-2 and DLC-3 has similarities with the large delta complex deposited east of the Viking graben in the Northern North Sea on the Horda platform (Ravnas et al., 2000). Ravnas et al. (2000) studied the sedimentary architecture on the Horda platform, containing the Krossfjord, Sognefjord and Fensfjords formations which are delta deposits representing a deposition similar to DLC-2 and DLC-3 in that the sediment supply has outpaced the subsidence/uplift rate and the accommodation development and a large well-established catchment area is feeding the delta. Furthermore, there are similarities in the rifting settings, the Horda platform corresponding to the El Qaa half-graben with the delta in the Horda platform prograding towards the Viking graben and in the Suez the delta progrades across the El Qaa syncline towards the large Nezzazat fault in the CFB, located closer to the rift axis. The Horda platform delta is expected to have a larger catchment area compare to the catchment area feeding the deltas in the El Qaa fault block, since it extends 50-60 km across towards the Viking graben (Figure 5-13), compare to the El Qaa delta extending ca. 13,5 km across towards the Nezzazat fault. The balance between sediment supply, subsidence/uplift rate and sea-level change controls the architecture (outbuilding and retreat) of the delta deposits. When the Sediment supply outpace the subsidence/uplift rate and the accommodation development the deltas prograde, and when the subsidence/uplift rate and accommodation development outpace the sediment supply the deltas aggrade or retreat. This is seen between the fan sequences in DLC-1, DLC-2 and DLC-3 (Gawthorpe et al., 1990) in the El Qaa half-graben, and also in the delta on the Horda platform, where the Krossfjord, Fensfjord and the Sognefjord Formation represent outbuild and retreat of delta deposits (Ravnas et al., 2000).

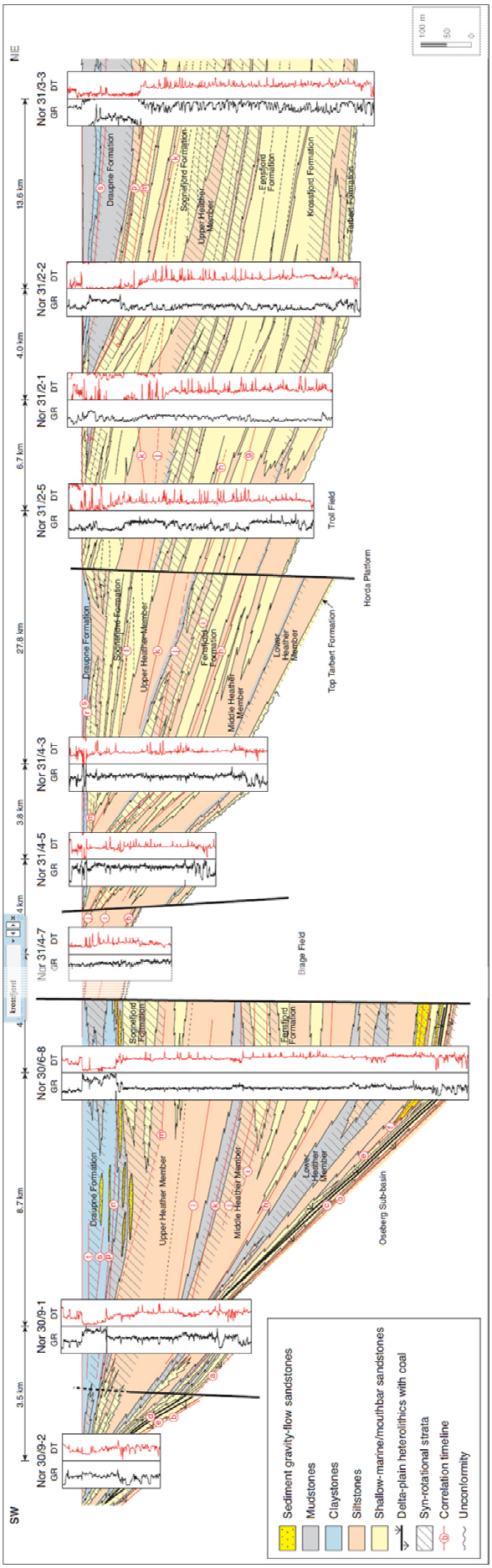

Figure 5-13: A cross section through the Horda Platform including the Krossfjord, Fensfjord and Sognefjord Formation (Ravnas et al., 2000).

Figure 5-14 is a schematic illustration of the different structural settings proposed for the upper and lower deltas, (A) is a smaller delta with the local footwall catchment-area and (B) represents a large catchment area, with a larger delta deposition.

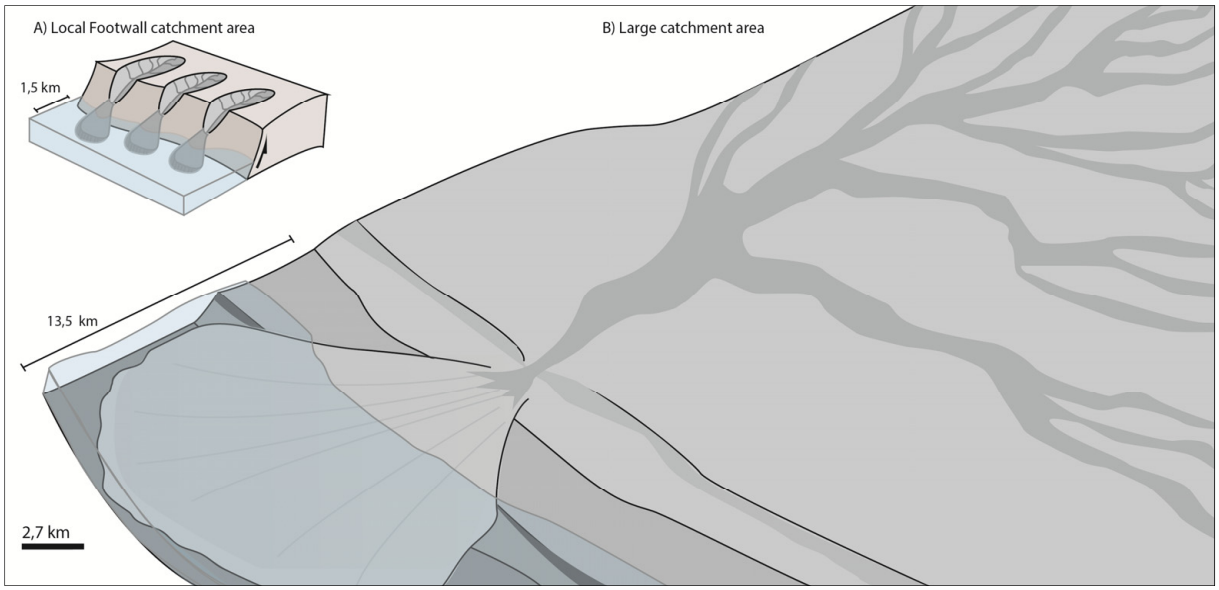

Figure 5-14: Illustration on the difference in structural settings, for a small delta with local footwall catchment-area and a larger delta with a large well-established catchment area.

The overall structure in the delta in El Qaa half graben follows the same three-fold architecture as the Horda platform delta (sandstone-mudstone-sandstone) suggested by Prosser (1993) and Ravnås and Steel (1998) illustrated in Figure 2-9 in chapter two. The lower part of the delta (DLC-1) represents the early rifting stage, dominated by coarse material with an overall fining-upward trend described by Gawthorpe et al. (1990). At the rift climax stage finer material is dominating, reflecting the high subsidence rate and increase in sea-level, this corresponds to when the Rudeis Formation was deposited and consists of deeper water (finer) sediments. The final stage reflects a large well established catchment area (hinterland) that feeds the delta, seen in DLC-2 and DLC-3, where the sediment supply has outpaced the subsidence/uplift rate and is prograding causing a coarsening-upward succession, similar to the overall dominated three-fold (sandstone-mudstone-sandstone) that Ravnas et al. (2000) describes for the Horda Platform delta.

5.3 Limitations and future work

The 2D/3D MOVE software was used to construct and restore the cross-sections and to construct a 3D modelling of the present day structural settings. For the restoration 2D/3D MOVE has different algorithms to use for different geological settings, described in the background chapter, but these work best with simple geological models with a simple geometry (layer-cake models), which is not the case in our restoration. In this thesis the synrift architecture is more complex, since it was deposited while the faults where active, this caused the strata to be dragged against the footwall scarp in the both the Hadahid fault and the Baba-Sidri fault, causing internal deformation within the bedding, 2D/3D MOVE does not handle these internal layer deformation well in the algorithms and therefore the process in restoring the syncline is more or less manual.

There are many possible solutions to form the lower part of the El Qaa syncline, regarding both the syncline axis and the amount of drag along the fault scarp, the restoration in this thesis are one possible solution. In order to make a more accurate reconstruction of the six cross-sections crossing the El Qaa syncline, I would need access to seismic data and/or well data from the El Qaa syncline area, this along with the geological map generated in this thesis including lithological boundaries, faults, folds and dip data, would have improved the results on both the interpreted cross-sections and the reconstruction of these. It would be an advantage to include offshore data, seismic and well data in future work in the reconstruction of the El Qaa fault block. In addition, access to offshore data on the hangingwall of the Nezzazat fault would have improved the results both for the restoration and for the 3D model, since I then would have some constrains on the Nezzazat faults displacement and could have included area west of the Nezzazat fault.

An attempted 3D reconstruction of the El Qaa fault block was made and is partly finished and used in this thesis, but due to the very slow work-process with the software when dealing with such a large 3D file for the entire El Qaa fault block, there was not enough time to finish it entirely before the thesis was handed in.

6 Conclusion

The purpose of this study was to improve the understanding of the tectono-stratigraphic evolution of the El Qaa fault block, by mapping the lithologies, faults and folds in addition to constructing and restoring six cross-sections and to make a present day 3D model, the main conclusions from this study are:

- The prerift and synrift stratigraphic units in the El Qaa fault block have been mapped using Google Earth and ArcGIS and have been incorporated into an ArcGIS project along with the dip data available in the study area.
- Furthermore, the key faults and folds in the El Qaa fault block have been mapped and also incorporated into the same ArcGIS project file.
- The entire ArcGIS project file was imported into 2D/3D MOVE, where six E-W dipping cross-sections have been constructed through the El Qaa Fault block by using traced sections through a DEM model, along with dip/strike data and line-intersections of the mapped surface boundaries.
- A restoration of the six interpreted cross-sections was made in 2D/3D MOVE using the following functions “Unfold”, “Move on fault” and “decompact”, the cross-sections were restored back to the top Thebes Formation
- A simplified 3D model of the present day structural settings in the El Qaa fault block was constructing based on the balanced interpretation of the six cross-sections and the traced faults.
- Based on integrating the mapped units, faults, dip data and cross-sections an interpretation of the tectono-stratigraphic evolution of the El Qaa fault block has been made and the key interpretations are:
    - The sedimentary response to folding and faulting is clearly observed in the restoration of the cross-sections that show the monocline developing in the early stages towards the surface breaking fault, in cross-section 3 the result of the development is preserved in the Hadahid fault block, where the anticline structure (part of the early monocline) now can be observed in the sub-blocks within the Hadahid fault block.

- Restoration of the six cross-sections illustrate the tectonic evolution of the El Qaa fault block, which has been divided into 4 main synrift stages; 1) synrift stage 1, 4° rotation of the prerift units (Burdigalian-Langhian); 2) synrift stage 2, 3,5° rotation from base synrift to the top of DLC-1 (Langhian); synrift stage 3, 1° rotation from the top DLC-1 to top DLC-3 (Seravallian); synrift stage 4, a further rotation of an angle of ca. 7°, caused by further displacement on the western Nezzazat fault (Seravallian-Present day), the dip measurements are from the western side of the El Qaa syncline measured on the dipslope south of Wadi Feiran.

- The stratigraphic differences in the deltas deposits (DLC-1 and DLC-2+3) illustrate the differences in early rift to later rift structural settings, the early delta deposit was fed by a local drainage catchment and was deposited against the steep Baba-Sidri footwall and the on-going fault displacement is evident in the increased rotation of the aggrading fan sequences, this is similar to the western delta in the Alkyonides half graben (Leeder et al., 2002). The upper deltas (DLC-2 and DLC-3) were deposited in a more tectonic quiet period with a large well established catchment area (hinterland) and are therefore prograding and extending much further out then DLC-1, which can be compared to the deltas deposited on the Horda platform, east of the Viking graben (Ravnas et al., 2000).

- The late fault activity on the Nezzazat fault causing both fault growth on the western limb of the EL Qaa Syncline and causing the latest delta deposits to rotate 7° down to the east (measured on the western side of the El Qaa syncline), the DLC-3 show not rotation in the center on the eastern limb the DLC-3 is rotated down to the west.

- This study shows the importance for understanding how the sedimentary architecture is build up and how it is affected by different controlling factors that influences the tectono-stratigraphic evolution of the basin.

ReferenǒŜă

Allen, P.A., and Allen, J.R., 1990, Basin Analysis Principles & Applications: Backwell Publishing, Oxford.

Alsharhan, A.S., 2003, Petroleum geology and potential hydrocarbon plays in the Gulf of Suez rift basin, Egypt: AAPG Bulletin, v. 87, no. 1, p. 143–180.

Behn, M., Lin, J., and Zuber, M., 2004, Effects of Hydrothermal Cooling and Magma Injection on Mid-Ocean Ridge Temperature Structure, Deformation, and Axial Morphology: The Thermal Structure of the ocean Crust and the Dynamics of Hydrothermal Circulation, p. 151–165, doi: 10.1029/148GM06.

Bosworth, W., and Mcclay, K., 2001, Structural and stratigraphic evolution of the Gulf of Suez Rift, Egypt: a synthesis: Mémoires du Muséum national d'histoire naturelle, v. 186, p. 567–606.

Corlett, H., Hollis, C., Hirani, J., Hodgetts, D., Gawthorpe, R., Rotevatn, A., and Bastesen, E. Characteristics of remobilised carbonate geobodies in the Eocene Thebes Formation, Hammam Faraun Fault Block, Gulf of Suez and the cause of slope instability on a shallowly dipping ramp after the Paleocene-Eocene Thermal Maximum, Unpublished.:.

Cowie, P. a., Attal, M., Tucker, G.E., Whittaker, a. C., Naylor, M., Ganas, a., and Roberts, G.P., 2006, Investigating the surface process response to fault interaction and linkage using a numerical modelling approach: Basin Research, v. 18, p. 231–266, doi: 10.1111/j.1365-2117.2006.00298.x.

Cowie, P. a., Gupta, S., and Dawers, N.H., 2000, Implications of fault array evolution for synrift depocentre development: Insights from a numerical fault growth model: Basin Research, v. 12, p. 241–261, doi: 10.1046/j.1365-2117.2000.00126.x.

Cowie, P. a., Underhill, J.R., Behn, M.D., Lin, J., and Gill, C.E., 2005, Spatio-temporal evolution of strain accumulation derived from multi-scale observations of Late Jurassic rifting in the northern North Sea: A critical test of models for lithospheric extension: Earth and Planetary Science Letters, v. 234, no. 3-4, p. 401–419, doi: 10.1016/j.epsl.2005.01.039.

Garfunkel, Z., and Bartov, Y., 1977, The Tectonics of the Suez Rift: Geological Survey of Israel Bulletin, , no. 71, p. 45.

Gawthorpe, R.L., Hurst, J.M., and Sladen, C.P., 1990, Evolution of Miocene footwall-derived coarse-grained deltas, Gulf of Suez, Egypt: implications for exploration: v. 74, no. 7, p. 1077–1086.

Gawthorpe, R.L., and Leeder, M.R., 2000, Tectono-sedimentary evolution of active extensional basins: Basin Research, v. 12, no. 3-4, p. 195–218, doi: 10.1046/j.1365-2117.2000.00121.x.

Gawthorpe, R.L., Sharp, I., Underhill, J.R., and Gupta, S., 1997, Linked sequence stratigraphic and structural evolution of propagating normal faults: Geology, v. 25, no. 9, p. 795–798, doi: 10.1130/0091-7613(1997)025<0795:LSSASE>2.3.CO;2.

Gupta, S., Underbill, J.R., Sharp, I.R., and Gawthorpe, R.L., 1999, Role of fault interactions in controlling synrift sediment dispersal patterns: Miocene, Abu Alaqa Group, Suez Rift, Sinai, Egypt: Basin Research, v. 11, no. 2, p. 167–189.

Harland, D.G., 1990, A Geologic Time Scale, 1989 edition (Cambridge University Press, Ed.): Cambridge University Press, Cambridge.

Huismans, R., and Beaumont, C., 2011, Depth-dependent extension, two-stage breakup and cratonic underplating at rifted margins.: Nature, v. 473, no. 7345, p. 74–78, doi: 10.1038/nature09988.

Huismans, R.S., and Beaumont, C., 2014, Rifted Continental Margins : The Case for Depth-Dependent Extension: Earth and Planetary Science Letters, v. 407, p. 148–162, doi: 10.1016/j.epsl.2014.09.032.

Jackson, C.A.L., 2008, Sedimentology and significance of an early syn-rift paleovalley, Wadi Tayiba, Suez Rift, Egypt: Journal of African Earth Sciences, v. 52, p. 62–68, doi: 10.1016/j.jafrearsci.2008.03.007.

Jackson, C.A.L., Gawthorpe, R.L., Leppard, C.W., and Sharp, I.R., 2006, Rift-initiation development of normal fault blocks : insights from the Hammam Faraun fault block , Suez Rift , Egypt: Journal of the Geological Society, London, v. 163, p. 165–183.

Krebs, W.N., Wescot, W. a., Nummedal, D., Gaafar, I., Azazai, G., and Karamat, S., 1997, Graphic correlation and sequence stratigraphy of Neogene rocks in the Gulf of Suez: Bulletin de la Societe Geologique de France, v. 168, no. 1, p. 63–71.

Leeder, M.R., Collier, R.E.L., Abdul Aziz, L.H., Trout, M., Ferentinos, G., Papatheodorou, G., and Lyberis, E., 2002, Tectono-sedimentary processes along an active marine/lacustrine half-graben margin: Alkyonides gulf, E. Gulf of Corinth, Greece: Basin Research, v. 14, p. 25–41, doi: 10.1046/j.1365-2117.2002.00164.x.

Leeder, M.R., and Gawthorpe, R.L., 1987, Sedimentary models for extensional tilt-block/half-graben basins: Geological Society, London, Special Publications, v. 28, no. 28, p. 139–152, doi: 10.1144/GSL.SP.1987.028.01.11.

Lewis, M.M., Jackson, C.A.L., Rob L. Gawthorpe, and Whipp, P.S., 2015, Stratal Architecture and along-strike variability of early syn-rift deposits: An example from the hadahid fault system, Suez rift, Egypt: Basins Research Group (BRG), v. In press.

Martinsson, A., and Bassett, M.G., 2010, International Commission on Stratigraphy: Time, v. 13, no. 1, p. 26–26, doi: 10.1111/j.1502-3931.1980.tb01026.x.

McClay, K., and Khalil, S., 1998, Extensional hard linkages, eastern Gulf of Suez, Egypt: Geology, v. 26, no. 6, p. 563–566, doi: 10.1130/0091-7613(1998)026<0563:EHLEGO>2.3.CO;2.

McClay, K.R., Nichols, G.J., Khalil, S.M., Darwish, M., and Bosworth, W., 1998, McClay et al 1998 Chapter D4.pdf, *in* Purser, B.H. and Bosence, D.W.J. eds., Sedimentation and Tectonics of Rift Basins: Red Sea-Gulf of Aden, Chapman & Hall, London, p. 223–238.

Miller, K.G., Kominz, M. a, Browning, J. V, Wright, J.D., Mountain, G.S., Katz, M.E., Sugarman, P.J., Cramer, B.S., Christie-Blick, N., and Pekar, S.F., 2005, The Phanerozoic record of global sea-level change.: Science (New York, N.Y.), v. 310, p. 1293–1298, doi: 10.1126/science.1116412.

Moustafa, A.R., 2004, Geological Maps of the Eastern Side of the Suez Rift (Western Sinai Peninsula) Egypt: AAPG Datapages, GIS Series, , no. 74.

Moustafa, A.R., 1993, Structural characteristics and tectonic evolution of the east-margin blocks of the Suez rift: Tectonophysics, v. 223, no. 3-4, p. 381–399, doi: 10.1016/0040-1951(93)90146-B.

Moustafa, A.R., and El-Raey, A.K., 1993, Structural characteristics of the Suez rift margins: , no. January, p. 101–109.

NASA, 2014, https://reverb.echo.nasa.gov: ASTER Global Digital Elevation Model V002, p. Retrieved 2014–12–08.

Patton, T.L., Moustafa, A.R., Nelson, R.A., and Abdine, S.A., 1994, Tectonic Evolution and Structural Settings of the Suez Rift: Interior Rift Basins: AAPG Memoir 59, v. 137, p. 9–55.

Prosser, S., 1993, Rift-related linked depositional systems and their seismic expression: Geological Society, London, Special Publications, v. 71, no. 1, p. 35–66, doi: 10.1144/GSL.SP.1993.071.01.03.

Ravnas, R., Nottvedt, a., Steel, R.J., and Windelstad, J., 2000, Syn-rift sedimentary architectures in the Northern North Sea:.

Ravnås, R., and Steel, R.J., 1998, Architecture of Marine Rift-Basin Successions: AAPG Bulletin, v. 82 (1998), no. 1, p. 110–146, doi: 10.1306/1D9BC3A9-172D-11D7-8645000102C1865D.

Rigon, R., Rodriguez-Iturbe, I., Maritan, A., Giacometti, A., Tarboton, D.G., and Rinaldo, A., 1996, On Hack's law: v. 32, no. 11, p. 3367–3374.

Sclater, J.G., and Christie, P.A.F., 1980, Continental stretching: An explanation of the Post-Mid-Cretaceous subsidence of the central North Sea Basin: Journal of geophysical research, v. 85, no. B7, p. 3711–3739, doi: 10.1029/JB085iB07p03711.

Sharp, I.R., Gawthorpe, R.L., Armstrong, B., and Underhill, J.R., 2000a, Propagation history and passive rotation of mesoscale normal faults: implications for synrift stratigraphic development: Basin Research, v. 12, no. 3-4, p. 285–305, doi: 10.1046/j.1365-2117.2000.00132.x.

Sharp, I.R., Gawthorpe, R.L., Underhill, J.R., and Gupta, S., 2000b, Fault-propagation folding in extensional settings: Examples of structural style and synrift sedimentary response from the Suez rift, Sinai, Egypt: Geological Society of America Bulletin, v. 112, no. 12, p. 1877–1899, doi: 10.1130/0016-7606(2000)112<1877:FPFIES>2.0.CO;2.

Steckler, M.S., Pichon, X. Le, Lyberis, N., and Berthelot, F., 1988, Subsidence in the Gulf of Suez : implications for rifting and plate kinematics: v. 153, p. 249–270.

Wescot, W. a., Krebs, W.N., Dolson, J.C., Karamat, S. a., and Nummedal, D., 1996, Rift basin sequence stratigraphy: some examples from the Gulf of Suez: GeoArabia, v. 1, no. 2, p. 343–358.

Whipp, P.S., 2011, Fault-propagation folding and the growth of normal faults, unpublished Pdh thesis: Imperial College London, 283 p.

Younes, A.I., Mcclay, K., and Younes, A.I., 2002, Egypt: AAPG Bulletin, v. 6, no. 6, p. 1003–1026.

.....

Amoco Field Guide

Appendix 1

Figures used for finding Sea-level for the prerift and synrift units in the El Qaa fault block. Figure 1 is the Field notes from the Amoco Field Guide, Figure 2 is a from Harland et al., 1989 showing some biozones from the Neogene period and 1c is the Sea-level curve from (Miller et al., 2005).

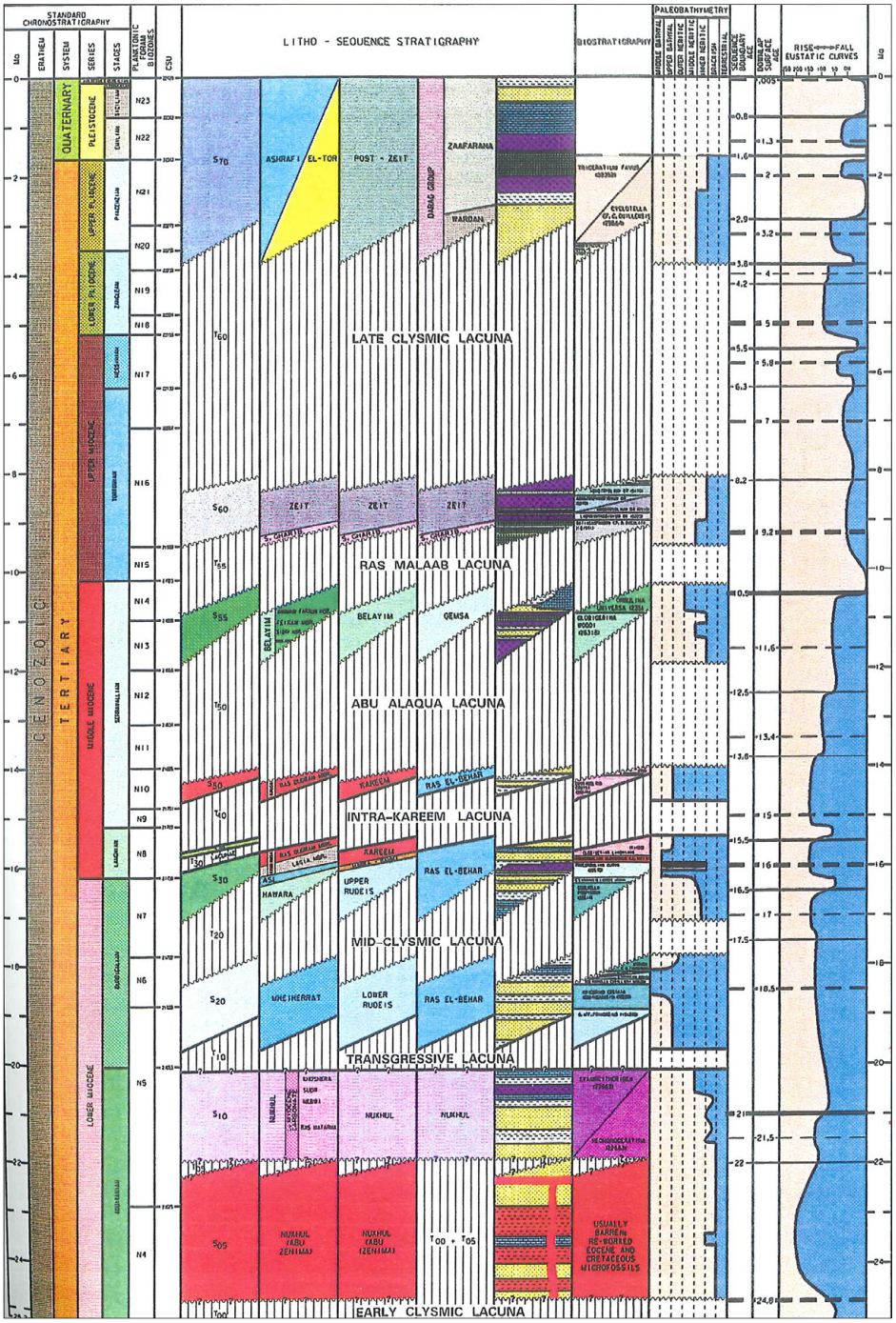

Figure 1: Notes for Amoco Field Guide, used for finding Sea-level (Source: Amoco Field Guide; Krebs et al. (1997)*)*

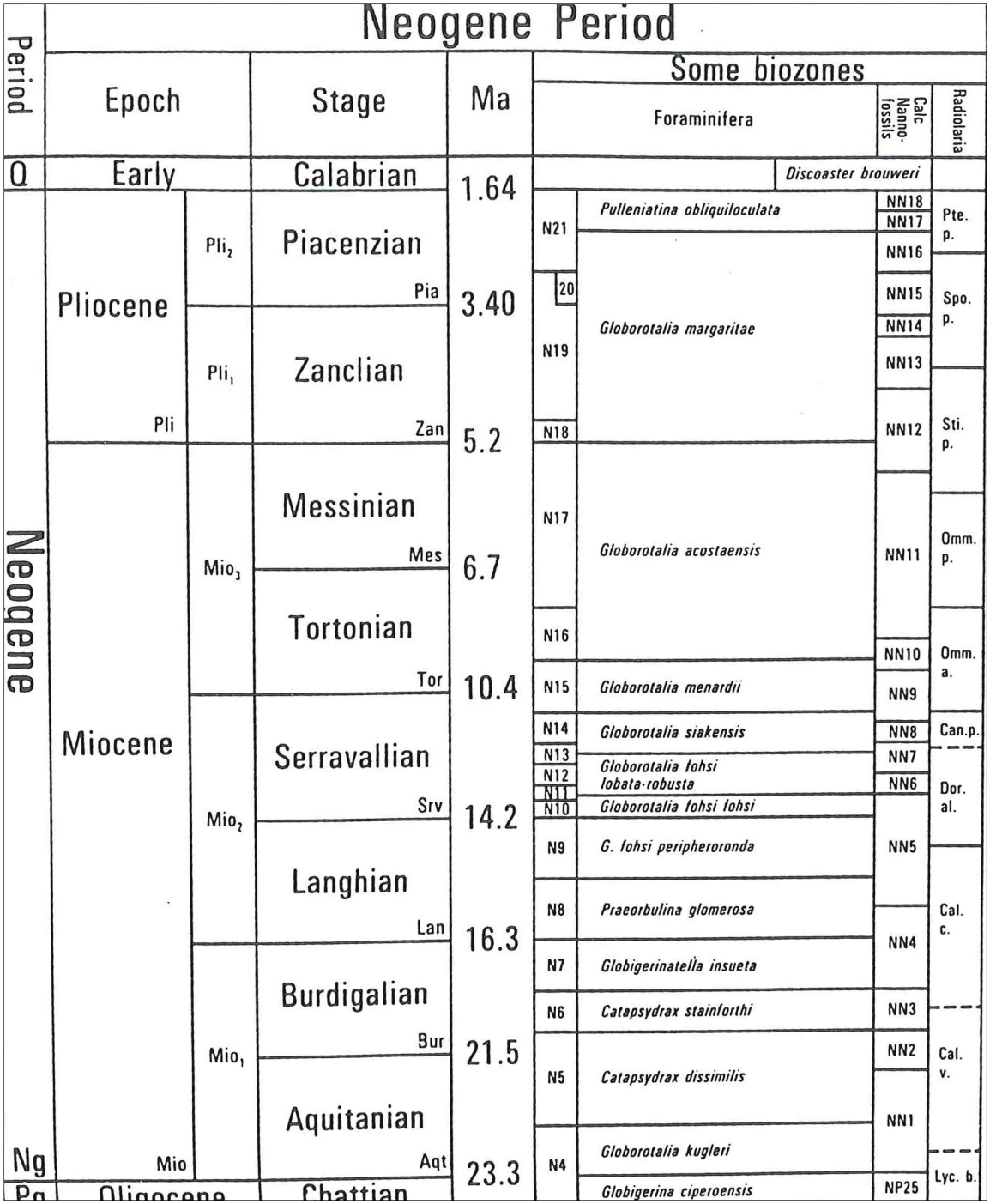

Figure 2: Neogene Timescale used for finding Sea-level (Harland, 1990).

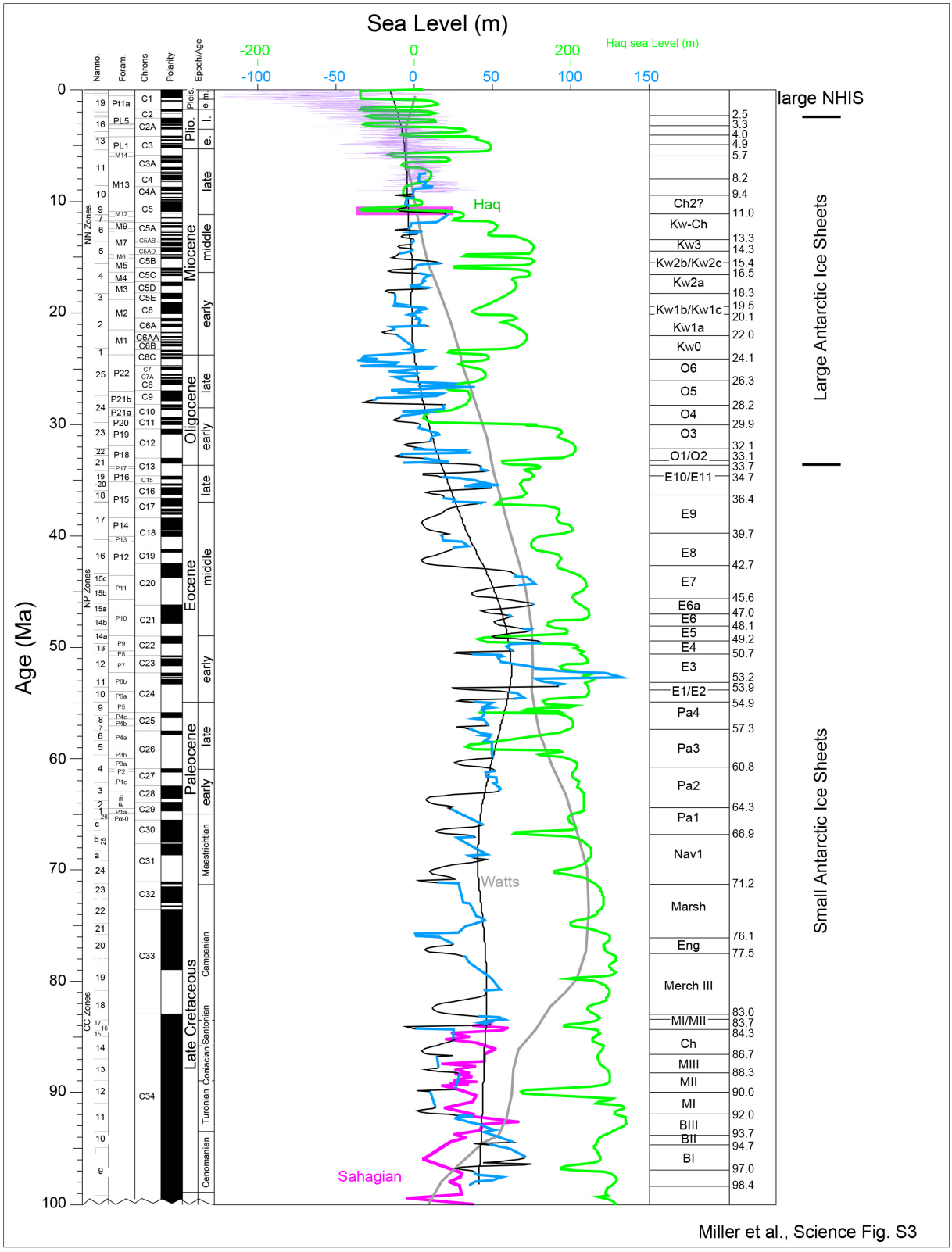

Figure 3: Global sea-level curve (Miller et al., 2005).

Appendix 2:

Restoration (Backstripping) results for all six cross-sections. Cross-section 1, 2 and 3 have fewer steps involved due to the lack of the delta deposits, instead a Carbonate platform (Qabeliat Formation) was simultaneously building up on the dipslope in the south-part of the El Qaa half graben.

- Figure 4: Restoration of cross-section 1
- Figure 5: Restoration of cross-section 2
- Figure 6: Restoration of cross-section 3
- Figure 7: Restoration of cross-section 4
- Figure 8: Restoration of cross-section 5
- Figure 9: Restoration of cross-section 6

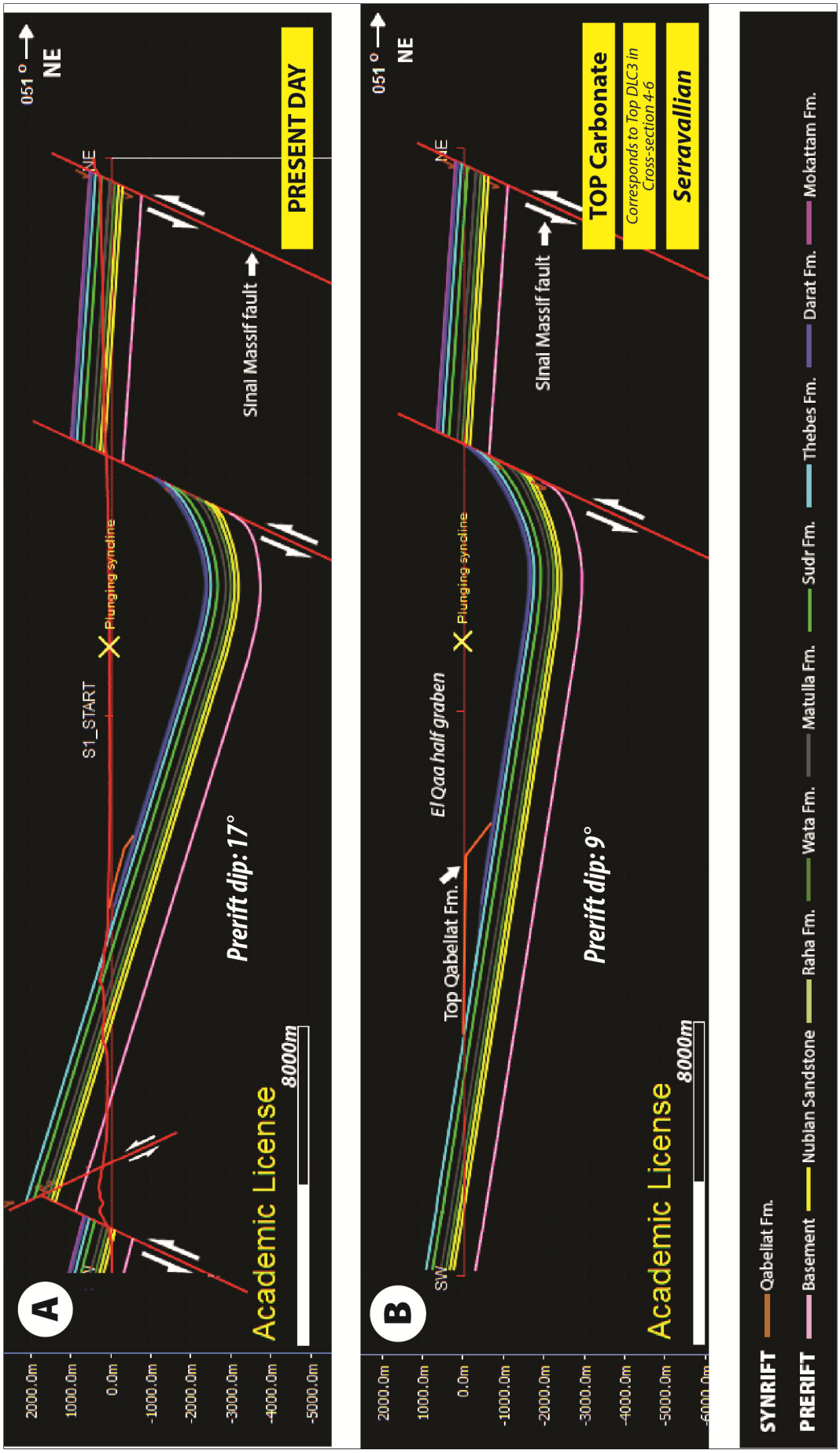

Figure 4: Restoration of cross-section 1 (A) Present day (B) Top of the Carbonates (Seravallian). (C) Base Synrift, Late Oligocene-Early Miocene. (D) Restored to the top of Mokattam Fm. of Mokattam Formation (Middle Eocene). Legend applies to A, B, C and D.

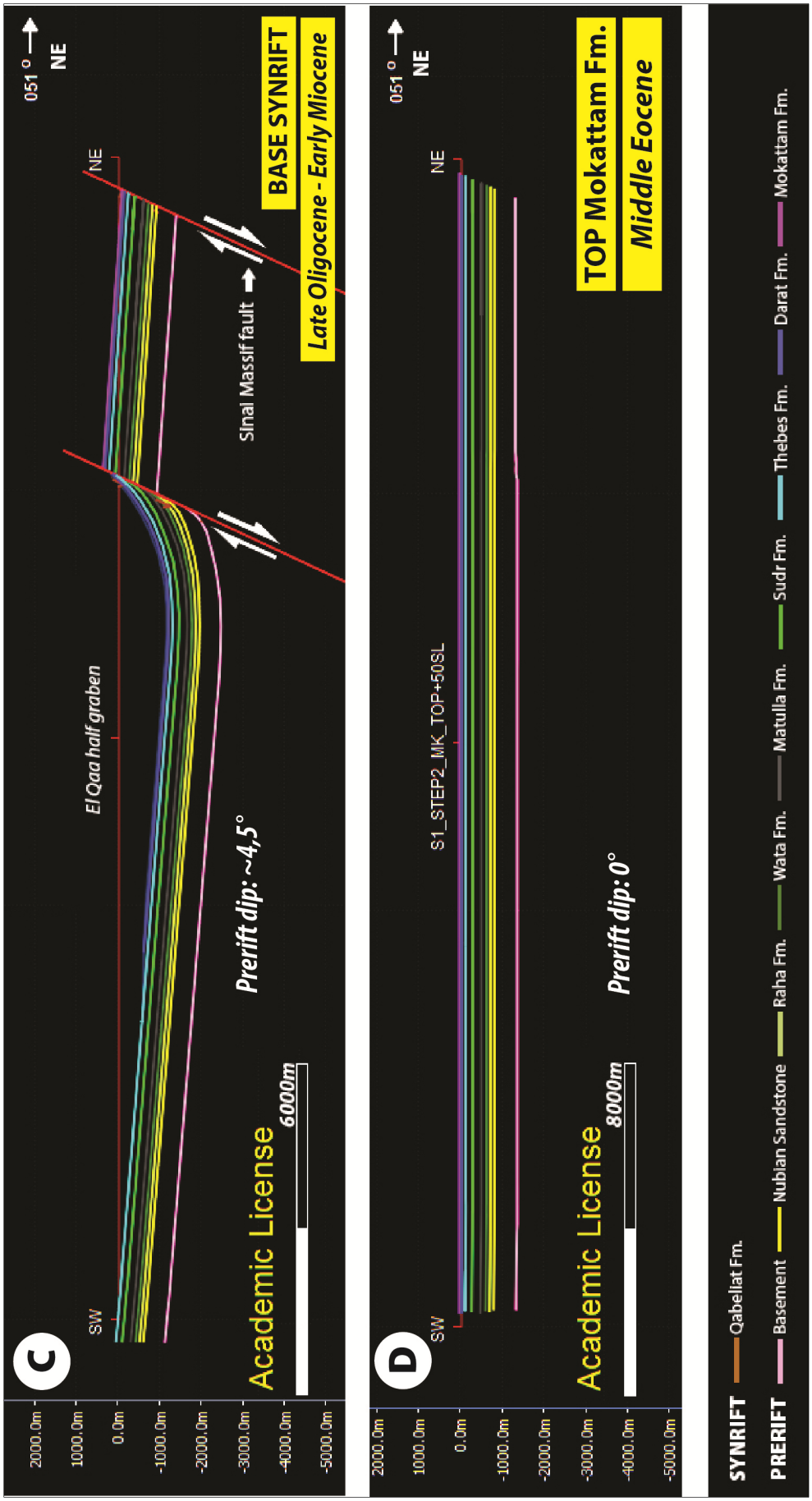
C
SW
NE
El Qaa half graben
Prerift dip: ~4,5°
Sinai Massif fault
NE
BASE SYNRIFT
Late Oligocene - Early Miocene
051 °
NE
Academic License
6000m
2000.0m
1000.0m
0.0m
-1000.0m
-2000.0m
-3000.0m
-4000.0m
-5000.0m
D
SW
S1_STEP2_MK_TOP+50SL
Prerift dip: 0°
NE
TOP Mokattam Fm.
Middle Eocene
051 °
NE
Academic License
8000m
2000.0m
1000.0m
0.0m
-1000.0m
-2000.0m
-3000.0m
-4000.0m
-5000.0m
SYNRIFT
Qabeliat Fm.
PRERIFT
Basement
Nubian Sandstone
Raha Fm.
Wata Fm.
Matulla Fm.
Sudr Fm.
Thebes Fm.
Darat Fm.
Mokattam Fm.

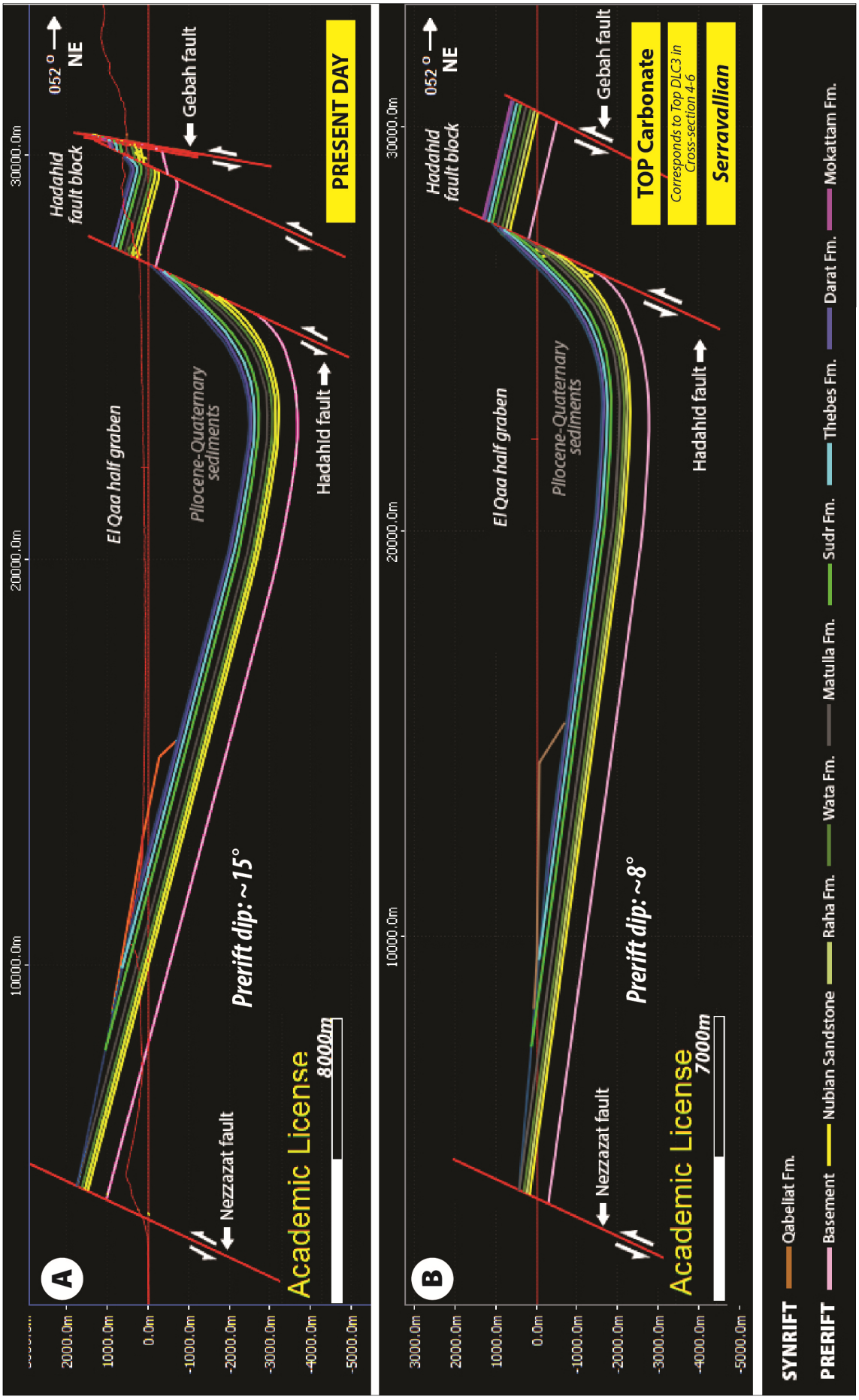

Figure 5: Cross-section 2 restoration. (A) Present day interpretation, (B) At Serravallian times, when the Qabeliat Formation was deposited (corresponds to the top of DLC-3 in cross-sections 4-6. (C) Base synrift at the Late Oligocene – Early Miocene. (D) Top Mokattam Formation (Middle Eocene). Legend applies to A, B, C and D.

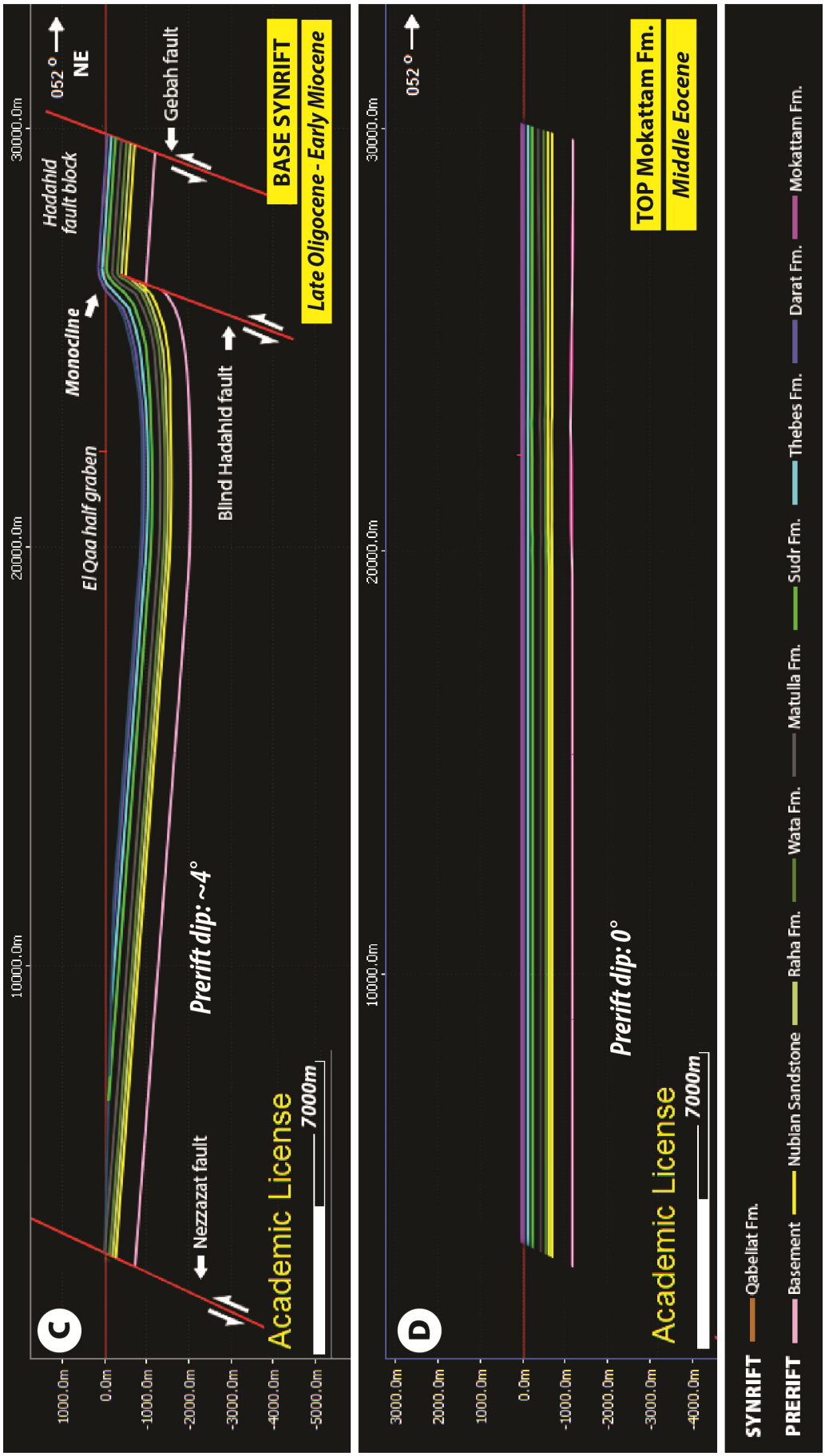
C
D
052 °
NE
Hadahid fault block
Monocline
El Qaa half graben
Gebah fault
Blind Hadahid fault
Nezzazat fault
BASE SYNRIFT
Late Oligocene - Early Miocene
Prerift dip: ~4°
Prerift dip: 0°
TOP Mokattam Fm.
Middle Eocene
Academic License
7000m
10000.0m
20000.0m
30000.0m
SYNRIFT
Qabeliat Fm.
PRERIFT
Basement
Nubian Sandstone
Raha Fm.
Wata Fm.
Matulla Fm.
Sudr Fm.
Thebes Fm.
Darat Fm.
Mokattam Fm.

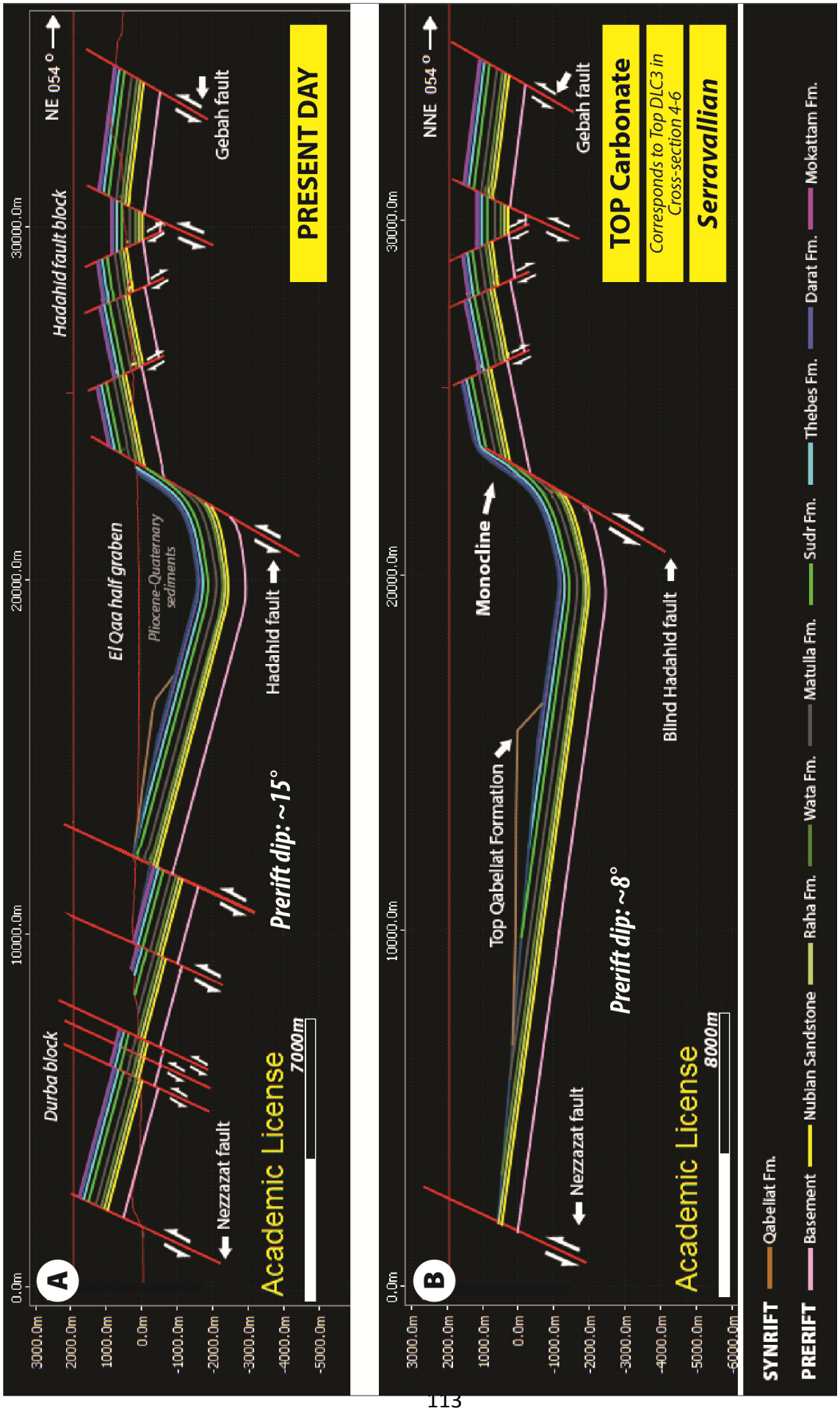

Figure 6: Cross-section 3 restoration. (A) Present day interpretation, (B) At Serravallian times, when the Qabeliat Formation was depositet (corresponds to the top of DLC-3 in cross-sections 4-6).(C) Base synrift (Late Oligocene – Early Miocene).Top of the Mokattam Formation (Middle Miocene). Legend applies to A, B, C and D.

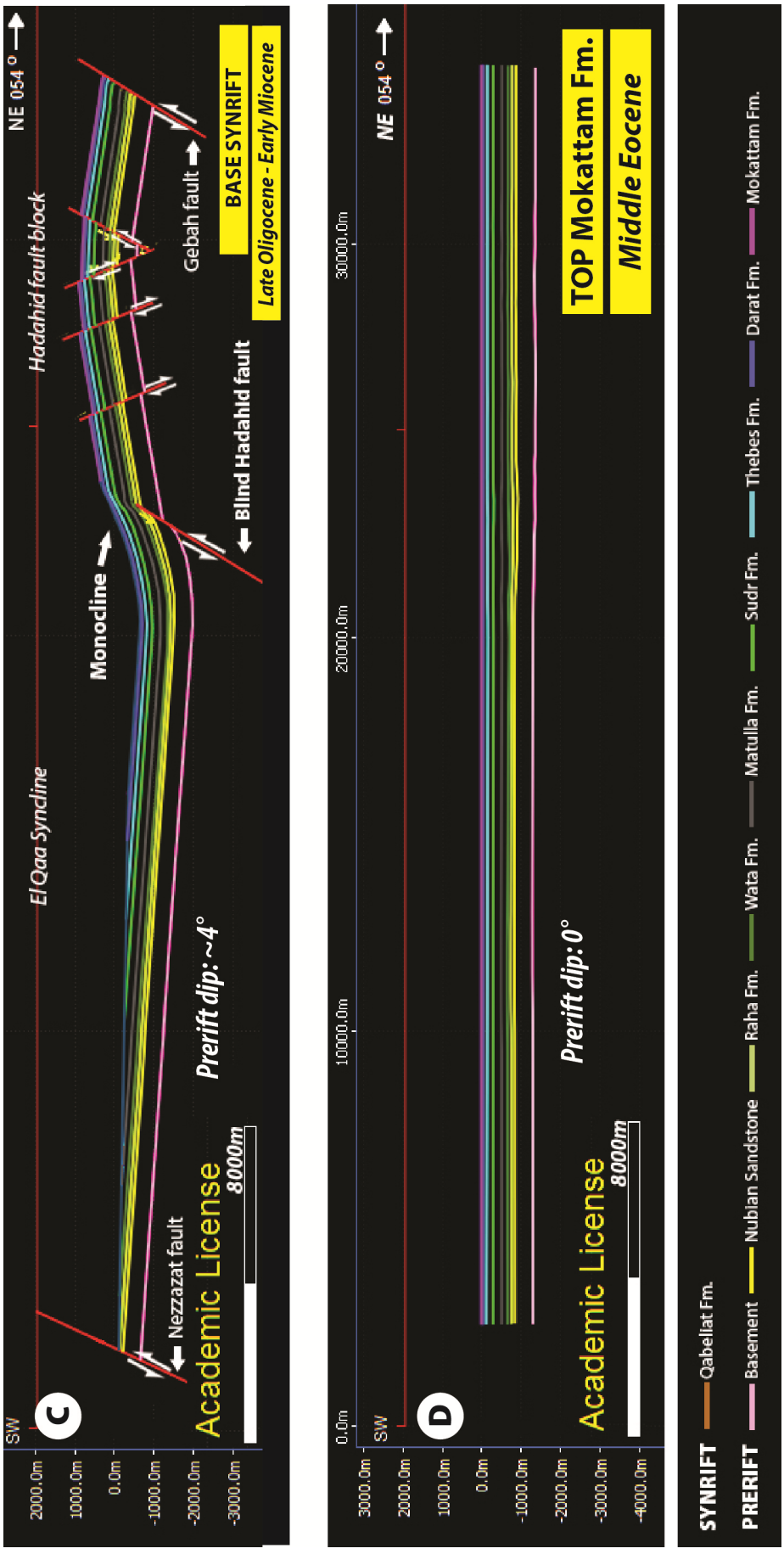
C
SW
NE 054 °
El Qaa Syncline
Hadahid fault block
Monocline
Gebah fault
BASE SYNRIFT
Late Oligocene - Early Miocene
Blind Hadahid fault
Nezzazat fault
Prerift dip: ~4°
Academic License
8000m
2000.0m
1000.0m
0.0m
-1000.0m
-2000.0m
-3000.0m
D
SW
NE 054 °
0.0m
10000.0m
20000.0m
30000.0m
TOP Mokattam Fm.
Middle Eocene
Prerift dip: 0°
Academic License
8000m
3000.0m
2000.0m
1000.0m
0.0m
-1000.0m
-2000.0m
-3000.0m
-4000.0m
SYNRIFT
Qabeliat Fm.
PRERIFT
Basement
Nubian Sandstone
Raha Fm.
Wata Fm.
Matulla Fm.
Sudr Fm.
Thebes Fm.
Darat Fm.
Mokattam Fm.

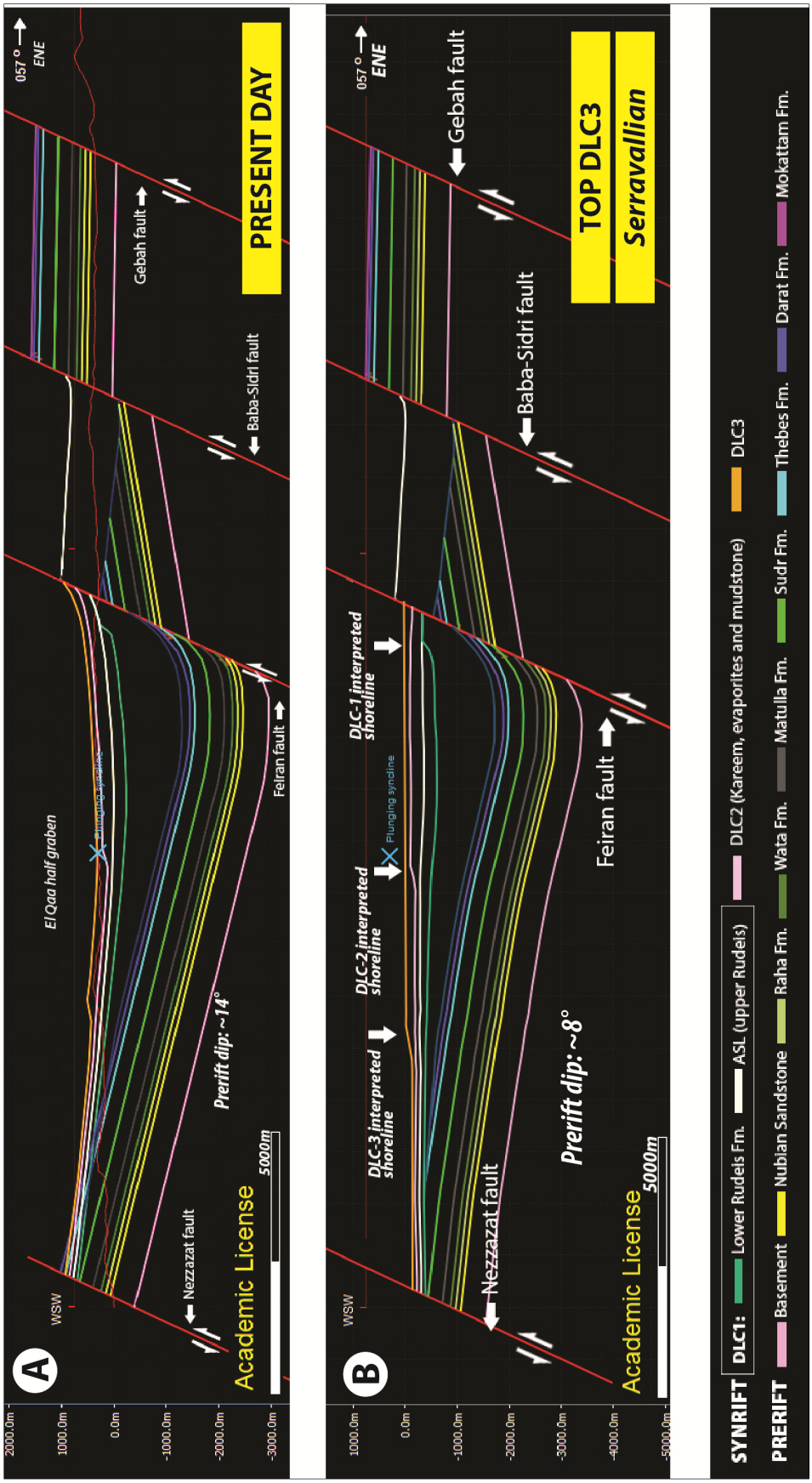

Figure 7: Cross-section 4 restoration. (A) Present day interpretation, (B) Top of DLC-3 (Seravallian. (C) Top DLC-2 in the Langhian-Seravallia. (D) Top DLC-1 (Langhian). (E) Base of the synrift at Late Oligocene - Early Miocene, (F) top of the Mokattam Formation at Middle Miocene.

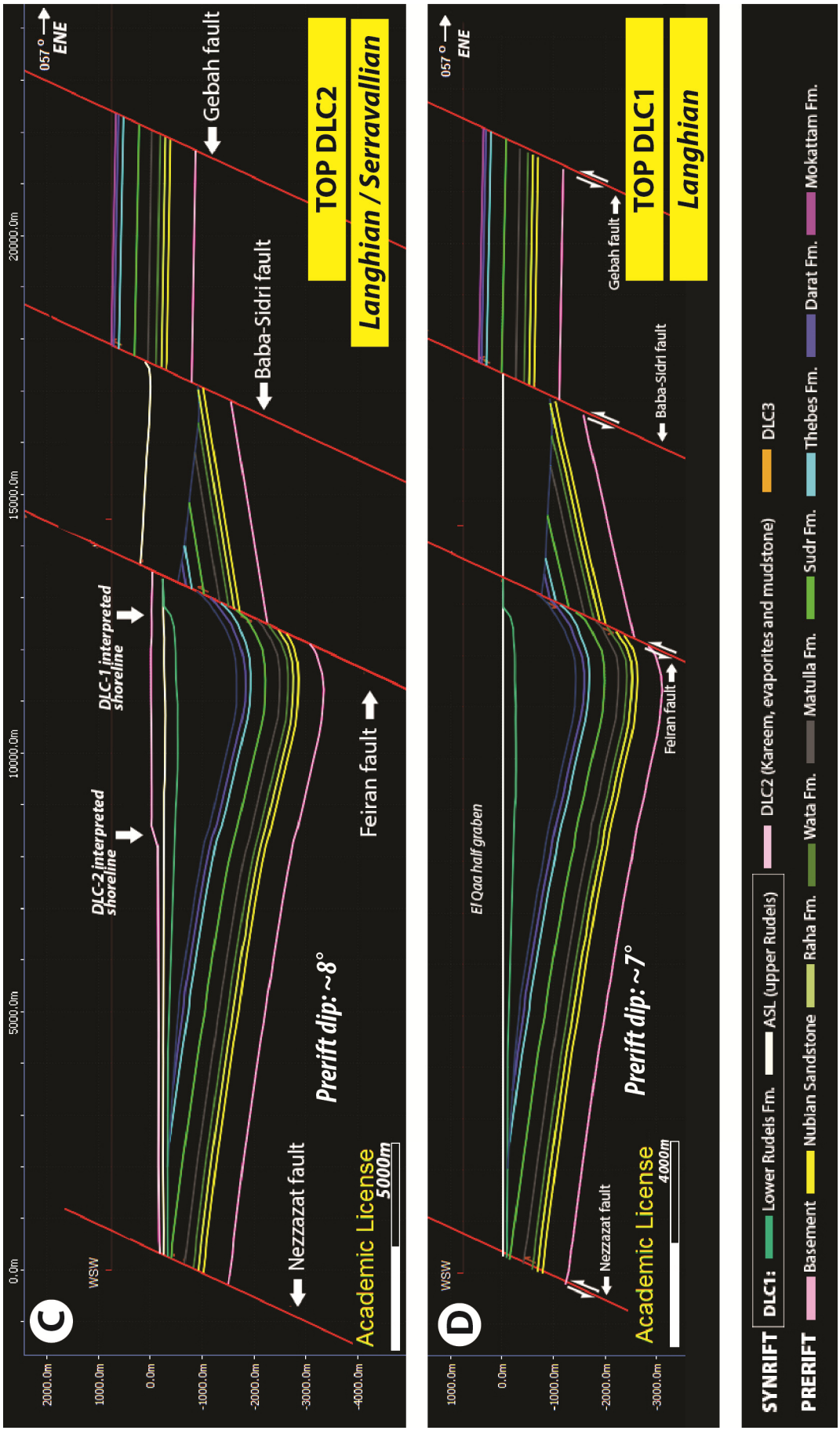
C
WSW
057 °
ENE
0.0m
5000.0m
10000.0m
15000.0m
20000.0m
2000.0m
1000.0m
0.0m
-1000.0m
-2000.0m
-3000.0m
-4000.0m
Gebah fault
Baba-Sidri fault
TOP DLC2
Langhian / Serravallian
DLC-1 interpreted shoreline
DLC-2 interpreted shoreline
Feiran fault
Prerift dip: ~8°
Nezzazat fault
Academic License
5000m
D
WSW
057 °
ENE
1000.0m
0.0m
-1000.0m
-2000.0m
-3000.0m
Gebah fault
TOP DLC1
Langhian
Baba-Sidri fault
El Qaa half graben
Feiran fault
Prerift dip: ~7°
Nezzazat fault
Academic License
4000m
SYNRIFT
DLC1:
Lower Rudeis Fm.
ASL (upper Rudeis)
DLC2 (Kareem, evaporites and mudstone)
DLC3
PRERIFT
Basement
Nubian Sandstone
Raha Fm.
Wata Fm.
Matulla Fm.
Sudr Fm.
Thebes Fm.
Darat Fm.
Mokattam Fm.

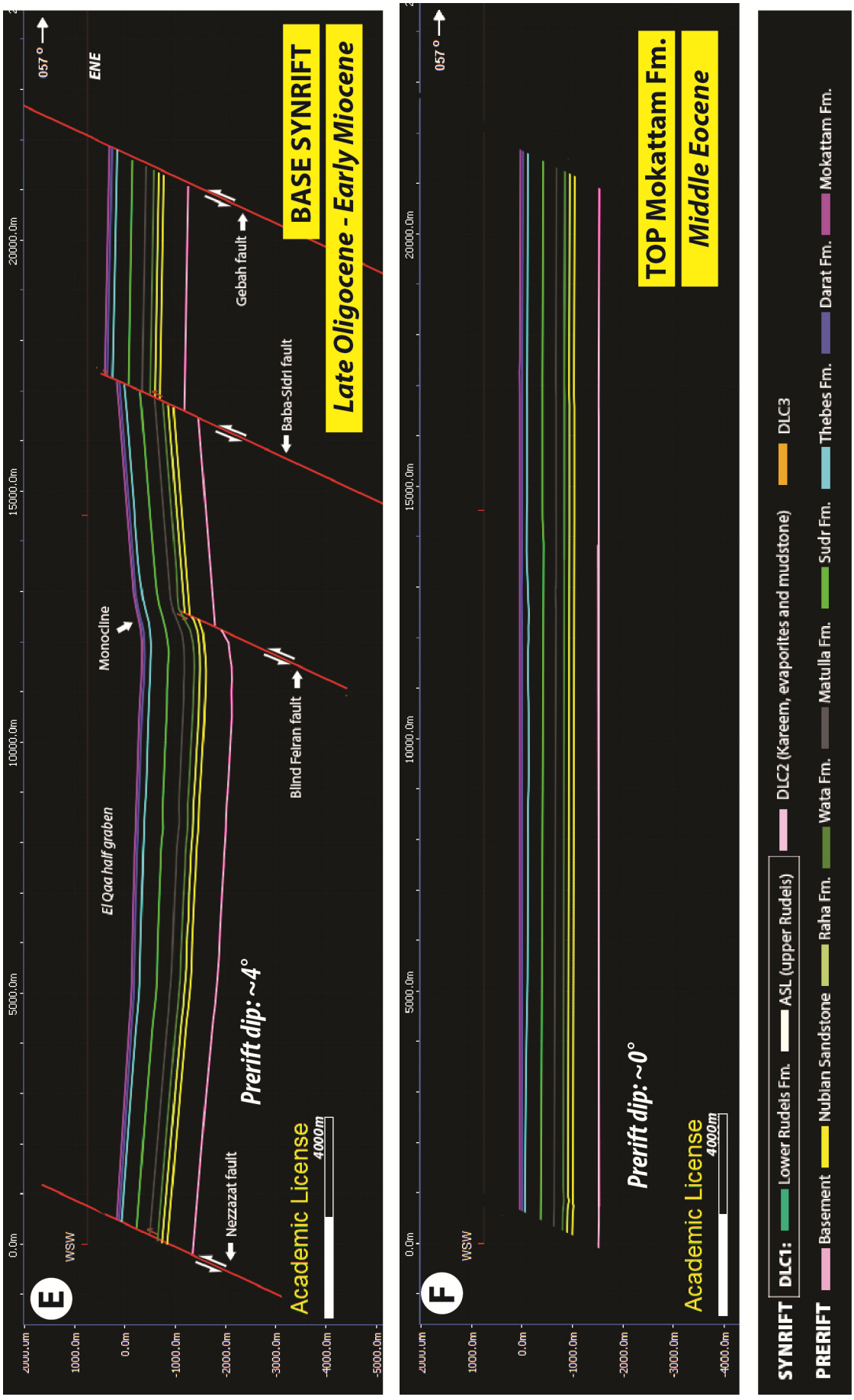
E
WSW
ENE
057 °
BASE SYNRIFT
Late Oligocene - Early Miocene
Gebah fault
Baba-Sidri fault
Monocline
El Qaa half graben
Blind Feiran fault
Nezzazat fault
Prerift dip: ~4°
Academic License
4000m
F
TOP Mokattam Fm.
Middle Eocene
Prerift dip: ~0°
SYNRIFT
DLC1:
Lower Rudeis Fm.
ASL (upper Rudeis)
DLC2 (Kareem, evaporites and mudstone)
DLC3
PRERIFT
Basement
Nubian Sandstone
Raha Fm.
Wata Fm.
Matulla Fm.
Sudr Fm.
Thebes Fm.
Darat Fm.
Mokattam Fm.

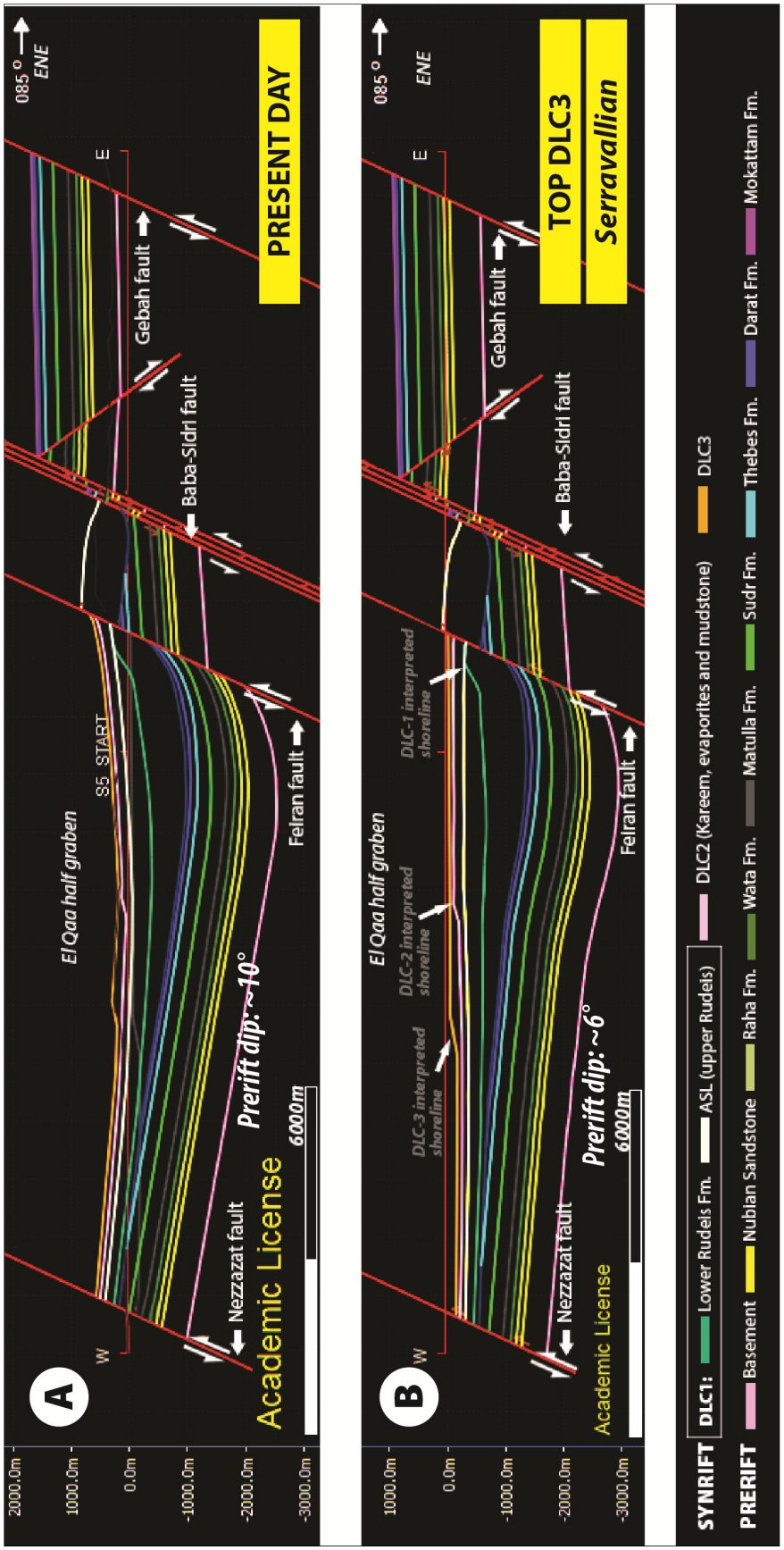

Figur 8: Cross-section 5 restoration. (A) Present day interpretation, (B) Top of DLC-3 (Seravallian). (C) Top DLC-2 in the Langhian-Seravallian, (D) top DLC-1 deposited in Langhian. (E) Base of the synrift at Late Oligocene - Early Miocene, (F) top of the Mokattam Formation at Middle Miocene.

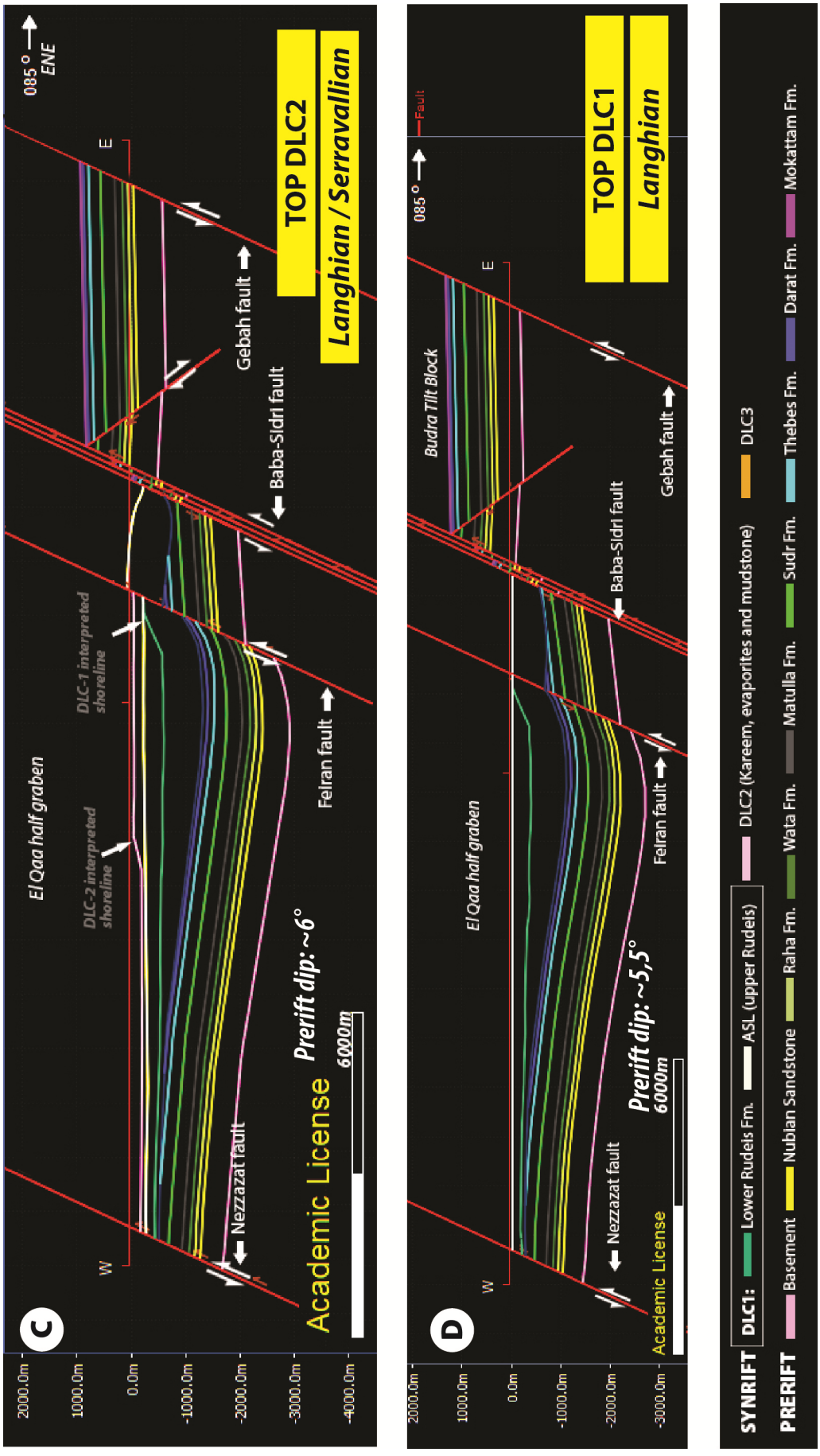
C
085 °
ENE
E
W
TOP DLC2
Langhian / Serravallian
Gebah fault
Baba-Sidri fault
Felran fault
Nezzazat fault
El Qaa half graben
DLC-1 interpreted shoreline
DLC-2 interpreted shoreline
Prerift dip: ~6°
6000m
Academic License
2000.0m
1000.0m
0.0m
-1000.0m
-2000.0m
-3000.0m
-4000.0m
D
Fault
085 °
TOP DLC1
Langhian
Budra Tilt Block
Gebah fault
Baba-Sidri fault
Felran fault
Nezzazat fault
El Qaa half graben
Prerift dip: ~5,5°
6000m
Academic License
SYNRIFT
DLC1:
Lower Rudeis Fm.
ASL (upper Rudeis)
DLC2 (Kareem, evaporites and mudstone)
DLC3
PRERIFT
Basement
Nubian Sandstone
Raha Fm.
Wata Fm.
Matulla Fm.
Sudr Fm.
Thebes Fm.
Darat Fm.
Mokattam Fm.

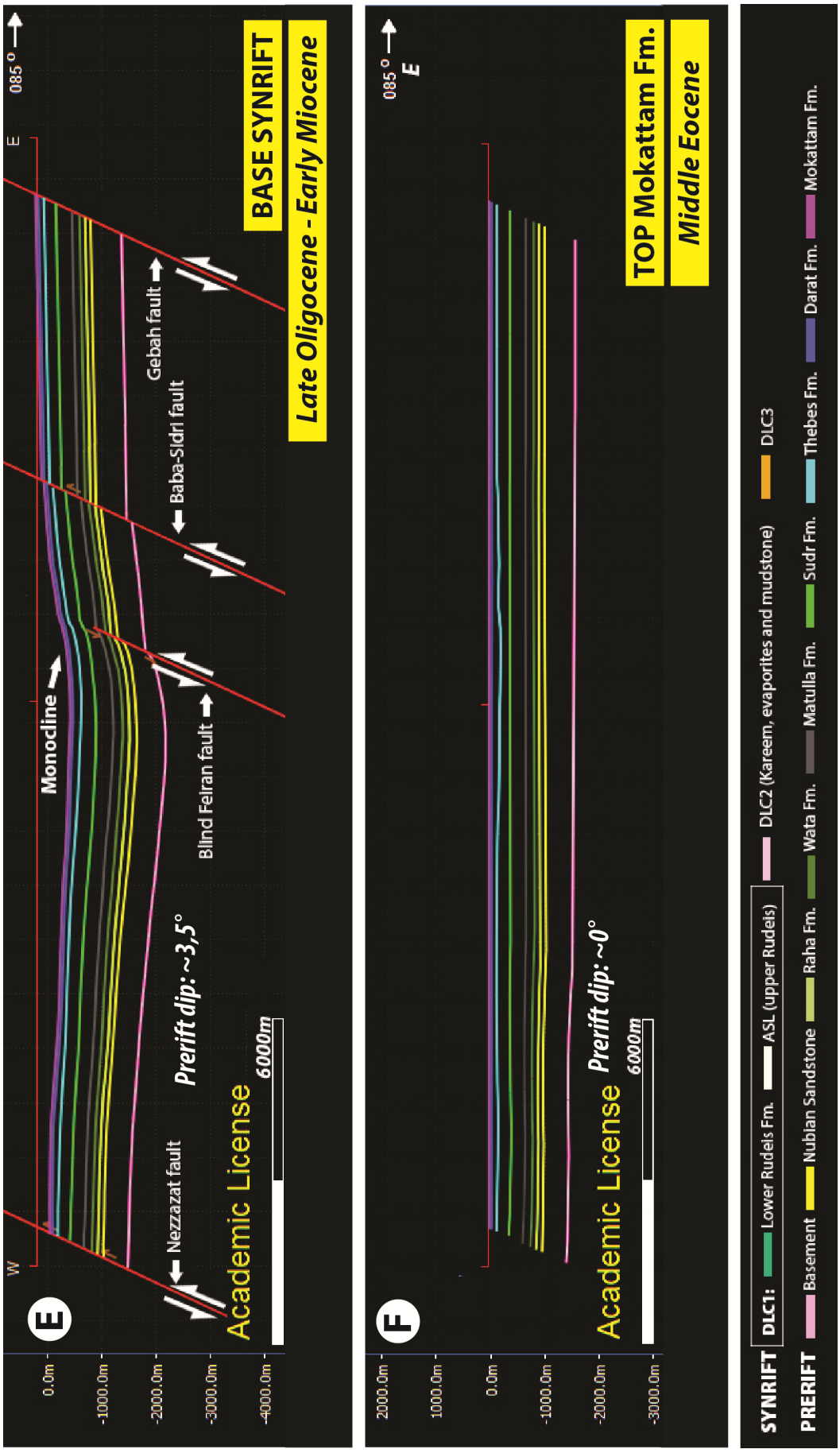
E
W
085 °
BASE SYNRIFT
Late Oligocene - Early Miocene
Gebah fault
Baba-Sidri fault
Monocline
Blind Feiran fault
Nezzazat fault
Prerift dip: ~3,5°
Academic License
6000m
0.0m
-1000.0m
-2000.0m
-3000.0m
-4000.0m
F
E
085 °
TOP Mokattam Fm.
Middle Eocene
Prerift dip: ~0°
Academic License
6000m
2000.0m
1000.0m
0.0m
-1000.0m
-2000.0m
-3000.0m
SYNRIFT
DLC1:
Lower Rudeis Fm.
ASL (upper Rudeis)
DLC2 (Kareem, evaporites and mudstone)
DLC3
PRERIFT
Basement
Nubian Sandstone
Raha Fm.
Wata Fm.
Matulla Fm.
Sudr Fm.
Thebes Fm.
Darat Fm.
Mokattam Fm.

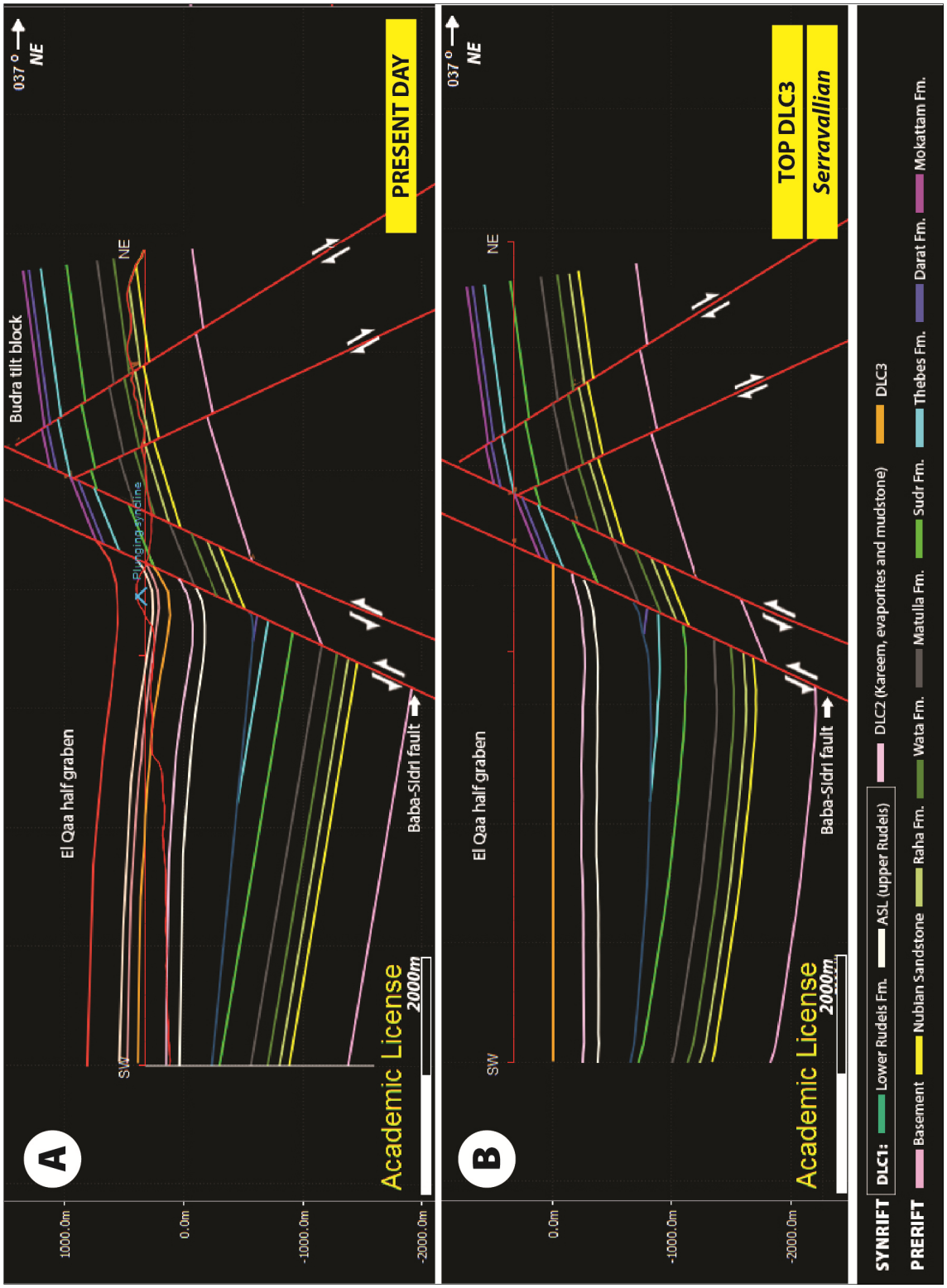

Figure 9: Cross-section 6 restoration. (A) Present day interpretation, (B) At Serravallian times top of DLC-3, (C) Top DLC-2 in the Langhian-Seravallian. (D) Top DLC-1(Langhian) (E) Base of the synrift at Late Oligocene - Early Miocene, (F) top of the Mokattam Formation at Middle Miocene.

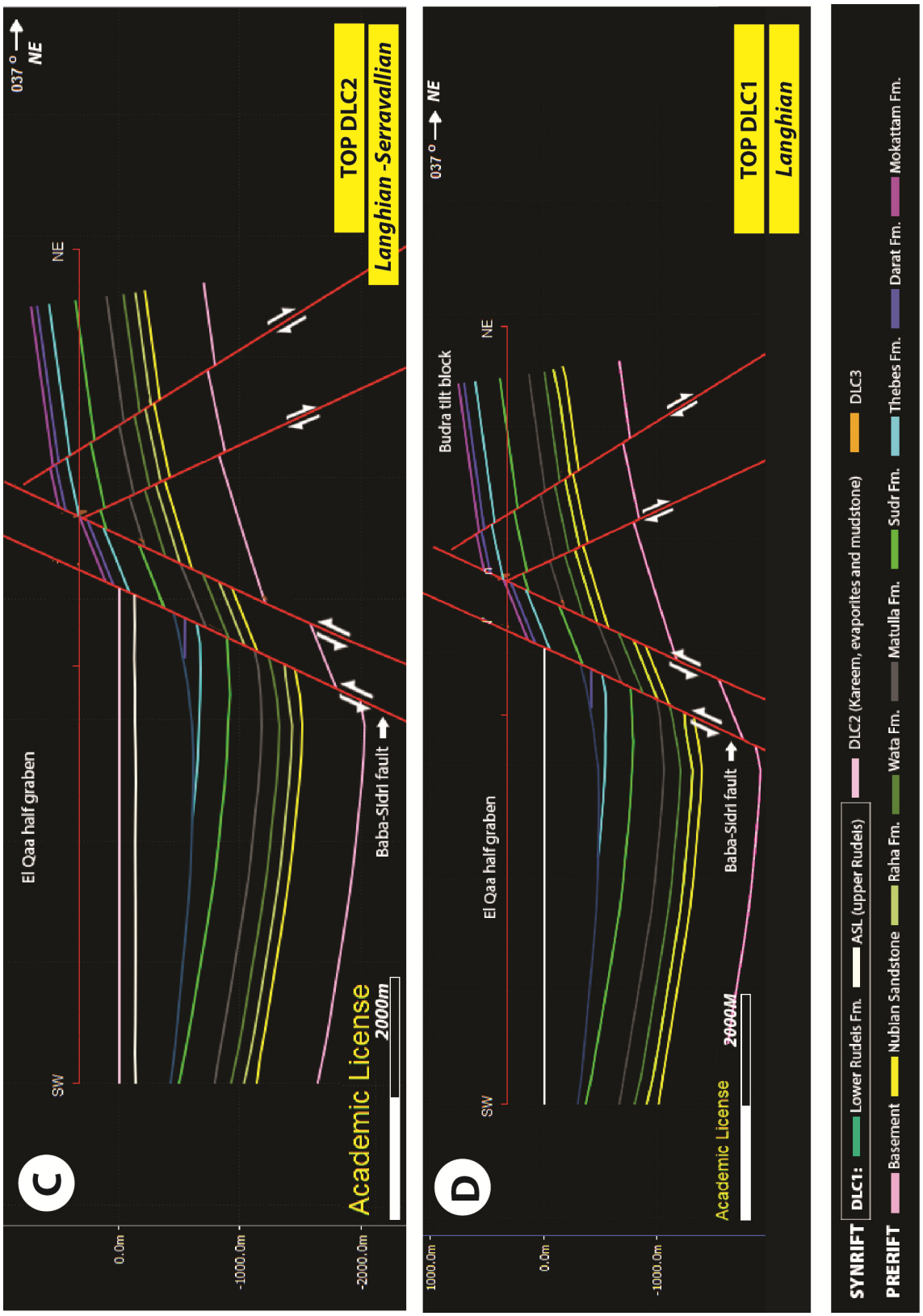
C
037 °
NE
SW
NE
El Qaa half graben
TOP DLC2
Langhian -Serravallian
Baba-Sidri fault
Academic License
2000m
0.0m
-1000.0m
-2000.0m
D
037 °
NE
SW
NE
Budra tilt block
El Qaa half graben
TOP DLC1
Langhian
Baba-Sidri fault
Academic License
2000M
1000.0m
0.0m
-1000.0m
SYNRIFT
DLC1:
Lower Rudeis Fm.
ASL (upper Rudeis)
DLC2 (Kareem, evaporites and mudstone)
DLC3
PRERIFT
Basement
Nubian Sandstone
Raha Fm.
Wata Fm.
Matulla Fm.
Sudr Fm.
Thebes Fm.
Darat Fm.
Mokattam Fm.

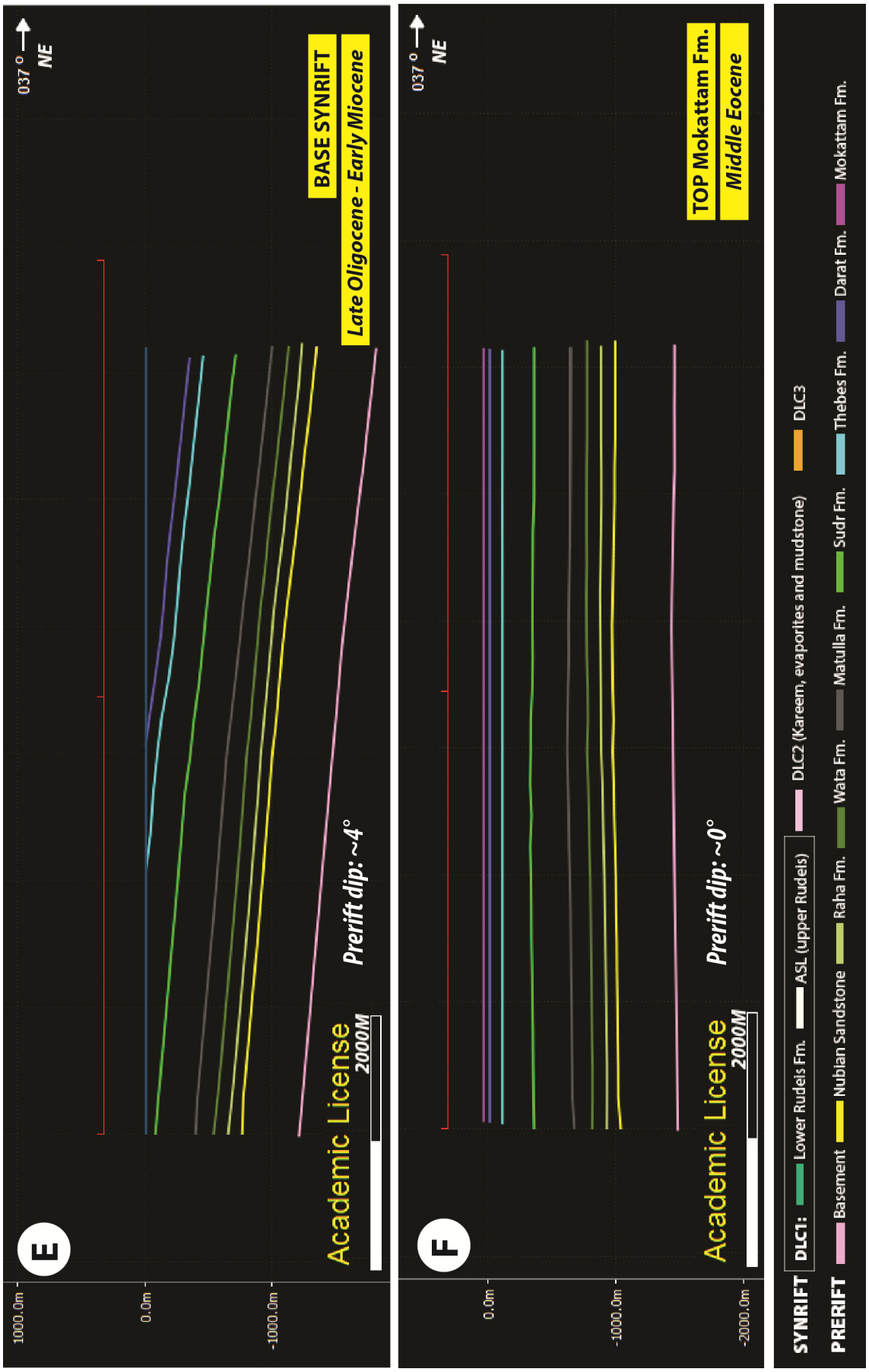
E
037 °
NE
BASE SYNRIFT
Late Oligocene - Early Miocene
Prerift dip: ~4°
Academic License
2000M
1000.0m
0.0m
-1000.0m
F
037 °
NE
TOP Mokattam Fm.
Middle Eocene
Prerift dip: ~0°
Academic License
2000M
0.0m
-1000.0m
-2000.0m
SYNRIFT
DLC1:
Lower Rudeis Fm.
ASL (upper Rudeis)
DLC2 (Kareem, evaporites and mudstone)
DLC3
PRERIFT
Basement
Nubian Sandstone
Raha Fm.
Wata Fm.
Matulla Fm.
Sudr Fm.
Thebes Fm.
Darat Fm.
Mokattam Fm.